U-Pb Geochronology and Trace Element Analysis of Apatite and Calcite from the Ernest Henry IOCG Deposit, NW Queensland.

Thesis submitted in accordance with the requirements of the University of Adelaide for an Honours Degree in Geology/Geophysics

Bradley Wade Cave

October 2017

THE UNIVERSITY of ADELAIDE

U-PB GEOCHRONOLOGY AND TRACE ELEMENT ANALYSIS OF APATITE AND CALCITE FROM ERNEST HENRY

ABSTRACT

Ernest Henry is the largest known IOCG deposit in the Eastern Succession of the Mount Isa inlier, NW Queensland. To improve our understanding of the timing of alteration and mineralisation in the Ernest Henry deposit, we attempt to date apatite from the Interlens (a pre-mineralization structure) and the ore-stage breccia, and calcite from the Interlens, ore-stage breccia and post-mineralization alteration using the in-situ U-Pb LA-ICP-MS method. This also approach provides the opportunity to examine the trace element composition of the minerals, which can be used to identify their sources and constrain metasomatic processes.

Coarse-grained apatite from Interlens was dated at 1581 ± 16 Ma, coeval with regional peak metamorphic conditions and D_2 deformation of the Isan Orogeny. Finer-grained apatite from the Interlens produced an age of 1557 ± 23 Ma, possibly representing regional D_2, $D_{2.5}$ or D_3 deformation, coeval with retrograde metamorphic conditions. Ore-stage apatite produced an age of 1529 ± 39 Ma, coeval with the accepted age for sulphide mineralisation, D_3 deformation and the formation of the nearby Mount Margaret granite. Calcite samples were unable to be dated by this method, as the samples were dominated by common lead.

Trace element analysis indicate that apatite from the Interlens and ore-stage assemblage were sourced from magmatic/hydrothermal fluids. Furthermore, metasomatism and coupled dissolution re-precipitation reactions of apatite were induced by a Na and/or Ca rich fluid, possessing varying amounts of Cl and S. Calcite from this study displays similarities with altered granites, and greisen type deposits, likely the result of fluid diffusing through the heavily altered Mount Fort Constantine host rocks. This study also geochemically links calcite from the Ernest Henry and the nearby E1 deposit, suggesting the REE composition of calcite may be used to link hydrothermal systems from various deposits.

KEYWORDS

Ernest Henry, Apatite, Calcite, U-Pb geochronology, IOCG, Trace Elements, Metasomatism.

TABLE OF CONTENTS

LIST OF FIGURS

LIST OF TABLES

1. INTRODUCTION

The Ernest Henry Iron Oxide Copper Gold (IOCG) deposit is located approximately 35Km NW of Cloncurry, NW Queensland (Figure 1) and represents the largest known deposit in the Proterozoic Eastern Succession of the Mount Isa Inlier, containing a total resource of 87.1Mt of ore at 1.18% Cu and 0.60 g/t of Au (Lilly, Case, & Miller, 2017). The four broad stages of alteration associated with this deposit include; regional Na-Ca alteration, pre-mineralization alteration, ore-stage mineralization and post-mineralization alteration (Mark, Oliver, and Williams, 2006). Economic mineralization consists of K-feldspar altered intermediate-volcanic clasts with a matrix consisting of magnetite, calcite, pyrite, biotite, barite, chalcopyrite and quartz with a range of accessory minerals that includes apatite (Mark et al., 2006). At depth, a weakly mineralized structure termed the Interlens separates the orebody into two distinct lenses (O'Brien, 2016). The discovery of this structure is recent, and therefore its presence has not been considered for current ore deposit models. This pre-mineralization structure commonly exhibits coarse grained apatite, brecciated by a mineralogy comparable to the ore grade assemblage (O'Brien, 2016). Previous research at Ernest Henry has constrained ages of regional Na-Ca alteration at 1529 +11/-8 Ma (Mark et al., 2006), biotite-magnetite alteration at 1514 ± 24Ma (Mark et al., 2006) and ore phase biotite at 1504 ± 3Ma (Twyerould, 1997). However, no dates have been established for either apatite or calcite from the deposit.

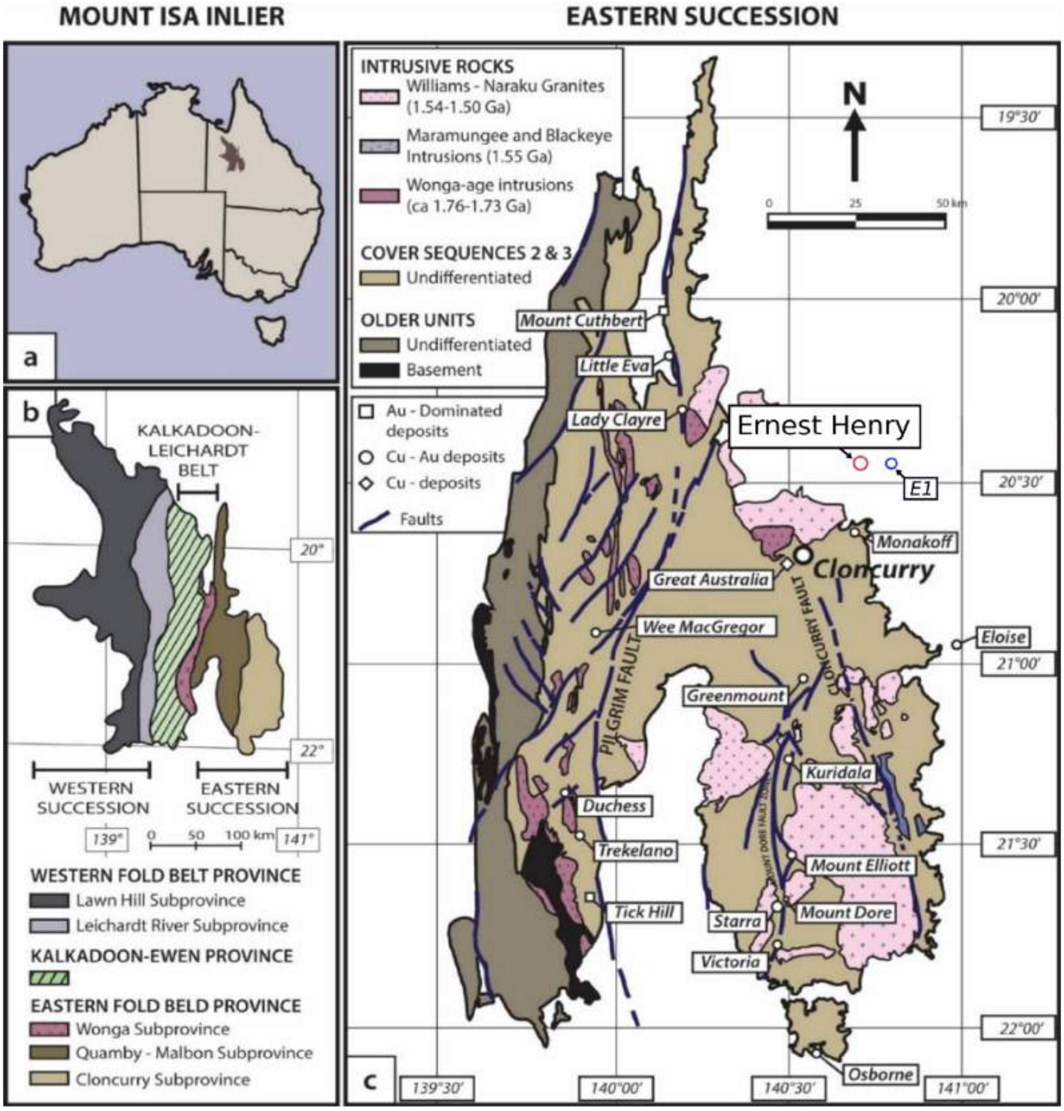

Figure 1: a) Location of the Mount Isa inlier in Australia. b) Sub-provinces of the Mount Isa inlier adapted from Hutton, Denaro, Dhnaram, and Derrick (2012). c) Simplified geological map of the Eastern Succession adapted from P. Williams (1998) with the Ernest Henry deposit shown in red and the nearby E1 deposit shown in blue.

Recent advances in U-Pb dating techniques allow for the in-situ dating of apatite and calcite via the laser ablation inductively coupled plasma mass spectrometry (LA-ICP-MS) method (Chew, Petrus, & Kamber, 2014; Roberts & Walker, 2016). This approach also provides the opportunity to examine the trace element composition of the minerals, which can be used to constrain the source of the minerals, and characterise metasomatic fluids (Debruyne, Hulsbosch, & Muchez, 2016; Harlov, 2015; Hughes & Rakovan, 2015).

The primary aim of this study is to constrain the age of apatite from the Interlens and the ore-stage breccia, and the age of calcite from the Interlens, the ore-stage breccia and later veins. This study will also use the REE composition of the various apatite and calcite samples to constrain their source, and to characterise metasomatic fluids.
This study will test the hypotheses:

- Apatite from the Ernest Henry deposit can be dated using the in-situ U-Pb LA-ICP-MS method.
- Calcite from the Ernest Henry deposit can be dated using the in-situ U-Pb LA-ICP-MS method.
- The trace element composition of apatite from the Ernest Henry deposit can be used to constrain its source, and characterise metasomatic fluids.
- The trace element composition of calcite from the Ernest Henry deposit can be used to constrain its source.

Testing the hypotheses above will add to our knowledge of the processes that formed the Ernest Henry orebody, assisting in the development of a more robust conceptual model of formation.

2. BACKGROUND GEOLOGY

2.1 Regional Geology

The Ernest Henry orebody is located in the Eastern Fold Belt of the Proterozoic Mount Isa Inlier, NW Queensland (Figure 1). Regional stratigraphy is divided into four major sequences; basement rocks, Cover Sequence 1, Cover Sequence 2 and Cover Sequence 3 (D. Foster & Austin, 2008; Mark et al., 2006). Economic mineralization is predominantly located proximal to the unconformable contact of Cover Sequence 2 and 3 (D. Foster & Austin, 2008). The Williams-Naraku Batholith intrudes these cover sequences, and consists of several I and A type granite plutons emplaced at 1750Ma and 1505Ma (D. Foster & Austin, 2008). Emplacement at 1505 Ma is synchronous with regional Na-Ca alteration, regional retrograde metamorphic conditions and D_3 deformation of the Isan Orogeny (Mark et al., 2006; Oliver et al., 2008).

2.2 Isan Orogeny

The Isan Orogeny is the youngest orogeny experienced by the Mount Isa Inlier, occurring synchronously with economic mineralization (Connors & Page, 1995). The Isan orogeny involved the shortening of a complex rift system from ~ 1610 to 1500 Ma and consisted of three deformation events (D_1, D_2 and D_3) (Giles, Ailléres, Jeffries, Betts, & Lister, 2006). D_1 was a N–S compressional event (~ 1610Ma), resulting in small scale E–W trending folds and thrusts (Page & Bell, 1986). D_2 was a W–E shortening event from 1595–1575 Ma, which correlates with regional peak metamorphic conditions and resulted in large scale N–S trending faults and folds (D Giles et al., 2006; Page & Sun, 1998). D_3 consisted of a W–E transpressional event from ~1532–1480Ma, resulting in the reactivation of D_2 faults and N–NE upright folding

(Betts et al., 2006; Connors & Page, 1995; Page & Bell, 1986). Regional metamorphic conditions were prograde during D_1, peak at D_2 and retrograde during D_3 (Sharib & Sanislav, 2013; Wyborn, 1998).

2.3 Deposit Geology

The Ernest Henry orebody is hosted in meta-andesitic rocks, interpreted as the temporal equivalent of the Mount Fort Constantine metavolcanics (∼1745Ma) (Mark et al., 2006). These host rocks are intercalated with metasedimentary units, which have been intruded by multiple fine- to medium-grained metadiorite dykes (Mark et al., 2006). The Ernest Henry orebody consists of a structurally controlled breccia with a pipe-like geometry, bound by two northeast trending shear zones termed the Hanging Wall Shear Zone (HWSZ) and Foot Wall Shear Zone (FWSZ) dipping at $\sim 45^{\circ}$ southeast (Twyerould, 1997) (Figure 2a). At depth, the orebody is divided into two distinct lenses separated by a package of strongly foliated (dominantly mafic) meta-volcanics and metasediments termed the Interlens (Figure 2a & 2b). This weakly mineralised structure predates Cu-Au mineralization and has a paragenesis comparable to the main orebody (Lilly et al., 2017; O'Brien, 2016).

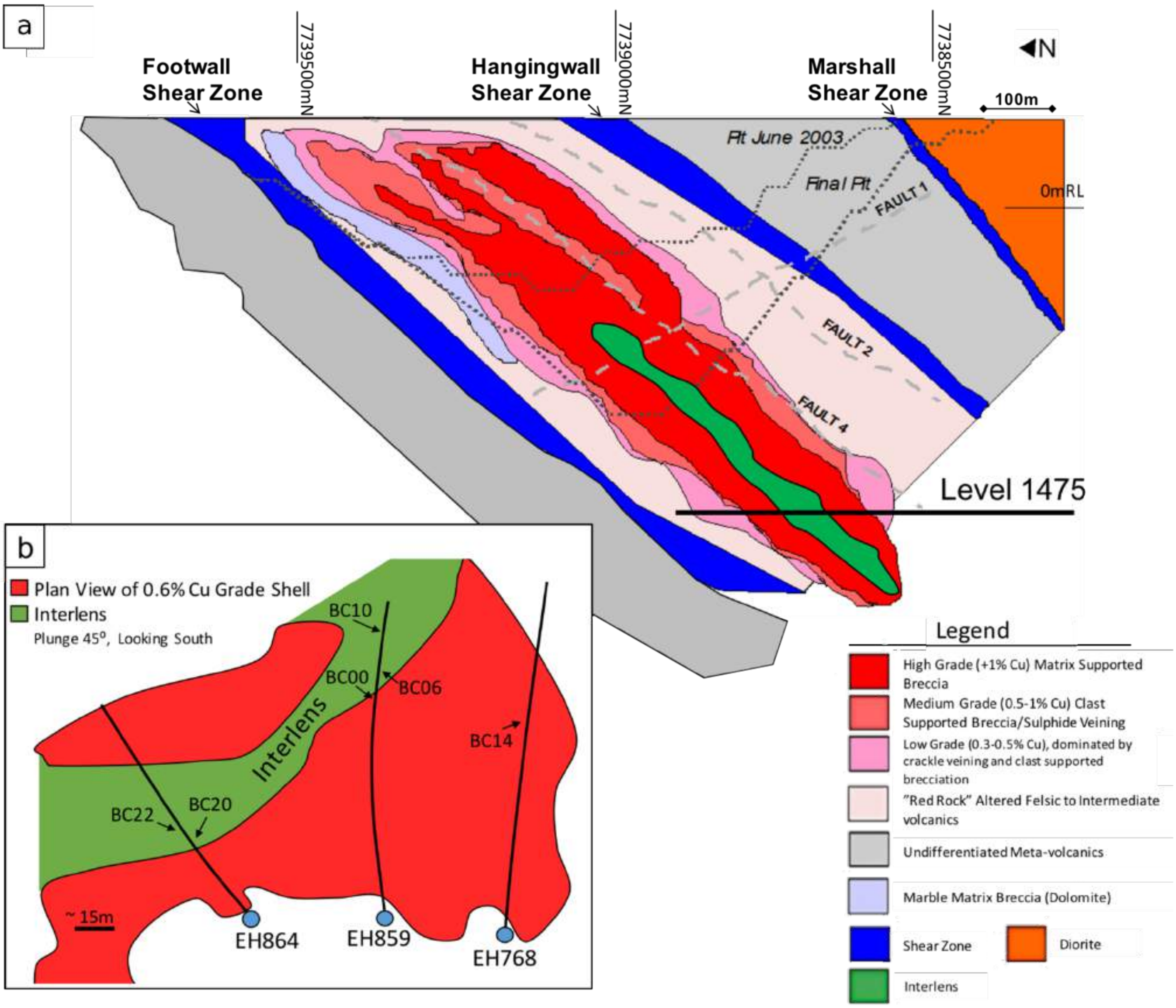

Figure 2: a) A cross section of the Ernest Henry orebody looking East, adapted from Lilly et al. (2017). b) Plan view of the 0.6% Cu grade shell and the Interlens at the 1475 level where samples used in this study were collected. This also shows the location of the main samples used in this study.

2.4 Alteration and Mineralization

The alteration and paragenesis of the Ernest Henry deposit (Figure 3) has been well documented by previous workers (Mark & Crookes, 1999; Mark et al., 2006; Twyerould, 1997), with seventeen individual stages of alteration described by Mark and Crookes (1999). However, several alteration stages are confined to minor areas of the orebody, resulting in a more conventional grouping of the four main alteration stages

(Mark et al., 2006). The extent of the alteration surrounding the Ernest Henry deposit is at least partly controlled by NE trending faults, proximal to local metadiorite intrusions (Mark et al., 2006). The four main stages of alteration are detailed below:

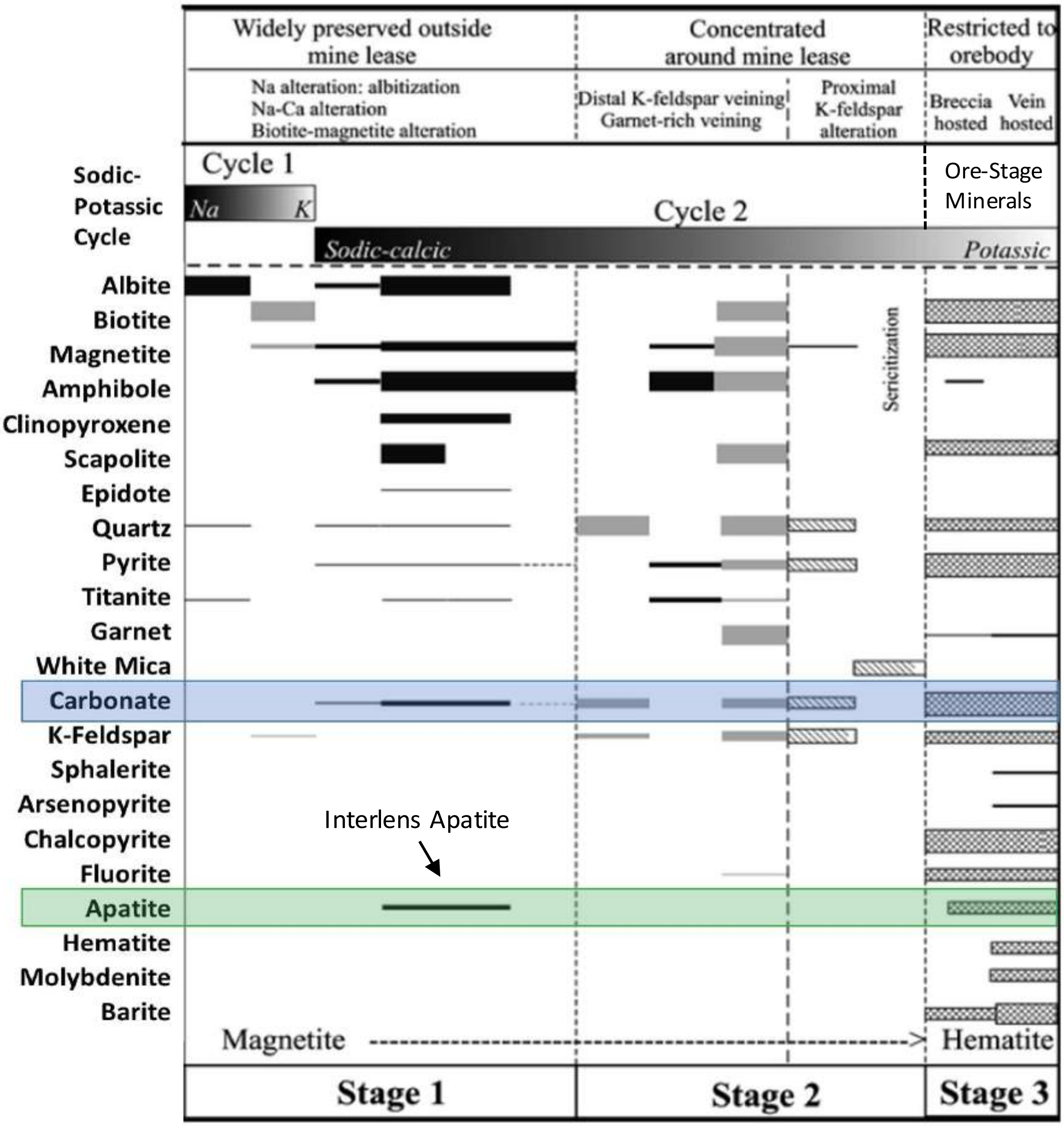

Figure 3: The paragenesis of the first three stages of Ernest Henry orebody from (Mark et al., 2006). The multiple generations of carbonate (blue) and apatite (green) are outlined.

1. REGIONAL SODIC-CALCIC ALTERATION

Regional sodic-calcic alteration describes a metasomatic event characterized by fine grained albitic-altered rocks found throughout the Eastern Fold Belt (Mark et al., 2006). This alteration formed is a result of relatively hot (400-500 °C) saline brines migrating along various fractures, faults and lithological contacts (Jong & Williams, 1995).

2. PRE-MINERALIZATION ALTERATION

A subsequent alteration style termed ‘pre-mineralization alteration’ displays similar chemical and mineralogical characteristics to the ore, with the exception of minor sulphides (Mark & Foster, 2000). This alteration type is divided into two groups. The first group is locally termed ‘dark rock’ alteration, and consists of fine grained biotite and magnetite rich alteration that overprints regionally altered rocks (Mark et al., 2006). The second group is termed ‘red rock’ alteration, and consists of garnet ± K-feldspar ± biotite ± pyrite bearing veins and alteration (Mark & Crookes, 1999).

3. ECONOMIC MINERALIZATION

Mineralization precipitated as a result of mixing between magmatic and sedimentary fluids, with the involvement of metamorphic volatiles (Kendrick, Mark, & Phillips, 2007). However, a combination of fluid mixing, wall rock interaction and changing pressure/temperature conditions are all factors that could have influenced ore deposition (Baker et al., 2008). The ore-grade assemblage consists predominantly of magnetite, calcite, pyrite, chalcopyrite and quartz with minor biotite, barite, specular hematite, K-feldspar and apatite. Copper mineralization is present as chalcopyrite, with gold mineralization occurring predominantly as native gold with minor electrum (A. Foster, Williams, & Ryan, 2007; Hewett, 2017).

4. POST MINERALIZATION ALTERATION

Post-mineralization alteration consists of carbonate-rich veins and breccia composed of medium-grained calcite, dolomite and quartz with fine grained barite, biotite, actinolite, pyrite, fluorite and magnetite (Mark & Foster, 2000). Calcite is the dominant mineral, typically recrystallized to fine or medium-grained assemblages (Mark & Foster, 2000).

2.5 Deposit Geochronology

Various studies have applied a range of geochronological techniques to the Ernest Henry deposit in an attempt to date the ore-stage mineralization and surrounding alteration. Twyerould (1997) used the ^{40}Ar / ^{39}Ar method to date early actinolite from actinolite-magnetite veining at 1610 ± 2 Ma and 1611 ± 4 Ma, ore-stage biotite at 1504 ± 3 Ma, post ore hydrothermal alteration biotite at 1514 ± 3 Ma, and actinolite from late ferroactinolite-magnetite veining at 1476 ± 3 Ma. Gauthier, Hall, Stein, and Schaltegger (2001) dated pre-ore hydrothermal alteration to 1595 ± 6 Ma via the ^{40}Ar / ^{39}Ar system, and ore-stage hornblende and biotite to 1595 ± 6 Ma and 1600 ± 6 Ma via the Re-Os system. Recently, Mark et al. (2006) used U-Pb titanite dating to constrain biotite magnetite alteration to 1514 ± 24 Ma and Na-Ca alteration to 1529 ± 11 Ma. The disagreement between geochronological data from the various studies highlights the complexity of the hydrothermal system, making it difficult to produce reliable and systematic ages for Cu-Au mineralization and the various stages of alteration.

2.6 Ernest Henry Apatite

Taylor (2017) and Mark et al. (2006) suggest at least three generations of apatite exist within the Ernest Henry Orebody; with a relatively early (first) generation existing within the host rocks of the Interlens, a second generation in the pre-mineralization alteration, and a third generation located in the ore-stage assemblage. Previous work illustrates that apatite in the Ernest Henry orebody possesses several stages of irregular concentric zoning, with the centre of the apatite grains relatively enriched in S (0.5 wt% SO_3) and the outer rims relatively enriched in As (up to 5 wt% As_2O_5) (Cleverley, 2006; Liu et al., 2017; Rusk et al., 2010). The U-Pb dating methodology used in this study is based upon Chew et al. (2014), with the apatite bearing samples sourced from the Interlens (representable of pre-mineralization alteration) (Figure 4a), and the ore-stage breccia (representable of ore-stage mineralization) (Figures 4b).

2.7 Ernest Henry Calcite

A recent study by Fuss (2014) classified the carbonate phases within the Ernest Henry orebody into two dominant stages. The first stage is associated with sulphide mineralization and thought to be sourced from metamorphic fluids (Fuss, 2014). The second stage is dominated by veining calcite with minimal sulphides, interpreted to be sourced from basinal fluids (Fuss, 2014). The U-Pb dating methodology used in this study is based upon a combination of methods used by Li, Parrish, Horstwood, and McArthur (2014) and Roberts and Walker (2016), with samples consisting of calcite from the Interlens (Figure 4a), the ore-stage breccia (Figure 4c), late veins (Figure 4c), and a calcite sample from the nearby E1 deposit (Figure 4d; see Figure 1 for the location of the E1 deposit).

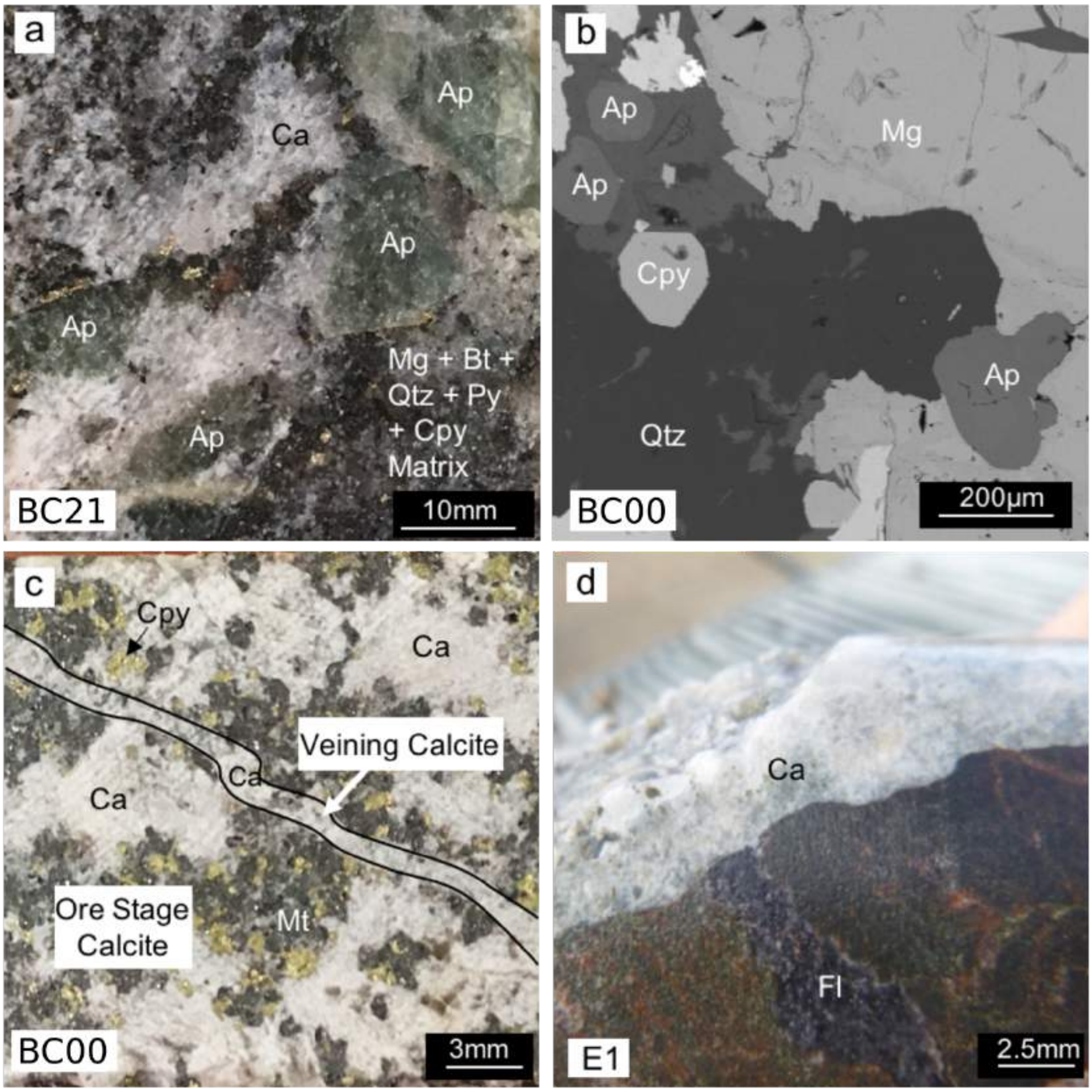

Figure 4: a) Typical coarse-grained apatite and calcite from the Interlens. b) Fine-grained apatite from the ore-stage assemblage. c) Depicts the textural relationship between the ore-stage calcite and veining calcite. c) Cross-cutting relationship between calcite and fluorite from E1 sample used in this study (see M. Williams, Holwell, Lilly, Case, and McDonald (2015) for details of fluorite paragenesis). (Sample numbers are located on the bottom left of the images).

3. METHODS

3.1 Sampling Procedure

Sampling was completed at the Ernest Henry Mine site during March 2017. Three drill cores (EH859, EH864 and EH768), representing typical sections through the orebody at level 1475 were made available for sampling (Figure 2b). The drill cores were logged for their rock types, alteration type and mineralogy (Appendix A). Areas of interest were flagged, cut into quarter core using a diamond saw and sent to Ingham Petrographics, resulting in 14 polished thin sections measuring 2cm x 3.5cm x 30µm thick. Sample descriptions and location details are available in Appendix B. A single additional sample was sourced from drill core from the E1 deposit (located 6km east of Ernest Henry) and used to compare calcite geochemistry.

3.2 Petrography

Petrography was completed at Adelaide Microscopy using an Olympus BX51 System Microscope with an attached DP21 Microscope digital camera.

3.3 Scanning Electron Microscope and Cathodoluminescence

Various samples were selected for Mineral Liberation Analysis (MLA) mapping on the Quanta SEM 600. Electron backscatter maps (EBS), and cathodoluminescence (CL) images were produced using specifications outlined in Table 1. To overcome phosphorescence during CL work, a method proposed by Reed and Milliken (2003) was used. This involved applying an external blue/UV filter to the machine, allowing wavelengths between 375-500nm to pass, resulting in clearer, and more distinguishable CL images.

Table 1: Parameters used for SEM and CL work during this study.

Method	EBS/MLA	CL
Samples	BC00, BC06, BC10, BC14, BC20, BC22	BC10, BC14, BC00, BC22, WC-1
Spot Size	7.2	7
Beam Energy	15Kv	15Kv
Working Distance	10mm	15mm
Minimum Grain Size	1µm	N/A

3.4 Laser Ablation Inductively Coupled Plasma Mass Spectrometry

During LA-ICP-MS work, apatite and calcite samples were grouped based on their sample number, location and CL reflectance (for apatite) (see Table 2). The specifications for LA-ICP-MS work completed on apatite and calcite samples are outlined in Table 3, with elemental acquisition parameters in Appendix C.

APATITE

Methods adapted from Chew et al. (2014) were utilised for LA-ICP-MS work with adjustments made to suit the equipment available at Adelaide Microscopy. Trace element analysis of apatite was performed simultaneously with the acquisition of isotopes for geochronology (eg ^{202}Hg, ^{204}Pb, ^{206}Pb, ^{207}Pb, ^{208}Pb, ^{232}Th and ^{238}U). Elemental mapping was also conducted on various apatite samples. Parameters that differed during the acquisition of elemental maps are displayed in blue on Table 3.

CALCITE

For geochronology, methods adapted from Roberts and Walker (2016) were used with adjustments made to suit the equipment available at Adelaide Microscopy. A separate run was conducted to examine the trace element composition of the calcite. Parameters that differed during the acquisition of trace element data is shown in red on Table 3.

Table 2: Details and nomenclature of apatite and calcite samples used in this study. This includes the names of the samples used in this study, the sample they are from and a brief description of their charachteristics.

Apatite Geochronology and Trace Element Analysis		
Name	Sample	Description
BC00	BC00	14 spots across 6 co-genetic apatite grains from apatite within ore-grade breccia. Spots are from intermediate zones within the apatite that show a similarly low CL reflectance.
BC10a	BC10	38 spots from co-genetic apatite grains from the Interlens which show a similarly high CL reflectance. This group is reflective of the core composition of the BC10 apatite.
BC10b	BC10	11 spots across apatite grains spatially associated with BC10a, however possess a significantly lower CL reflectance. Termed Ap2 in petrographic observations, this group reflects the composition of apatite rimming the BC10a group.
BC22a	BC22	15 spots across 2 co-genetic apatite grains from the Interlens which possess a similarly high CL value. (Same co-genetic grains used for all BC22 analysis.) This group represents the core composition of the BC22 samples.
BC22b	BC22	14 spots across zones from the 2 co-genetic apatite grains mentioned above, which display a comparatively intermediate CL reflectance (brighter than BC22c samples, darker than BC22a samples). This group represents an intermediate zone between the BC22a and BC22c samples.
BC22c	BC22	8 spots from a single grain in sample BC22 which possesses a comparatively lower reflectance under CL (darker than BC22b). This group represents the composition of apatite rimming the BC22 sample.
Calcite - Geochronology		
BC00CAL1	BC00	A 30 spot grid of data points within an ore-stage calcite grain
BC00CAL3	BC00	A 30 spot grid of data points from a calcite vein cross-cutting mineralization
BC00CAL4	BC00	A 30 spot grid of data points within an ore-stage calcite grain
BC00CAL5	BC00	A 30 spot grid of data points from a calcite vein cross-cutting mineralization
BC10CAL1	BC10	A 30 spot transect of data points along a coarse-grained calcite vein from the Interlens which is brecciating a coarse-grained apatite.
BC10CAL2	BC10	A 30 spot transect along a coarse-grained calcite vein from the Interlens which shows to be brecciating a coarse-grained apatite.
BC14CAL1	BC14	A 30 spot grid of data points from a calcite grain in the Interlens spatially associated with sulphide mineralization.
Calcite - Trace Element Analysis		
BC10	BC10	A 20 spot transect along a calcite vein from the Interlens brecciating a coarse-grained apatite.
ORE	BC00	20 spots across co-genetic ore stage calcite grains.
VEIN	BC00	A 20 spot transect along a calcite vein showing to cross-cutting ore-stage mineralization.
E1	RML	A 20 spot transect across co-genetic calcite grains from the nearby E1 deposit which shows to be cross-cutting fluorite and ore-stage mineralization.

Table 3: Parameters used during LA-ICP-MS work for apatite (left) and calcite (right). Parameters in black were used for geochronology work. Parameters in blue were used for constructing elemental maps of apatite and parameters in red were used for the trace element analysis of calcite.

ICP-MS		
	Apatite	Calcite
Brand and model	Agilent 7900x ICP-MS	Agilent 7900x ICP-MS
Forward power	1350W	1350W
Gas flow (L/min)		
Cool (Ar)	15	15
Auxiliary (Ar)	0.89	0.89
Carrier (He)	0.35	0.35
Sample (Ar)	1.06	1.06
Laser		
Type of laser	ArF Excimer	ArF Excimer
Brand and model	Resolution LR (Resonetics)	Resolution LR (Resonetics)
Laser wavelength	193nm	193nm
Pulse duration	20ns	20ns
Spot Size	29µm 7µm	110 µm
Laser Energy	40mJ 65mJ	75mJ
Repetition rate	5Hz 10Hz	10Hz
Energy attenuation	50% 100%	100%
Laser Fluence	2.8 J/cm^{-2} 3.5 J/cm^{-2}	~9.5 ~J/cm^{-2}
Laser warm up (background collection)	30s 10s	30s
Data Acquisition Parameters		
Data acquisition protocol	Time-resolved analysis	Time-resolved analysis
Cleaning method	Firing 5 pulses followed by washout Single blast along transect	Firing 5 pulses followed by washout
Scanned masses	24, 29, 31, 35, 43, 51, 55, 75, 88, 89, 90, 139, 140, 141, 146. 147, 153, 157, 159, 163, 165, 166, 169, 172, 175, 202, 204, 206, 207, 208, 232, 238	43, 202, 204, 206, 207, 208, 232, 238, 24, 29,43, 51, 55, 75, 88, 89, 90, 139, 140, 146. 147, 153, 157, 159, 163, 165, 166, 169, 172, 175
Detection mode	Pulse counting	Pulse counting
Detector Deadtime	3.68ns	3.68ns
Background collection	30s	30s
Ablation Time	30s Variable	30s
Washout	20s	20s
Settling Time	0.053s 0.089s	0.018s 0.053s
Ablation Sequence	2 x NIST610, 2 x Madagascar, 2 x McClure Mountain, 15 x Unknown 1 x NIST610, 10 x Unknown	2 x NIST614, 2 x NIST610, 4 x WC-1, 15 x Unkown. 2 x NIST612, 2 x NIST610, 15 x Unknown
Standardisation and Data Reduction		
Primary standard	Madagascar, NIST610	WC-1, NIST610
Secondary standard	McClure Mountain, NIST610	NIST-614, NIST-610, JS
Data reduction software	Iolite, In House Excel	Iolite, In House Excel

3.5 Data Reduction

GEOCHRONOLOGY

The Iolite software package (Paton, Hellstrom, Paul, Woodhead, & Hergt, 2011) was used to correct for instrumental drift and downhole fractionation using the VizualAge_UcomPbine data reduction scheme (DRS) (Chew et al., 2014) for apatite and the U-Pb_Geochronology DRS (Paton et al., 2011) for calcite. Isoplot (Ludwig, 2003) was used to construct Tera-Wasserburg plots for apatite and calcite, and to produce a ^{207}Pb corrected $^{238}U/^{206}Pb$ weighted mean age plot for apatite.

For apatite, this study follows procedures outlined in Chew et al. (2014). Corrections for common Pb were made by calculating a best-fit common Pb line through the data in a Tera-Wasserburg plot. The upper-intercept of this common Pb line with the concordia estimates the initial common Pb in the system ($^{207}Pb/^{206}Pb$ ratio), to which the unknown samples are corrected to produce a ^{207}Pb corrected $^{238}U/^{206}Pb$ weighted mean age, interpreted as the best estimate of the U-Pb cooling/formation age (Chew et al., 2014). Madagascar apatite (U-Pb TIMS 473.5 ± 0.7 Ma; (Chew et al., 2014)) was used as a primary standard and the McClure Mountain apatite (U-Pb TIMS 523.51 ± 1.47 Ma; (Schoene, Crowley, Condon, Schmitz, & Bowring, 2006)) was used as a secondary standard to perform accuracy checks. Data containing concentrations less than 0.5ppm of ^{238}U, or possessed an abnormally large ^{206}Pb concentrations were not utilised for age calculation as they often plotted outside concordant space.

For calcite, NIST614 was used as a primary standard and NIST610, WC-1 (U-Pb TIMS 251 ± 2 Ma; (Li et al., 2014)) and calcite with a known stratigraphic age (calcite from the late Silurian section in the Prague Basin ~ 424 Ma; (Farkaš, Frýda, & Holmden, 2016)) used as secondary standards. As the NIST614 glass is not a matrix matched standard, and the $^{206}Pb/^{238}U$ ratio of the glass is not known precisely enough for this application, it is important to first normalise the LA-ICP-MS data to the NIST614 glass, then compare the measured $^{238}U/^{206}Pb$ ratio of the WC-1 standard to its measured TIMS ratio of 0.045 (Li et al., 2014). The difference between the measured $^{238}U/^{206}Pb$ ratio and the known value is then used to correct the final $^{206}Pb/^{238}U$ ratio. The measured $^{207}Pb/^{206}Pb$ ratio of the WC-1 standard is also compared to its known ratio of 0.83 ± 0.01, with the difference between the measured values and the known value used to produce a correction factor that is applied to the unknown samples (Li et al., 2014).

TRACE ELEMENTS

Elemental maps of the apatite were produced in Iolite software (Paton et al., 2011) using the Trace_Element DRS (Paton et al., 2011). The trace element composition of apatite and calcite were calculated using the Trace Element_IS DRS (Paton et al., 2011), with an internal standard value of 39.36 wt% Ca in apatite and 40.04 wt% Ca in calcite.

4 OBSERVATIONS AND RESULTS

4.1 Apatite and Calcite Petrography and Mineral Liberation Analysis (MLA)

Apatite from the ore-stage mineralization is generally small (~200µm) and has no preferential mineralogical associations with regards to its distribution, commonly located adjacent to calcite, pyrite, quartz, chalcopyrite, magnetite and hematite (Figure 5a). Apatite from the Interlens is often coarse (up to cm scale) and brecciated by calcite, quartz, pyrite, chalcopyrite, magnetite, hematite and biotite; a mineralogy comparable to the ore-stage assemblage (Figure 5b). Smaller (~100µm) grains of rounded apatite are also found within this matrix, usually located proximal to the boundary of coarse-grained apatite, or within fractures of coarse-grained apatite (Figure 5c). In many cases, a reaction front is visible between apatite and calcite grains, exhibiting high order interference colours. Samples from the Interlens also display several textures. For example, sample BC10 contains coarse-grained euhedral apatite mildly brecciated by a finer grained groundmass (Figure 5d), whist sample BC22 contains a much larger proportion of groundmass with smaller and less brecciated apatite (Figure 5e).

Ore-stage calcite co-exists with chalcopyrite, pyrite, magnetite, hematite and quartz, and is shown to be cross-cut by later, calcite dominated veins (Figure 5f). Calcite from the Interlens is often medium- to fine-grained and found within the groundmass of the samples, with coarser-grained calcite usually located proximal to coarse-grained apatite (Figure 5d). Calcite from the E1 deposit is coarse-grained (cm scale) and cross-cuts fluorite veins and economic mineralization. Additional petrography is located in Appendix D.

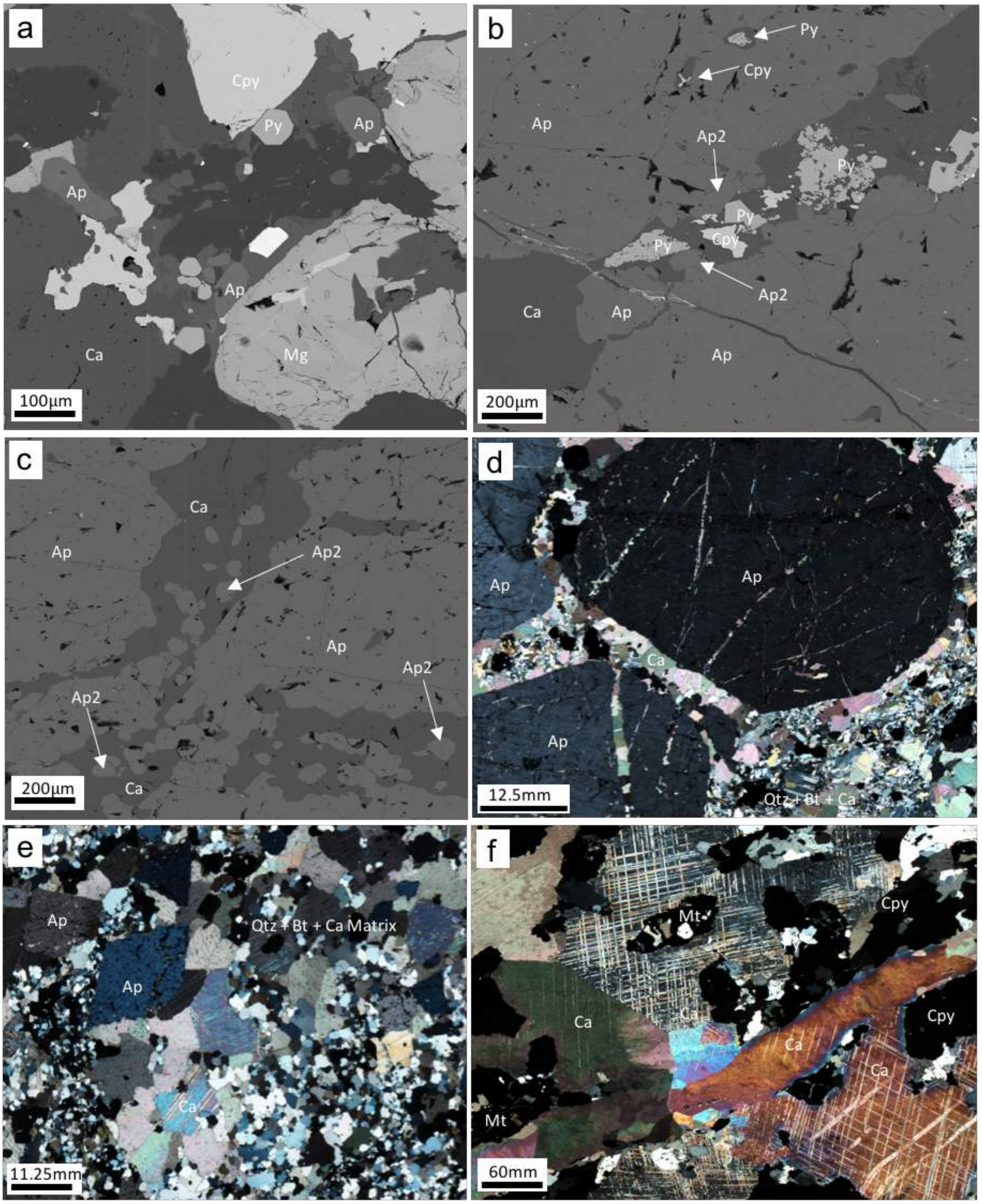

Figure 5: a) Distribution of small-grained apatite in sample BC00. b) Coarse grained apatite brecciated by a mineralogy of calcite, chalcopyrite and pyrite. c) Shows Ap2 in calcite surrounding coarse-grained apatite. d) Shows a texture from the Interlens consisting of coarse-grained apatite mildly brecciated by a mineralogy of qtz, ca, bt, py, cpy. e) Shows a highly brecciated sample from the Interlens consisting of smaller fragmented apatite grains in a groundmass of qtz, ca, bt, py and cpy. f) An xpl image depicting the textural relationship between the calcite generations present in sample BC00. Note a similar interference colour and a similar orientation of twinning planes between the two calcite generations.

4.2 Cathodoluminescence (CL)

CL work revealed multiple stages of concentric and irregular zonation in apatite. Fine-grained apatite from the ore-stage assemblage (sample BC00) consistently possess light cores surrounded by darker intermediate zone and a bright rim (Figure 6 a,b,c). Coarse grained apatite from the Interlens display a relatively consistent internal reflectance (BC10a), with dark irregular zonation on the outer rims of large brecciated grains (BC10b) (Figure 6d). Some medium sized apatite (~500µm) from the Interlens display varying degrees of CL reflectance across the length of the grain (BC22a, b, c) (Figure 6e). CL of calcite samples proved unsuccessful, perhaps the result of large Fe^{2+} concentrations, considered to quench luminescence dramatically (Machel & Burton, 1991). CL and SEM studies on the WC-1 calcite standard show no zonation. However, inclusions of celestite, dolomite and fluorite were observed (Figure 6f).

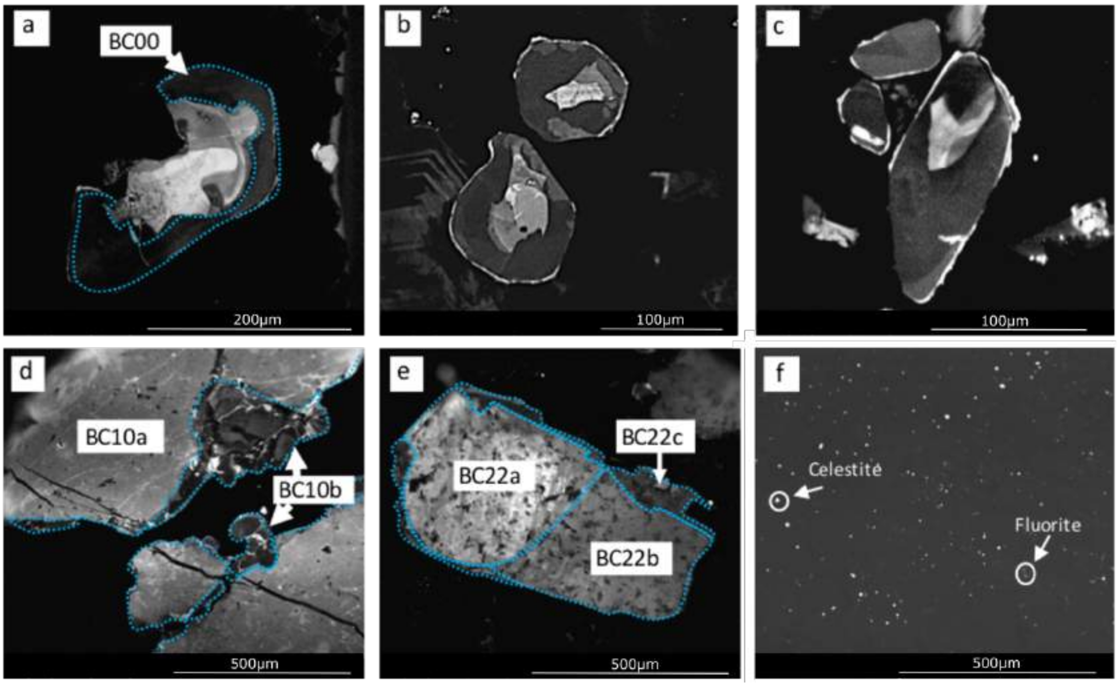

Figure 6: a, b & c) CL images of apatite from the BC00 sample showing a bright core consistently surrounded by a dark intermediate zone and a light rim. d) A grain from sample BC10 showing the BC10a (light) and BC10b (dark) zones. The BC10b CL reflectance is consistent with the Ap2 generation of apatite made in petrographic observations (see section 4.1). e) A grain from sample BC22 showing a gradient from high (BC22a) to low (BC22c) CL reflectance. f) The WC-1 calcite standard showing celestite and fluorite inclusions.

4.3 Apatite Geochronologyy

The ^{206}Pb and ^{238}U concentrations, $^{238}U/^{206}Pb$ and $^{207}Pb/^{206}Pb$ ratios and error correlations, along with the ^{207}Pb corrected age and 2σ propagated errors associated with each analysis are available in Appendix E.

STANDARDS AND ACCURACY

The Madagascar apatite standard produced a concordant age of 473.6 ± 3.4 Ma, whilst the McClure Mountain standard produced a ^{207}Pb corrected $^{238}U/^{206}Pb$ weighted mean age of 520.9 ± 6.1 Ma (Figure 7 a & b). These ages agree with the published Madagascar age of 473.5 ± 0.7 Ma (Chew et al., 2014) and the published McClure Mountain age of 523.51 ± 1.47 Ma (Schoene et al., 2006), suggesting acceptably high accuracy for the obtained U-Pb apatite ages presented in this study.

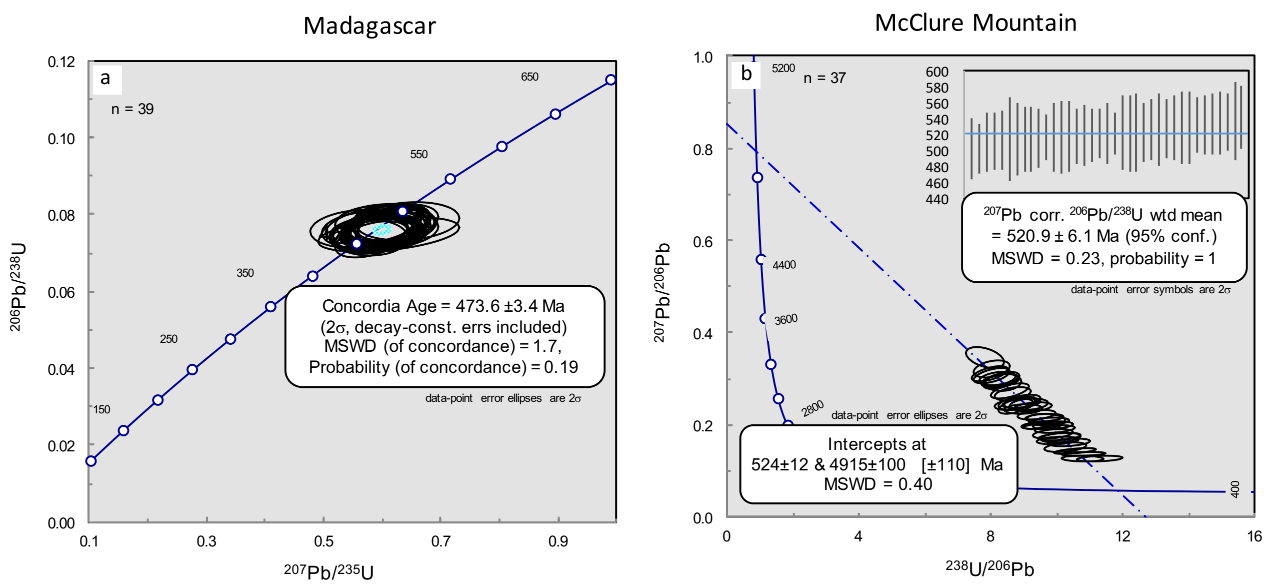

Figure 7: a) Concordia plot of the Madagascar primary standard. b) A Tera-Wasserburg plot and the corresponding ^{207}Pb corrected $^{238}U/^{206}Pb$ weighted mean age plot of the McClure Mountain secondary standard. Ellipses represent the 2σ error associated with each measurement and n = sample population used for age calculation.

APATITE SAMPLES

BC10a: A ^{207}Pb corrected $^{206}Pb/^{238}U$ weighted mean age of 1581 ± 16 Ma (MSWD = 1.3; Probability = 0.058) was produced for this sample (Figure 8a). This age has a high precision due to a large sample population (n = 61) and variable ^{238}U (1.0 −7.8ppm) and ^{206}Pb (2.2 − 5.8ppm), producing a relatively well-resolved common Pb line with a $^{207}Pb/^{206}Pb$ ratio of 0.65.

BC10b: A ^{207}Pb corrected $^{206}Pb/^{238}U$ weighted mean age of 1572 ± 40 Ma (MSWD = 0.14; Probability = 0.999) was produced for this sample (Figure 8b). ^{238}U concentrations ranged from 0.64 − 4.7ppm and ^{206}Pb ranged from 1.6 − 8.1ppm. As the common Pb line appears to be well resolved with a $^{207}Pb/^{206}Pb$ ratio of 0.77, the large error in the age calculation is likely due to the small sample population (n = 11).

BC22a: A ^{207}Pb corrected $^{206}Pb/^{238}U$ weighted mean age of 1557 ± 23 Ma (MSWD = 3.1; Probability = 1.4) was produced from this sample (Figure 8c). ^{238}U concentrations ranged from 4.3 − 7.91ppm and ^{206}Pb from 7.2 −12.7ppm. The Tera-Wasserburg plot depicts highly variable data possessing large errors and a relatively low $^{207}Pb/^{206}Pb$ ratio of 0.55.

BC22b: A ^{207}Pb corrected $^{206}Pb/^{238}U$ weighted mean age of 1564 ± 56 Ma (MSWD = 2.9; Probability = 0.001) was produced from this sample (Figure 8d). ^{238}U concentrations ranged from 0.766 − 5.58ppm and ^{206}Pb concentrations ranged from 0.65 − 7.5ppm. This sample displays a highly variable Tera-Wasserburg plot possessing large errors, possibly affecting the placement of the common Pb line, which produced a $^{207}Pb/^{206}Pb$ ratio of 0.66.

BC22c: No meaningful age could be extracted from the data from this sample due to the low concentration of ^{238}U (>1ppm) and the high amount of common Pb. When the few (n=8) analyses that could be performed on this sample are plotted in Tera-Wasserburg space, they are all reversely discordant and do not produce a linear array that intercepts the concordia (Figure 8e).

BC00: This group produced a ^{207}Pb corrected $^{206}Pb/^{238}U$ weighted mean age of 1529 ± 39 Ma (MSWD = 0.95; Probability = 0.5) (Figure 8f). The error associated with this age is likely due to the low concentrations of ^{238}U (0.7 − 3.5ppm) and the small quantity of data (n=14). It should also be noted that the $^{207}Pb/^{206}Pb$ intercept is relatively low (0.51), which would affect the final ^{207}Pb corrected $^{238}U/^{206}Pb$ weighted mean age.

As the 2σ propagated errors associated with each age calculation in this study overlap, the ages produced from the samples are within error of one another, and therefore are not statistically significant from each another.

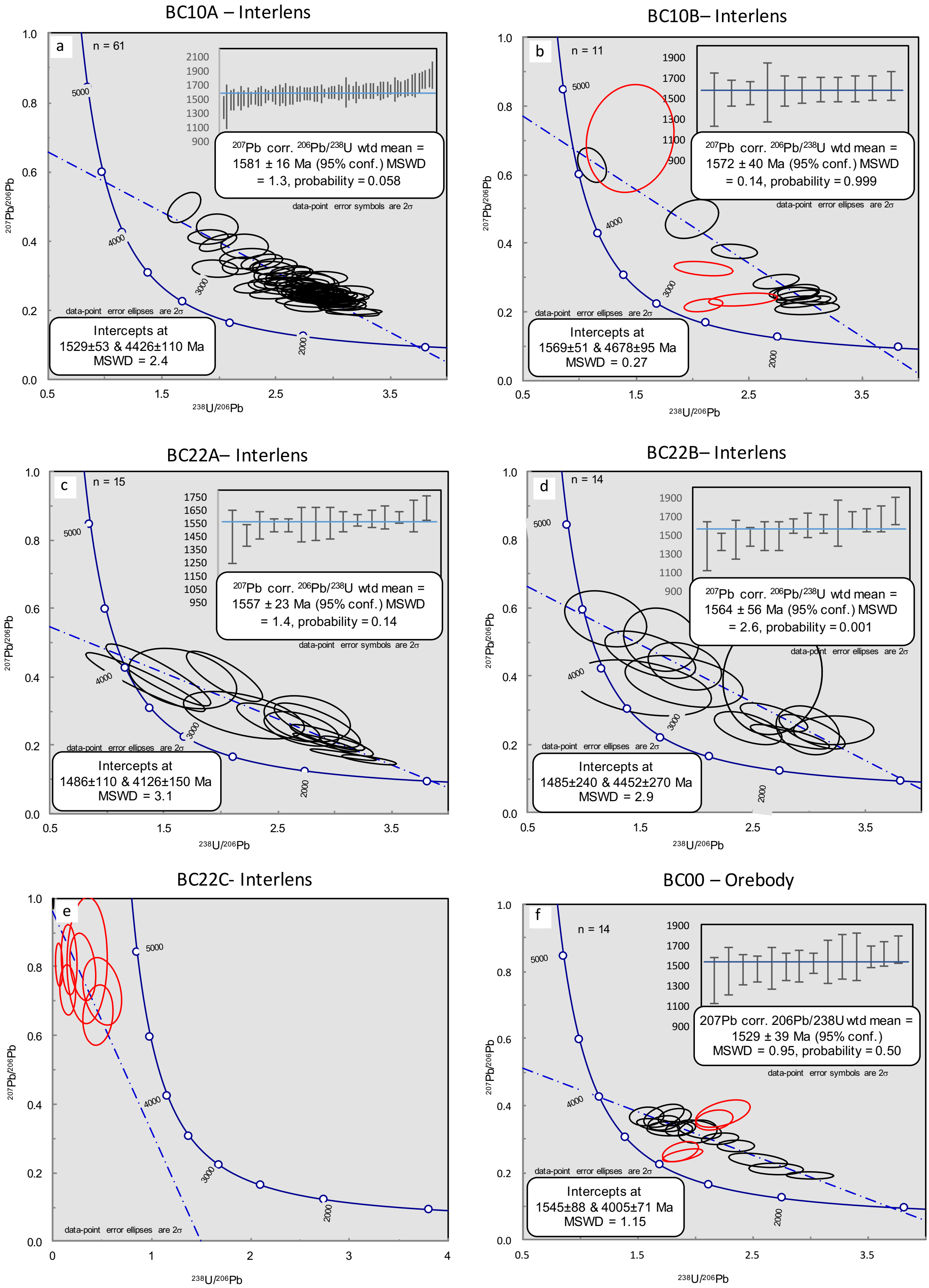

Figure 8: Tera-Wasserburg plots and corresponding ^{207}Pb corrected ^{238}U/^{206}Pb weighted mean ages for apatite samples: a) BC10a. b) BC10b. c) BC22a. d) BC22b. e) BC22c. f) BC00. Ellipses represent the 2σ error associated with each measurement. The line represents the best fit used to calculate the common lead line. n = the sample population used for age calculation. Red ellipses represent data considered to be outliers that do not fall onto the linear array, and were not used for age calculation.

4.4 Calcite Geochronology

The ^{206}Pb and ^{238}U concentrations, $^{238}U/^{206}Pb$ and $^{207}Pb/^{206}Pb$ ratios and error correlations, along with the corrected $^{238}U/^{206}Pb$ and $^{207}Pb/^{206}Pb$ ratios and 2σ propagated errors associated with each analysis are available in Appendix F.

STANDARDS AND ACCURACY

The WC-1 and Prague Basin standards were successfully dated to within error of their known age (Figure 9a & b), suggesting a viable dating method for future studies. The WC-1 standard produced an uncorrected age of 271.9 ± 8.5 Ma (MSWD = 0.46), compared to the published values of 251 ± 2 Ma (Li et al., 2014) and 254 ± 7 Ma (Roberts & Walker, 2016). The Prague Basin standard produced an uncorrected intercept age of 417 ± 47 Ma, relatively close to the known stratigraphic age of ~ 424 Ma (Farkaš et al., 2016). When the correction method described by Li et al. (2014) is used, the WC-1 standard produced an age of 257.6 ± 7.3 Ma (Figure 9c) and the Prague Basin produced an age of 428 ± 14 Ma (Figure 9d). It should also be noted that the resulting $^{207}Pb/^{206}Pb$ intercept of theWC-1 standard was 0.87, compared to the known TIMS ratio of 0.83 ± 0.01 (Li et al., 2014), producing a $^{207}Pb/^{206}Pb$ correction factor of 0.94. The average $^{206}Pb/^{238}U$ ratio of the WC-1 standard was measured at 0.046, analogous to the known ratio of 0.045 (Li et al., 2014), resulting in a correction factor of 0.98.

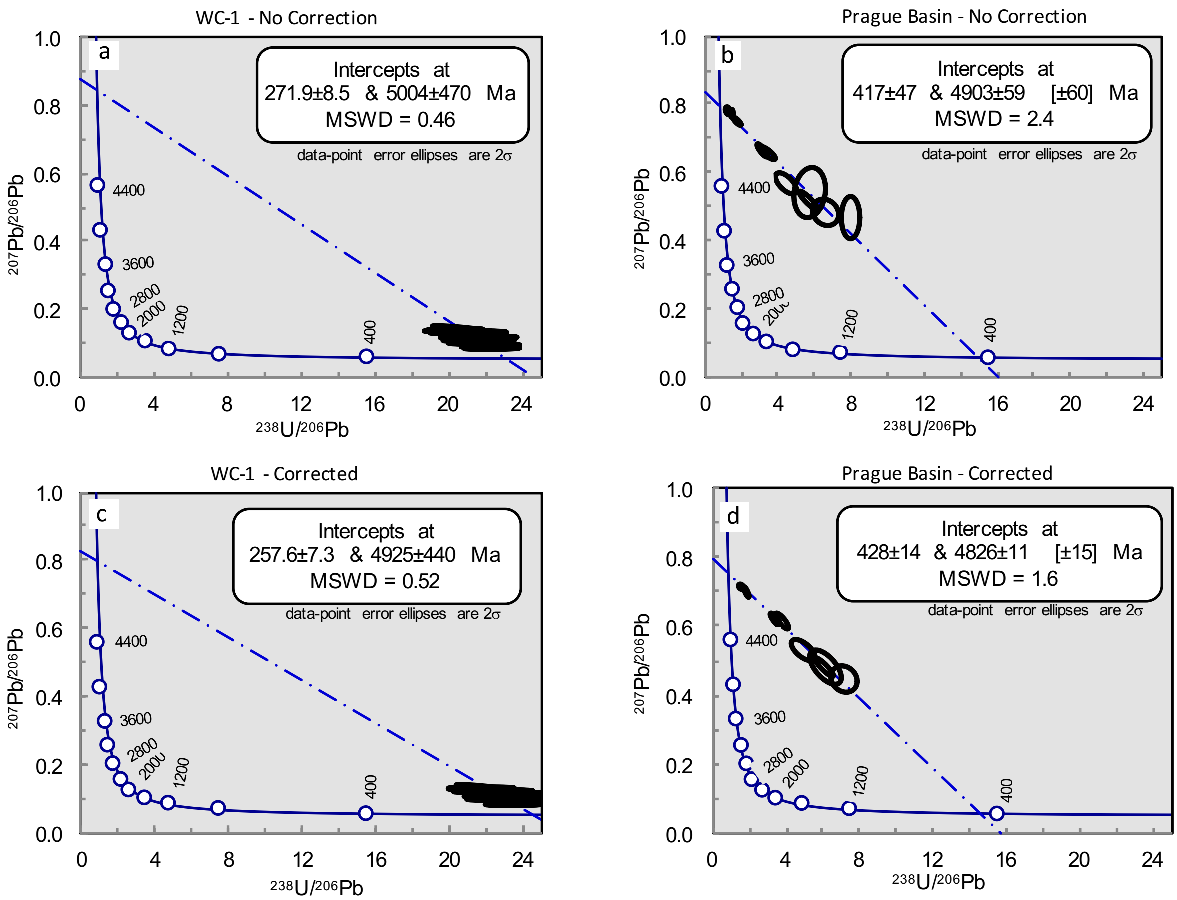

Figure 9: Tera-Wasserburg plots showing the uncorrected age calculation of the (a) WC-1 and (b) Prague Basin secondary standards. Using the correction method based on Li et al (2014), the $^{207}Pb/^{206}Pb$ ratio was corrected by a factor of 0.94 and the $^{206}Pb/^{238}U$ ratio was corrected by a factor of 0.98, which was used to calculate the final $^{238}U/^{206}Pb$ ratio and the corrected age for the (c) WC-1 and (d) Prague Basin standards. Ellipses represent the 2σ error associated with each measurement and n = the sample population used for age calculation

UNKNOWN SAMPLES

U-Pb dating was attempted on 7 grains from multiple samples (Figure 10 a to g). Unfortunately, because of low ^{238}U concentrations (0.3-0.45ppm) and relatively high ^{206}Pb concentrations (3.2-11.8ppm), the dating was unsuccessful on every sample, and therefore was not pursued any further in this study.

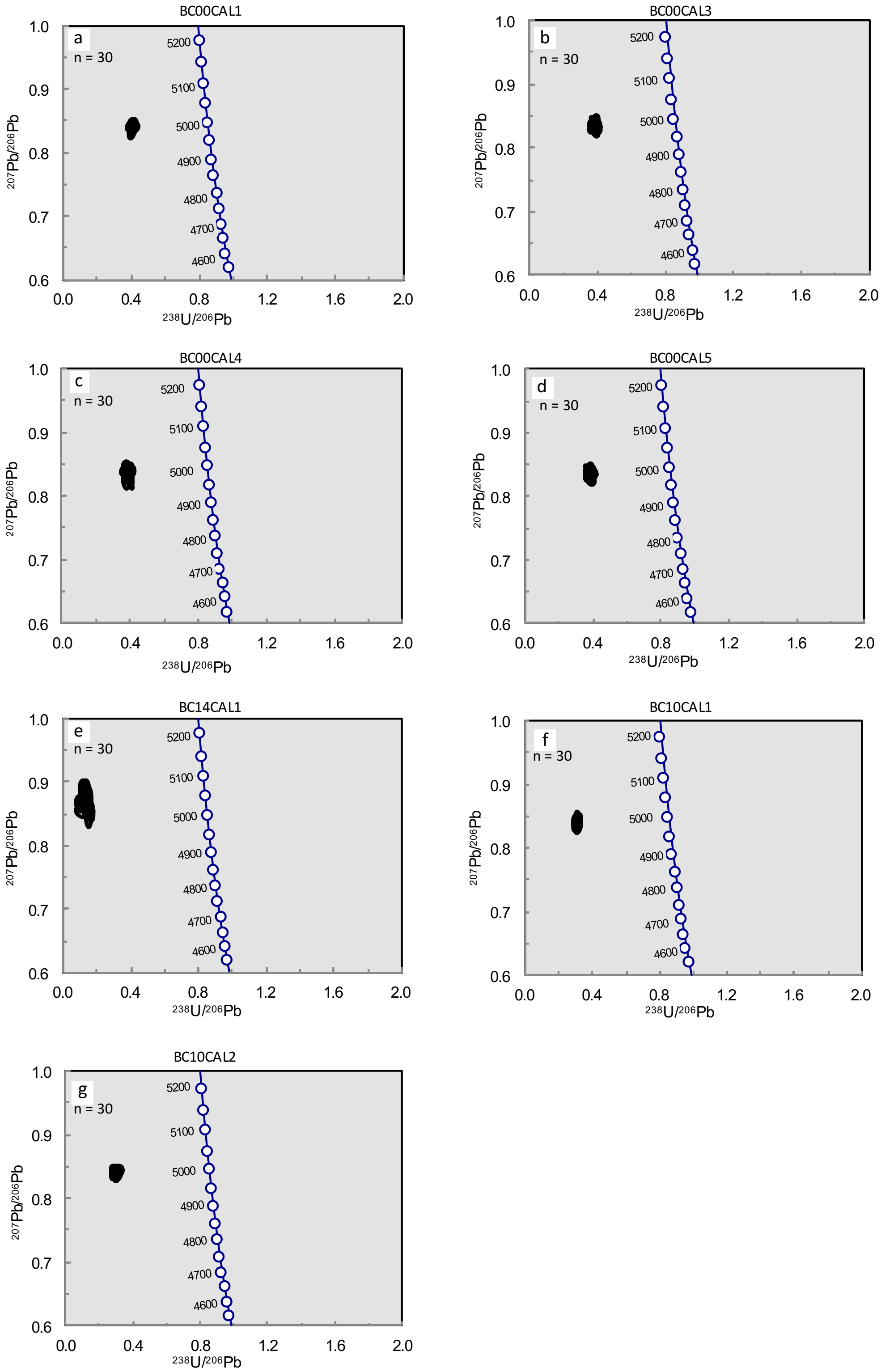

Figure 10: Tera-Wasserburg concordia plots displaying the result of geochronology attempted on calcite samples a) BC00CAL1. b) BC00CAL3. c) BC00CAL4. d) BC00CAL5. e) BC14CAL1. f) BC10CAL1. g) BC10CAL2. Ellipses represent the 2σ error associated with each measurement and n = the sample population.

4.5 Apatite Trace Elements

DISCRIMINATION PLOTS

Apatite data from this study was plotted on geochemical discrimination diagrams using fields from Belousova et al. (2002), the only published apatite trace element data from the Eastern Succession. Figure 11 shows the samples from this study plotting within the granitoid/carbonatite field on the Eu/Eu* vs Y discrimination diagram. This is replicated in Figure 12, where the samples predominantly plot within the granitoid field on the Y vs Sr discrimination diagram.

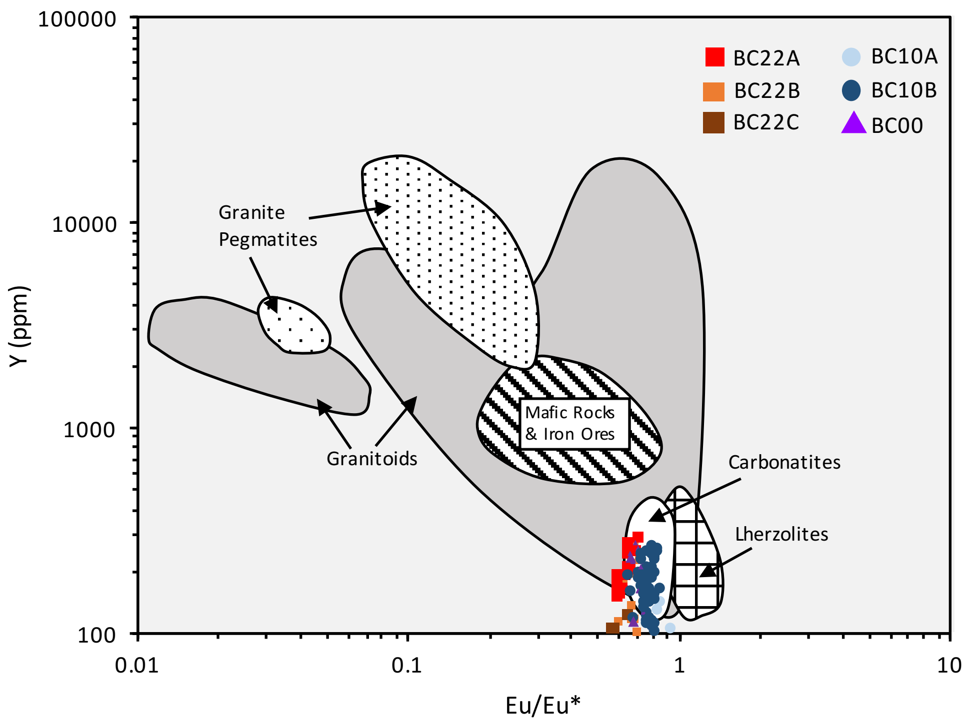

Figure 11: A Eu/Eu* vs Y(ppm) discrimination diagram with corresponding fields from Belousova et al. (2002). Eu* = Average of the chondrite-normalised Sm and Gd concentrations and E = chondrite-normalised Eu value. This plot shows no discrimination between apatite samples with the majority plotting within the carbonatite/granitoid fields.

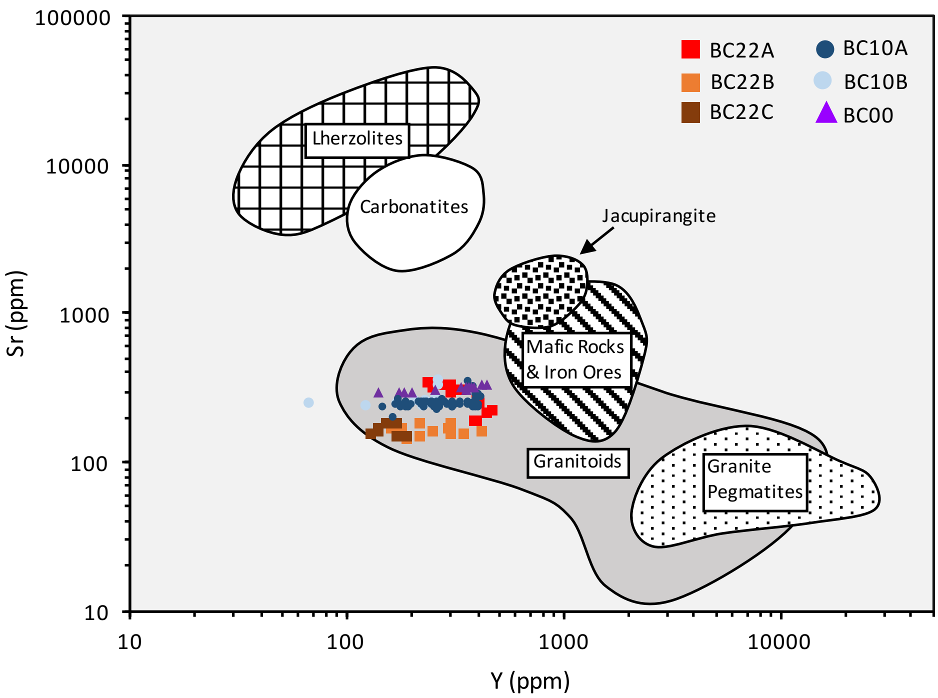

Figure 12: Y(ppm) vs Sr (ppm) discrimination diagram with corresponding fields from Belousova, Griffin, O'Reilly, and Fisher (2002). This plot shows no discrimination between apatite samples with the majority plotting within the granitoid field.

ELEMENTAL MAPS

The elemental maps produced in this study display elemental zonation consistent with the zonation observed in CL images. Elemental maps of apatite from the BC00 sample are comparable (Figure 13 a & b), and depict relatively high levels of enrichment (up to 3.5 wt%) in As located on the intermediate to outer rim of the grain. In the same location, these samples are also relatively enriched in the elements Y, La, Ce, Pr, Nd, Sm, Eu, Gd, Tb, Dy, Ho, Er, Tm, Yb, and Lu, with the core of the grains relatively enriched in ^{238}U and ^{206}Pb. Apatite from the Interlens (Figure 13c) also display a relative enrichment of As on the rim of the grain. However, possesses a relative enrichment of Y, La, Ce, Pr, Nd, Sm, Eu, Gd, Tb, Dy, Ho, Er, Tm, Yb, Lu, ^{206}Pb and ^{238}U in the core of the grain. These maps indicate that the enrichment of REE's differ between apatite from the ore-stage assemblage and apatite from the Interlens.

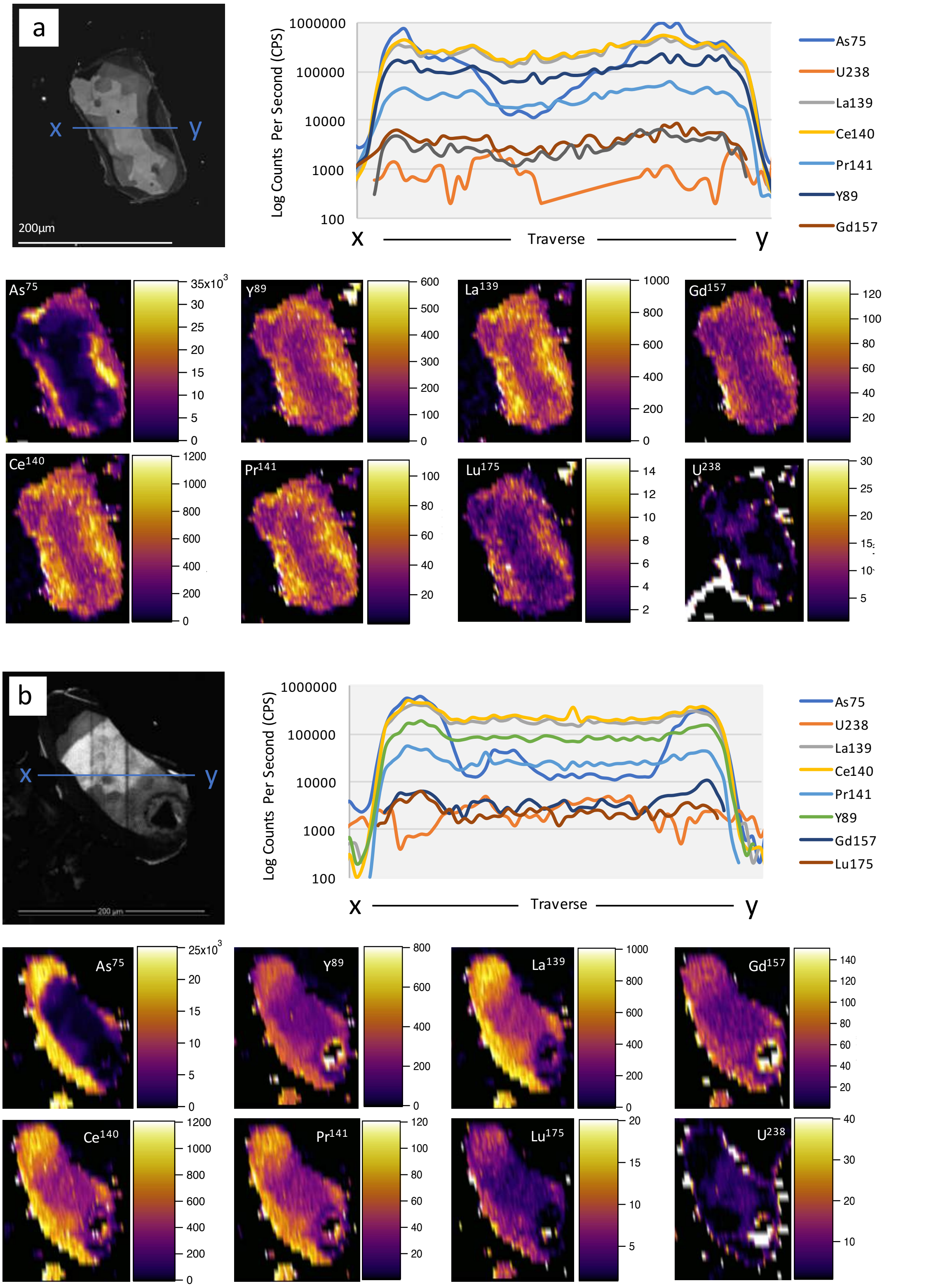
a
200μm
x
y
1000000
100000
10000
1000
100
Log Counts Per Second (CPS)
Traverse
As75
U238
La139
Ce140
Pr141
Y89
Gd157
As75
Y89
La139
Gd157
Ce140
Pr141
Lu175
U238
35x10^3
b
200 μm
Lu175
25x10^3

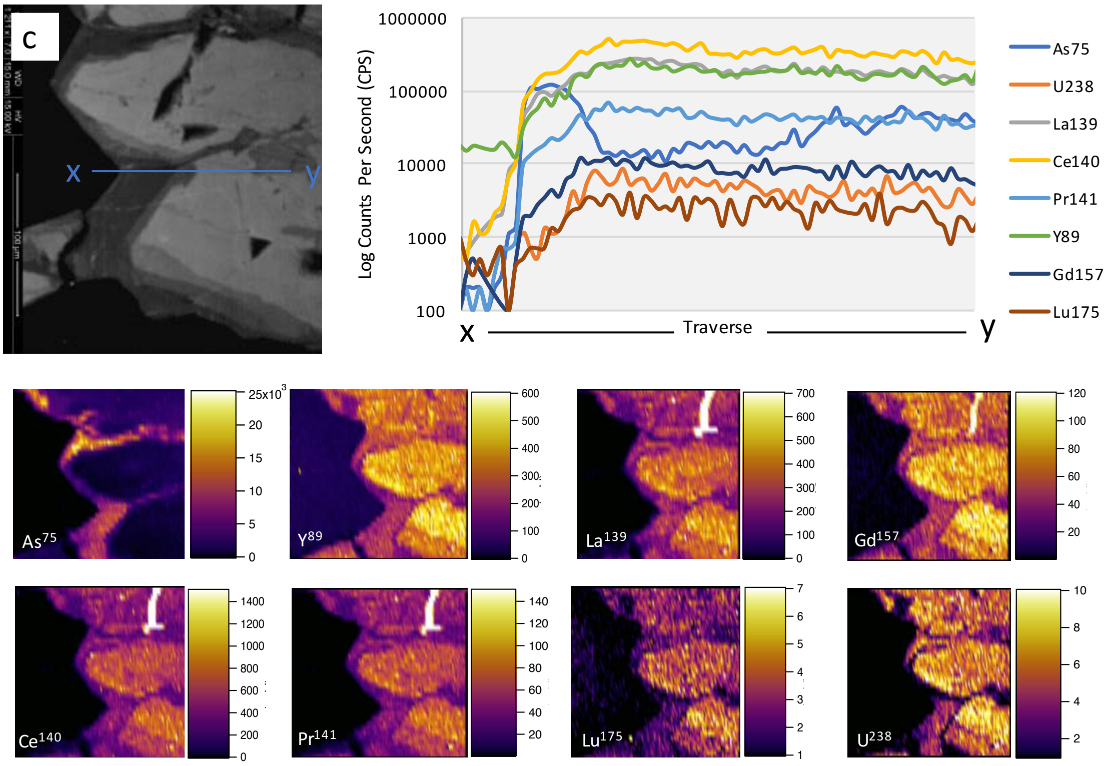

Figure 13: a & b) Trace element maps of apatite showing the distribution of As, Y, La, Gd, Ce, Pr, Lu & ^{238}U in grains from the BC00 (ore-stage) samples and c) BC10 (Interlens). All concentrations are in ppm unless otherwise specified. Images in the top left corner depict CL images of the sample, whilst the graph in the top right represents the abundance of the elements (CPS) across the transect from x to y. These images show that the zonation of various elements in the ore-stage apatite are not consistent with zonation present in apatite from the Interlens. However, the zonation of trace elements are consistant the zonation seen in CL images.

Elemental maps of Mg, Si, P, Cl, V, Mn, Si, Zr, Nd, Sm, Eu, Tb, Dy, Ho, Er, Tm, Yb, ^{204}Pb, ^{206}Pb, ^{207}Pb, ^{208}Pb and ^{232}Th are located in Appendix G.

CHONDRITE-NORMALIZED REE PLOTS

Chondrite-normalized REE plots of apatite show the REE concentrations vary across samples (Figure 14). The BC22 sample (Figure 14a) displays a large range in LREE's, with concentrations decreasing in order of BC22a (core) to BC22c (rim). This is accompanied by a decrease in the overall REE concentration from the core to the rim of the grain. Samples BC10a and BC10b possess broadly similar REE profiles, although

BC10b contains on average a lower concentration of REE's. The BC10 samples are both enriched in LREE relative to the MREE and HREE, and enriched in MREE relative to HREE. This is in contrast to the BC22 samples, where the cores are relatively enriched in LREE's and the rims are relatively enriched in MREE's. BC00 (Figure 14c) has a broadly similar trend of LREE enrichment to the BC10a, BC10b and BC22a samples, however is flat through the MREE and HREE's, with a slight enrichment in the HREE's Tm, Yb and Lu. In general, the apatites analysed in this study are enriched in LREE relative to HREE's, with the exception of the BC22b and BC22c samples, which are flat to slightly enriched in MREE's.

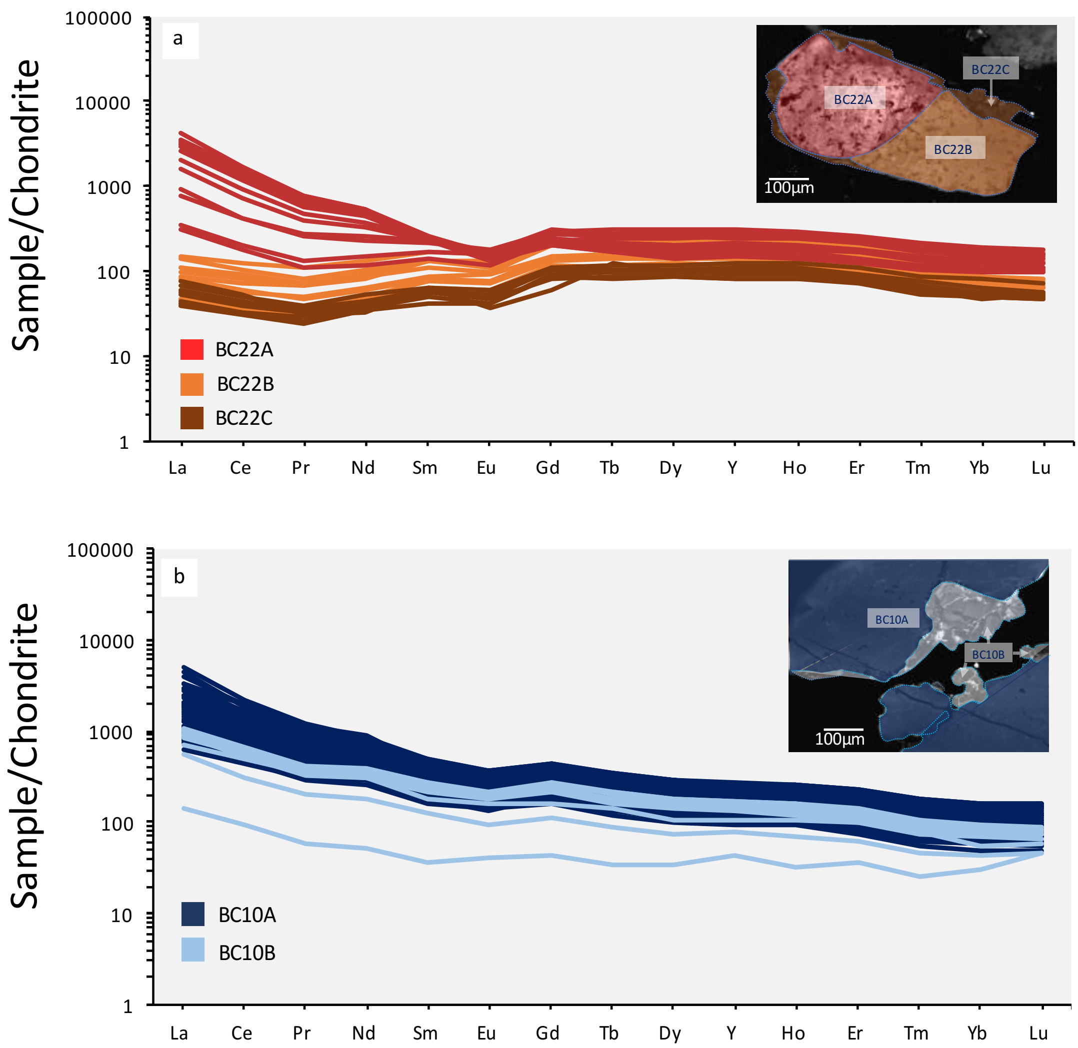

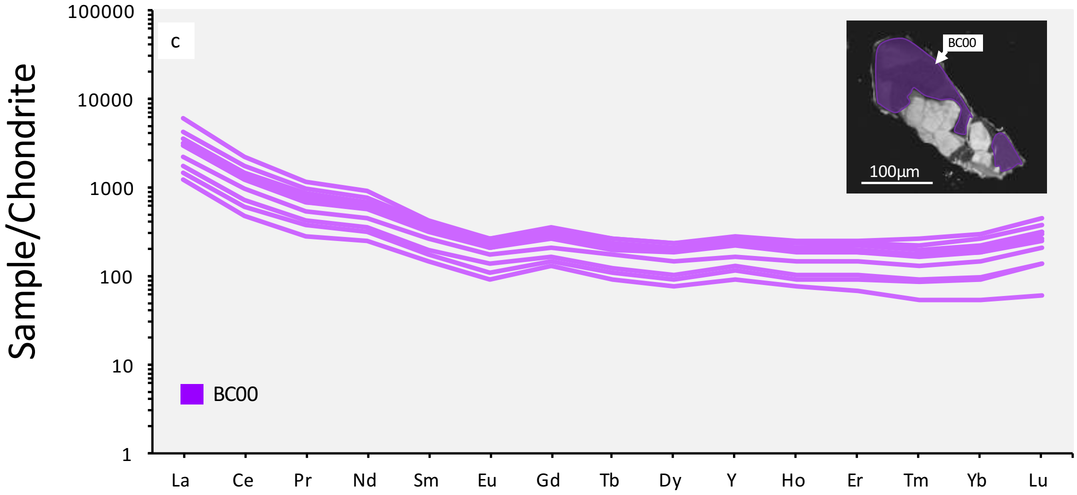

Figure 14: Chondrite-normalized REE diagrams for a) BC22a, BC22b and BC22c samples. b) BC10a and BC10b samples. c) BC00 samples. Chondrite values used from Sun and McDonough (1989). Images in the top right of the diagrams depict the relative sampling sites under CL. The apatite samples are mostly enriched in LREE relative to HREE, with the exception of BC22b and BC22c.

REE TRENDS ACROSS APATITE GRAINS

Figure 15 displays various correlations of REE compositions that vary from the core to the rim of the grains. The HREE + Y vs LREE plot (Figure 15a) shows a general decrease in REE concentrations from the core to the rim of the grains. BC10 samples follow a linear depletion trend (similar to the BC00 sample), whilst the BC22 sample shows a rapid decrease in LREE's, before becoming relatively depleted in HREE + Y, representable of the LREE depletion in seen Figure 13a. The Th vs U diagram (Figure 15b) shows a large decrease in Th from the core to the rim of the samples. A loss of ^{238}U from the core (BC22a) to the rim (BC22b) of the BC22 sample is observed, however is not replicated by the BC10 or BC00 samples. The V vs Mn/Sr diagram (Figure 15c) shows a general trend of decreasing V concentration accompanied by an increasing Mn/Sr ratio from the core to the rim of the samples. This diagram can also be used to discriminate the apatite samples, with each sample plotting in a different location on the diagram. The Sm/Yb vs La/Nd diagram (Figure 15d) shows a general negative correlation between the La/Nd and Sm/Yb ratios from the core to the rim of the samples, producing a similar trend seen in Figure 15a and in Figure 14. This diagram can also be used to discriminate the BC10 and BC22 samples, as they contain different Sm/Yb ratios. Overall, the diagrams depicted in Figure 15 (a to d) show that the trace element composition of the various apatite samples can be used to discriminate the samples, and highlight differences in depletion trends from the core to the rim of the grains. Apatite trace element data can be found in Appendix H.

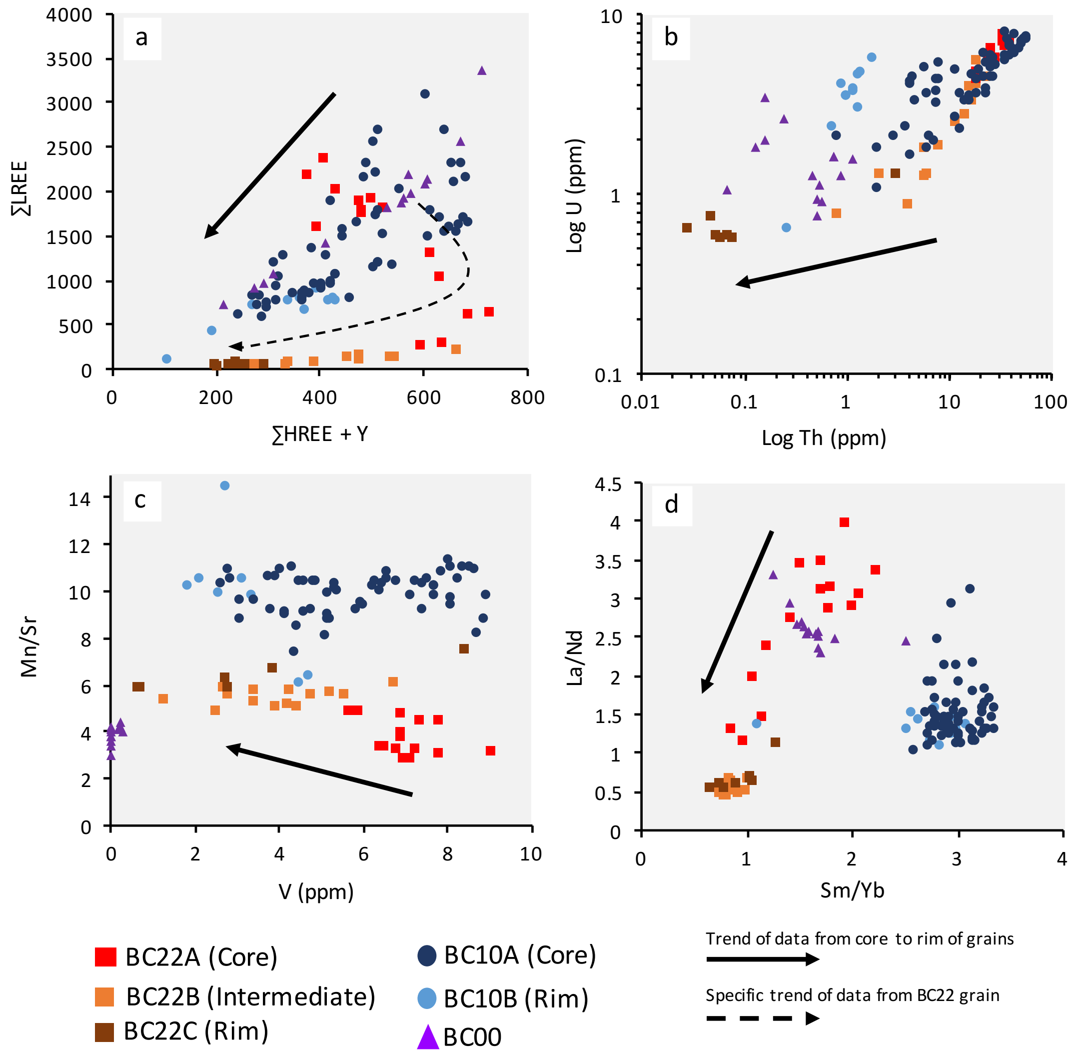

Figure 15: Various diagrams depicting the relationships between certain REE concentrations from the core to the rims of the grains. a) ∑HREE + Y vs ∑LREE diagram. b) Th (ppm) vs U (ppm) diagram. b) V (ppm) vs Mn/Sr diagram. d) Sm/Yb vs La/Nd diagram. Solid arrows show the general trend of the data, whilst dotted arrows show a specific separate trend in the data from the BC22 grain.

4.6 Calcite Trace Elements

DISCRIMINATION PLOTS

When plotted against a range of trace element data of calcite from different host rocks (Figure 16a), data from this plots predominantly within the range of calcite from altered granites. The BC10 (Interlens) and E1 calcite also broadly resemble the greisen type REE profile, although they possess a smaller negative Eu anomaly and a lower concentration of MREE's. Figure 16b also provides a comparison to previously published REE data of calcite from a variety of deposits and environments. The calcite samples from this study plot within the greisen type deposit and magmatic calcite fields, consistent with the data presented in Figure 16a.

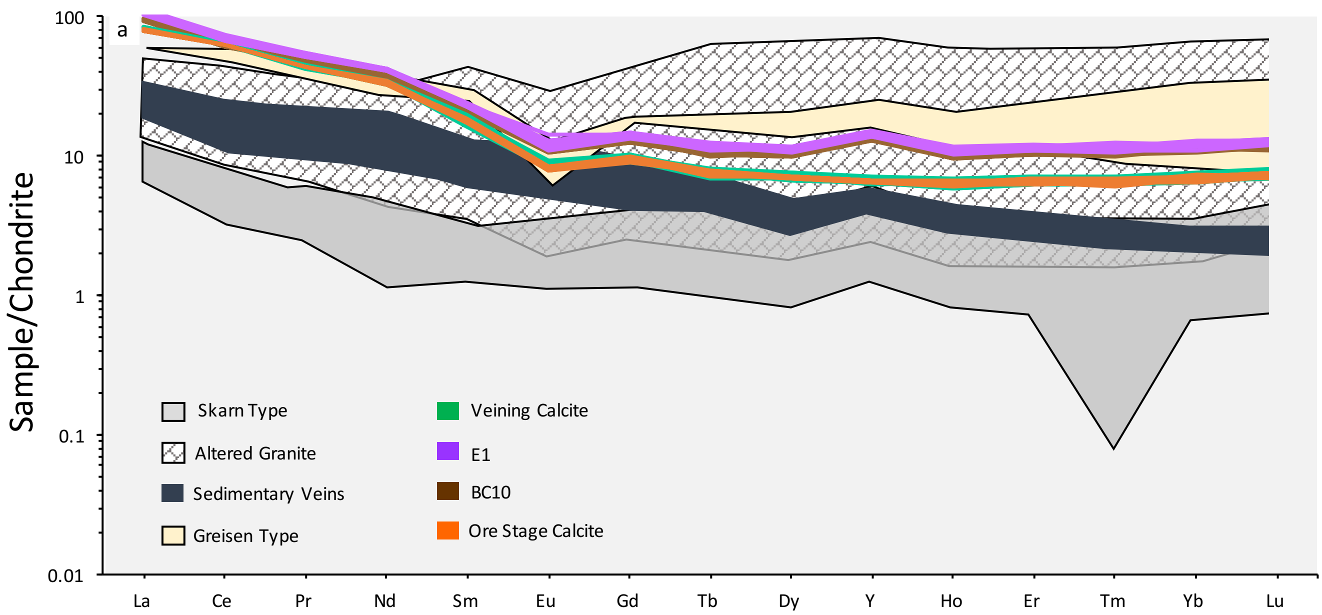

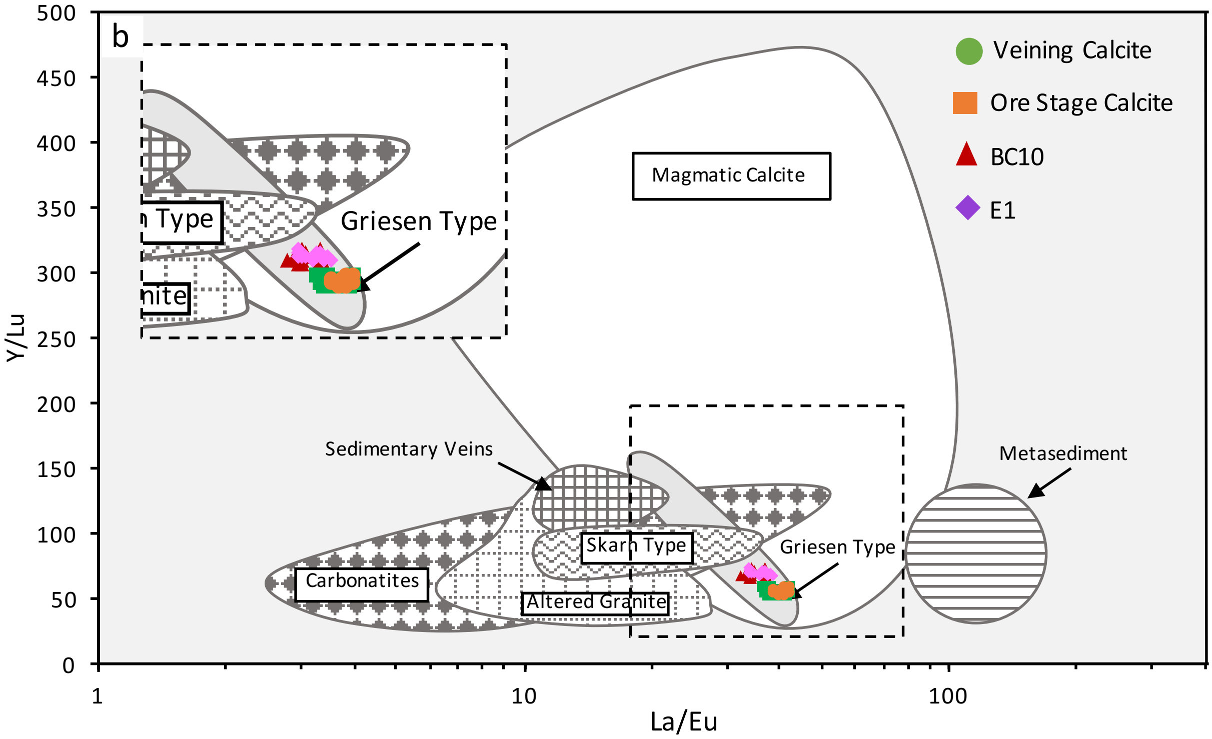

Figure 16: a) A REE plot comparing calcite from this study with calcite from a variety of lithologies. b) Y/Lu vs La/Eu calcite discrimination diagram. Values from skarn type ore, altered granite-type ore and greisen-type ore from Shuang et al. (2010), values from sedimentary veins (Dolníček, Kropáč, Uher, & Polach, 2010) and magmatic calcite (Ionov & Harmer, 2002) with additional data for altered granite from Kontonikas-Charos, Ciobanu, and Cook (2014). This diagram shows the data from this study plotting within the greisen type deposit calcite field, consistent with similarities seen in Figure 18b.

THE CHONDRITE-NORMALISED REE PLOT

Chondrite-normalised REE plots of calcite show two distinct populations within the data (Figure 17). The ore-stage calcite and the veining calcite form one population, possessing very similar REE profiles. Likewise, the E1 and the BC10 samples form a second population, possessing very similar REE profiles. The E1 and BC10 calcite samples possess an overall higher REE abundance, and a positive Y anomaly when compared to the ore stage and veining calcite samples. Overall, the calcite samples from this study are enriched in LREE relative to MREE and HREE, and are relatively flat across the MREE and HREE's.

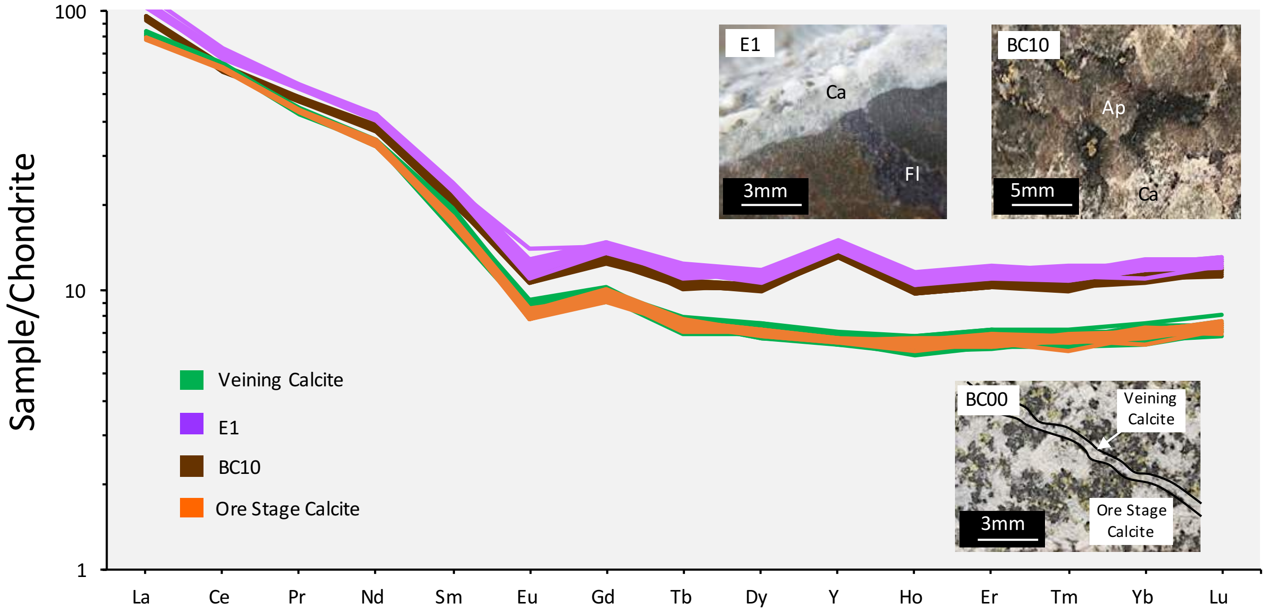

Figure 17: A REE plot of calcite samples from this study. Inserts depict the calcite used for trace element analysis. The calcite from this study appear to form two distinctive groups with similar REE profiles. The BC10 (Interlens) sample and the E1 samples form one group, whilst the Ore-stage calcite and veining calcite form a second group.

REE TRENDS IN CALCITE SAMPLES

Diagrams presented in Figure 18 (a to d) illustrate the similarities and differences in the trace element composition of the calcite samples used in this study. The Sr vs As diagram (Figure 18a) clearly discriminates between the two populations, with the ore stage and veining calcite containing higher concentrations of Sr, and a lower concentration of As when compared to the BC10 and E1 samples. The Y/Ho and La/Ho (Figure 18b) diagram also discriminates the two populations, with the BC10 and E1 samples possessing a higher Y/Ho value and a lower La/Ho ratio compared to the ore-stage and veining calcite. Figure 18c shows no correlation between Mn concentration and the samples locality, however, shows that the concentration of V can be used to discriminate the two populations. The HREE + Y vs LREE diagram in Figure 18d shows that the REE concentration of veining and ore-stage calcite are similar. However, shows that the E1 sample is more enriched in REEs compared to the BC10 sample. The figures presented below clearly illustrate a correlation between the Interlens and E1 calcite samples, and between the ore stage and veining calcite samples, re-affirming the populations seen in Figure 17. Calcite trace element data can be found in Appendix I.

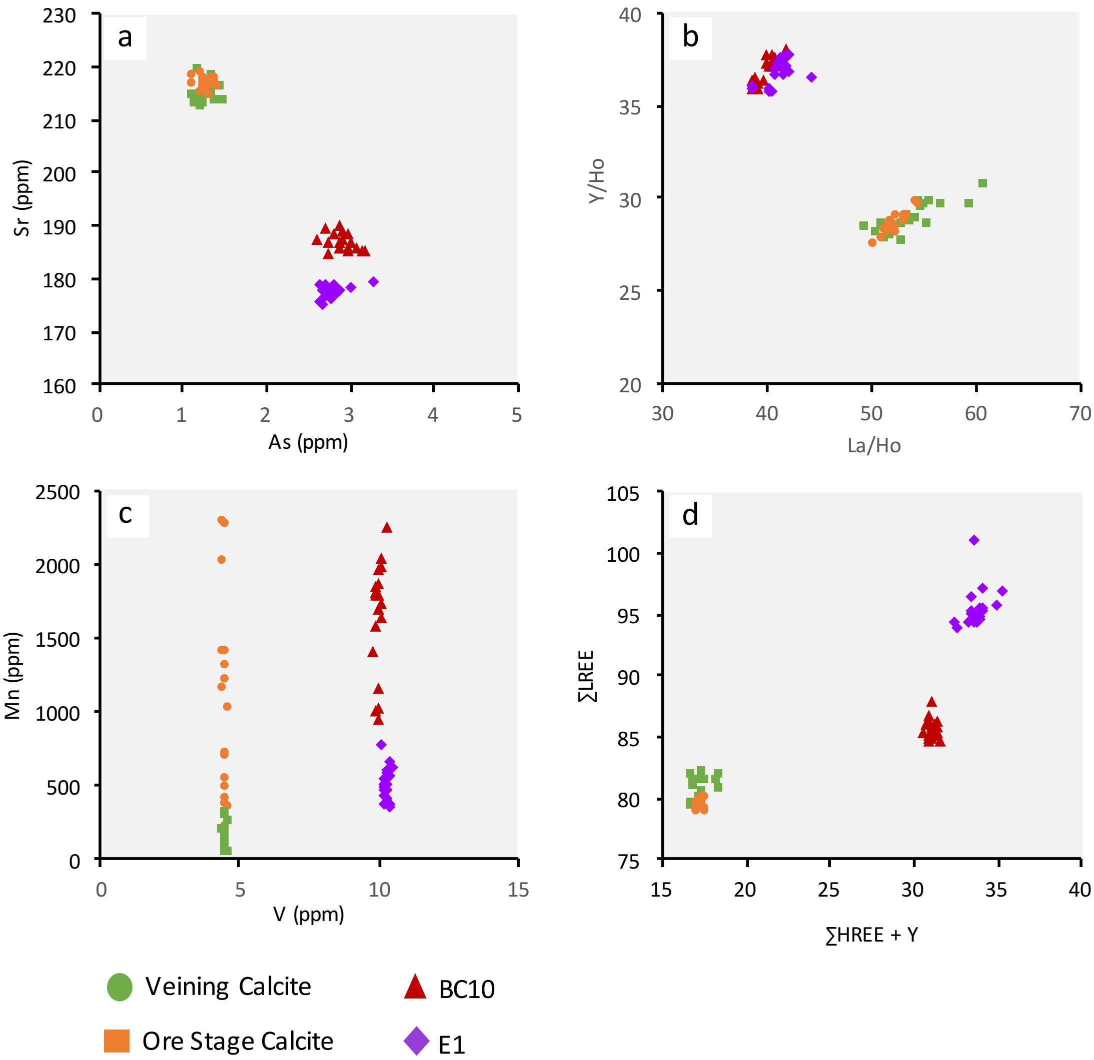

Figure 18: Multiple plots highlighting the similarities and differences in calcite geochemistry of the samples. a) Sr vs As plot. b) Y/Ho vs La/Ho diagram. c) Mn vs V diagram. Note: the limited range of data is not the result of the instrument detection limit. d) LREE vs HREE + Y diagram. These plots illustrate a correlation between the geochemistry of the BC10 and E1 samples, and the ore stage and veining samples.

5. DISCUSSION

5.1 Apatite Geochronology

The U-Pb apatite ages produced in this study are statistically within error of each other, (Figure 8) and are consistent with previously published ages corresponding with events in the Eastern Succession (as seen in Figure 19). Apatite from the Interlens is texturally early in the Ernest Henry paragenetic sequence (Mark et al., 2006), and provide the opportunity to constrain the age of this structure. Sample BC10a produced a U-Pb age of 1581 ± 16 Ma (Figure 9a), whilst the BC22a sample produced an age of 1557 ± 23 Ma (Figure 9c). The BC10a age corresponds temporally with regional peak metamorphic conditions at 1584 ± 17 Ma, and is synchronous with D_2 deformation at 1595−1575 Ma (Page & Sun, 1998; Rubenach et al., 2008). The calculated BC22a age is within uncertainty of D_2 deformation, however, may also represent a local sub-vertical deformation event termed $D_{2.5}$ (Coward, 2001), or the later deformation stage of D_3 from ~1532 to 1480 Ma (Bell & Hickey, 1998; Page & Sun, 1998). BC10a samples represent data from the core of coarse-grained apatite, of which CL and trace element analysis suggest are unaltered (see Section 5.3). Dates produced from this sample likely corresponding to the earliest formation of apatite in the Interlens, or the cooling of the mineral below ~ 350°C (Chew et al., 2014). The BC22a samples are smaller in size, display a shearing texture associated with their distribution, and record multiple stages of alteration (see Section 4.1 and Figure 5e). Therefore, the age of this sample may have been partially reset as a result of alteration above ~350°C, or may also correspond to a later growth of apatite in the Interlens.

The zoning of apatite in this study is likely the result of metasomatism (see Section 5.3), and therefore any difference in the ages between the core and rim may be used to constrain the timing of metasomatic events. However, as samples BC10a and BC10b did not produce a statistically different age (1581 ± 16 Ma and 1572 ± 40 Ma), nor did samples BC22a and BC22b (1557 ± 23 Ma and 1564 ± 56 Ma), the age of alteration is unable to be constrained from this study. This could be attributed to either low temperature alteration (< 350°C), or relatively quick alteration of the minerals following formation.

Apatite from the BC00 samples are from ore-stage mineralization and therefore may represent the formation of the ore-stage assemblage, allowing for the discrimination of paragenetic sequences in the Ernest Henry deposit based on age. Sample BC00 produced an age of 1529 ± 39 Ma, which is consistent with the timing of Na-Ca alteration at 1529 ± 11 Ma (Mark et al., 2006), ore-stage biotite at 1504 ± 3 Ma (Twyerould, 1997), the emplacement of the Mount Margaret granite at 1530 ± 8 Ma (Page & Sun, 1998), and the nearby Saxby Granite at 1527 ± 4 Ma (Rubenach et al., 2008). Furthermore, this age also corresponds with D_3 deformation from ~1532 to 1480 Ma (Connors & Page, 1995; Page & Bell, 1986). The age of this sample likely reflects the timing of D_3 deformation, and the addition of fluids (as discussed by Kendrick et al. 2007)) to form the ore-stage assemblage (see Section 5.3). However, as the age produced from this apatite generation is within error of the Interlens samples, it is not possible to discriminate the apatite from different paragenetic sequences based on age.

5.2 Calcite Geochronology

The calcite samples from Ernest Henry proved unsuitable for geochronology due to a high abundance of common Pb and a low concentration of ^{238}U, resulting in all the analyses falling into the reversely discordant field in the Tera-Wasserburg plot. However, the WC-1 standard, and the Prague Basin standard were successfully dated to within error of their published values, indicating a viable dating technique for future use. It is unclear how the correction method proposed by Li et al. (2014) affects the errors associated with the final calculated age, as this error should inherit the uncertainty in the age of the WC-1 standard, uncertainties in the $^{207}Pb/^{206}Pb$ and $^{206}Pb/^{238}U$ ratios of the WC-1 standard and any uncertainties associated with the measured $^{207}Pb/^{206}Pb$ and $^{206}Pb/^{238}U$ ratios of the samples. Therefore, further research will be required to produce a method to propagate the uncertainties associated with the use of this correction method.

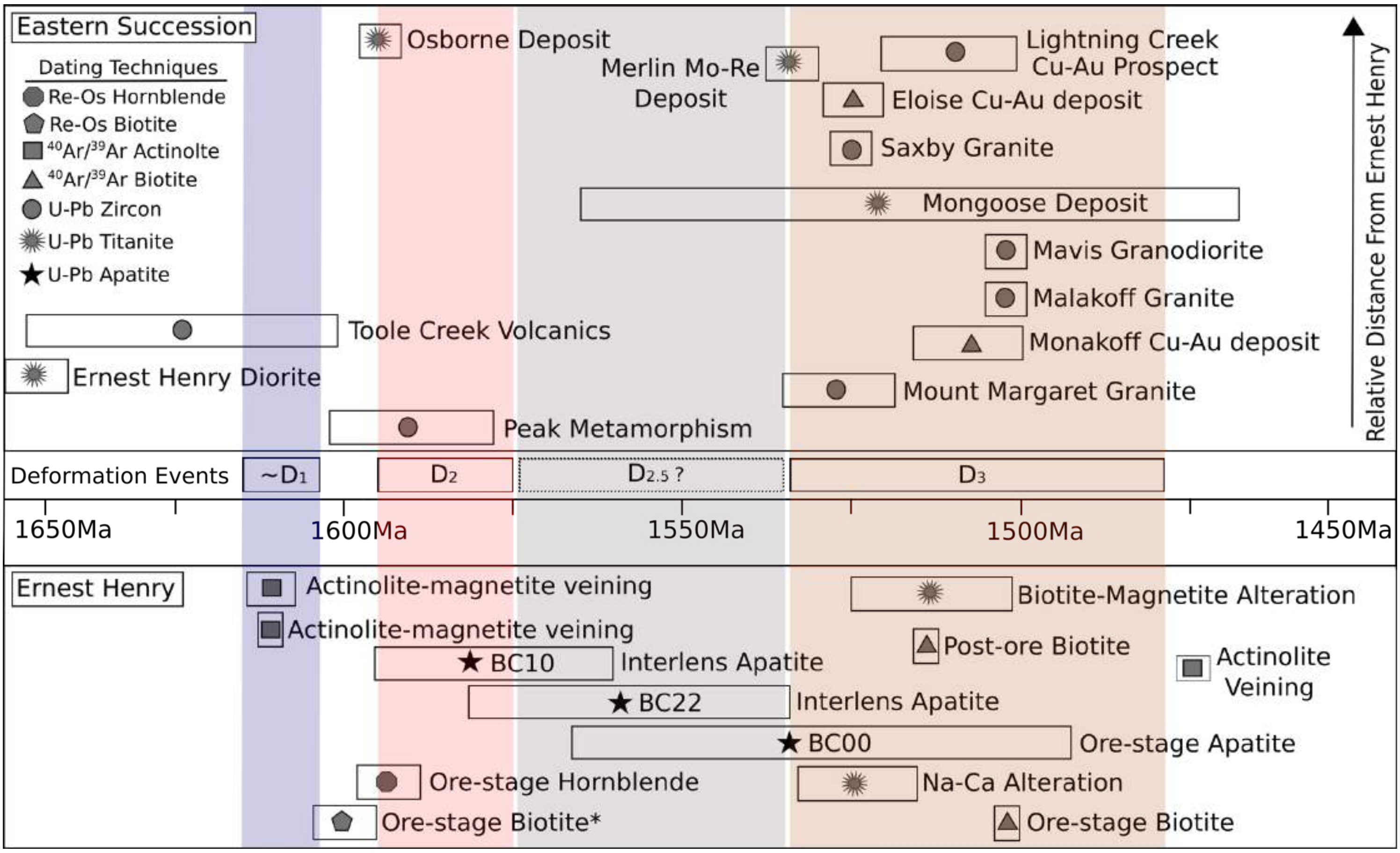

Figure 19: An outline of geochronology data from this experiment compared to work completed by previous authors. The top half of the diagram consists of data from various deposits and large scale events from the Eastern Succession, the y-axis represents their relative distance from Ernest Henry. The bottom half of the diagram consists of data from previous geochronology work completed on the Ernest Henry deposit. It is shown above that the BC10 age correlates with D_2, Peak metamorphism and the timing of the Osborne deposit. The BC22 sample corresponds to the peak metamorphism, D_2, D_3 and a theorised $D_{2.5}$ event. The age of the BC00 sample corresponds to D_3 deformation, a series of mineralization events throughout the Eastern Succession and the occurrence of various granitic units. Boxes indicate the 2σ error associated with each age and the symbol located within each box represents the method used to acquire the age. Data from D_1, (~1610 Ma; Page & Bell, 1986), D_2 (1595−1575 Ma; Page & Sun, 1998), D_3 (1562−1480 Ma Betts et al., 2006). From the Ernest Henry deposit dates produced for actinolite - magnetite veining (1610 ± 2 Ma & 1611 ± 4 Ma), ore-stage biotite (1504 ± 3 Ma), post-ore biotite (1514 ± 3 Ma), and actinolite veining (1476 ± 3 Ma) from Twyerould (1997). Ore-stage biotite* (1595 ± 6 Ma) and ore-stage hornblende (1600 ± 6 Ma) from Gauthier et al., (2001). Na-Ca alteration (1529 ± 11Ma) and biotite-magnetite alteration (1514 ± 29Ma) from Mark et al., (2006). Interlens apatite (1581 ± 16 Ma) and (1557 ± 23 Ma) and ore-stage apatite (1529 ± 39 Ma) from this study. Throughout the eastern succession, dates from the Ernest Henry Diorite (1660 ± 13 Ma; Pollard & McNaughton, 1997), Toole Creek Volcanics (1625 ± 27 Ma; Griffin, Belousova, Walters, & O'Reilly, 2006), Osborne Deposit (1595 ± 6 Ma; Gauthier et al., 2001), Peak Metamorphism (1584 ± 17 Ma; Page & Sun, 1998), Mongoose Deposit (1515 ± 55 Ma; Maughan, 2016), Merlin Mo-Re Deposit (1535 ± 6 Ma; Babo et al., 2017), Mount Margaret Granite (1530 ± 8 Ma; Page & Sun, 1998), Eloise Cu-Au deposit (1530 ± 3 Ma; Baker, Perkins, Blake, & Williams, 2001), Saxby Granite (1527 ± 4 Ma; Rubenach, Foster, Evins, Blake, & Fanning, 2008), Lightening Creek Prospect (Perring, Pollard, & Nunn, 2001), Mavis Granidiorite (1505 ± 3 Ma; Davis, Pollard, Lally, Blake, & Williams, 2001), Malakoff Granite (1505 ± 5 Ma; Page & Sun, 1998) and the Monakoff Cu-Au deposit (1508 ± 10 Ma; Pollard & Perkins, 1997).

5.3 Apatite Trace Element Analysis

SOURCE OF APATITE

The source of the apatites in this study can be used to infer the source of fluids responsible for the formation of different paragenetic stages, developing a greater understanding of the orebody. The REE content of apatite is related to the composition and source of enclosing host rocks, allowing apatite to be used as a petrogenetic tool (Belousova et al., 2002; Belousova et al., 2001). The apatites from this study plot on the granitiod field in Figure 11 and 12, and show a similar, however overall depleted REE profile when compared to nearby intrusive units (Figure 20 (Belousova et al., 2001)). The apatite from this study also show variable REE profiles, however the core samples (BC10a & BC22a) which likely preserve its original composition show a relative LREE enrichment. A relatively LREE rich profile is typical of magmatic-hydrothermal mineralization (Harlov, Andersson, et al., 2002), IOCG deposits (P. Williams et al., 2005) and high temperature magnetite-dominated assemblages (Krneta, Cook, Ciobanu, Ehrig, & Kontonikas-Charos, 2017). Correlations with previously published data suggest the apatite from Ernest Henry was likely sourced from a magmatic/hydrothermal fluid, correlating with the source of apatite from various other IOCG deposits (Krneta, Ciobanu, Cook, Ehrig, & Kontonikas-Charos, 2017; Krneta, Cook, et al., 2017). For Interlens samples, it could be suggested that the fluid was derived from the partial melting of metasedimentary and metavolcanic lithologies within the Interlens, to produce Eu, Y and Sr values similar to those of granitoids and carbonatites. For the ore-stage apatite, the formation fluids are suggested to be at least in some part magmatic and metamorphic (Kendrick et al., 2007), explaining the similarity this sample shares with granitoids and magmatic-hydrothermal mineralization.

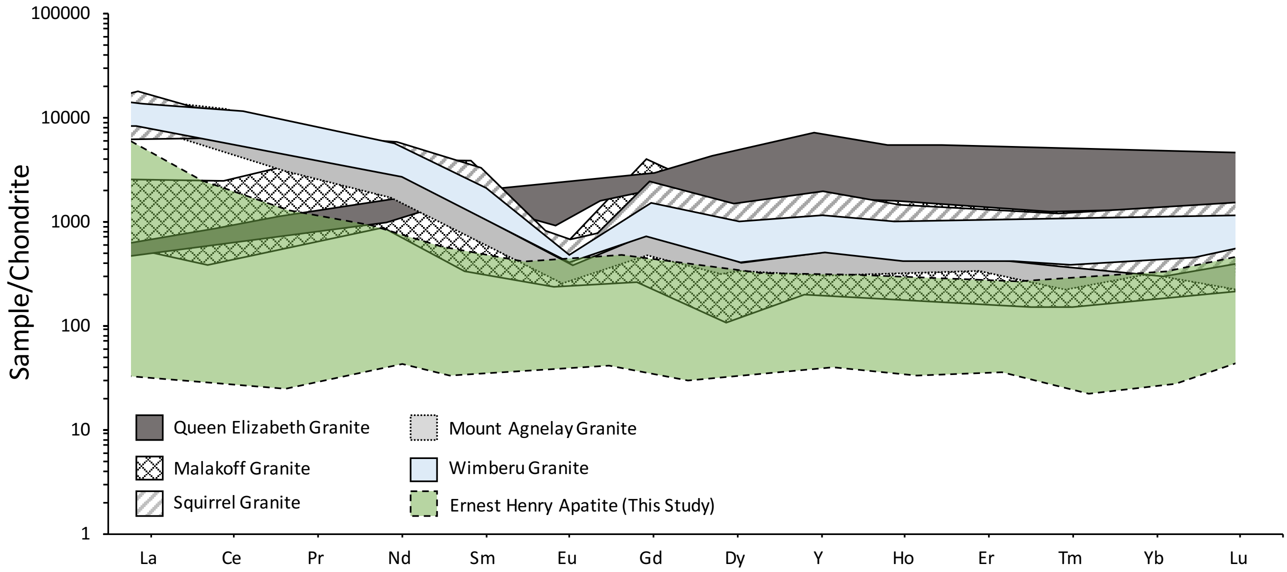

Figure 20: Chondrite-normalized REE diagram showing values from various granite units within the Cloncurry district from Belousova, Walters, Griffin, and O'Reilly (2001) compared to apatite from this study. Chondrite values from Sun and McDonough (1989) Note that no Tb values were included in this plot as they were not included in data from Belousova et al. (2001). This diagram shows no correlation between the samples from Ernest Henry and surrounding granitic units. However, shows that the apatite from Ernest Henry is generally depleted in REE compared to surrounding lithologies.

HYDROTHERMAL ALTERATION AND REE DEPLETION

The REE composition of altered regions in apatite can be used to infer the characteristics of fluids responsible for alteration (Harlov, 2015), and therefore can be used to provide information regarding the composition of fluids responsible for ore-stage mineralization and surrounding alteration. As a high abundance of fluid has been documented throughout the deposit (Mark & Crookes, 1999), and textural observations correlate with criteria outlined in Putnis (2009), it is interpreted that the geochemical changes of the apatite within this study are a result of metasomatism. Experimental studies (Harlov & Förster, 2003; Harlov, Förster, & Nijland, 2002; Harlov, Wirth, & Förster, 2005) show a decrease in Th and REE’s, occasionally accompanied by an increase in Sr in metasomatized regions, directly comparable to the results presented in

Figure 15 and Section 4.6, providing further evidence of metasomatism. Compared to the experimental studies listed above, the presence of REE-bearing minerals such as monazite found within metasomatized regions is minor. This is characteristic of alteration by a Na and/or Ca rich fluid, as the availability of Na^{+} and Ca^{2+} maintain a charge balance if Y + REE are removed, hindering the formation of REE-bearing minerals (Harlov et al., 2005). Therefore, it is interpreted that the change in the trace element composition across the apatite grains from this study is likely the result of metasomatism by a Na and/or Ca rich fluid. This correlates with the general geological setting of Ernest Henry (eg abundance of calcite and sodic-calcic alteration), and fluid inclusion studies from the ore-grade assemblage, which are found to contain both NaCl and CaCl bearing fluids (Kendrick et al., 2007; Mark, Williams, Oliver, Ryan, & Mernagh, 2005).

BC22 samples display a noticeable vuggy texture, which is likely the result of increased porosity due to a high degree of metasomatism (Harlov, Förster, et al., 2002; Putnis, 2009). This sample is comparable to results from Harlov, Andersson, et al. (2002), showing a large decreases in LREEs from relatively unaltered (BC22a) to heavily metasomatized regions (BC22c). This is likely associated with the dominant transport mechanism of the REE's during metasomatism. REE are transported predominantly as sulphate and chloride complexes, where fluorite, carbonate and phosphate complexes play an important role as depositional ligands (Haas, Shock, & Sassani, 1995; Migdisov, Williams-Jones, Brugger, & Caporuscio, 2016). LREE's and HREE's can be fractionated hydrothermally due to the stability of the transport complexes they form, as LREE-chlorite complexes are considerably more stable than HREE-chlorite complexes

(Migdisov et al., 2016). This mechanism is likely responsible for the preferential LREE depletion of the BC22 grain from sample BC22a to BC22c, suggesting the fluids responsible for alteration were relatively rich in Cl. This fluid could be associated with the ore-stage assemblage, of which Kendrick et al. (2007) found fluid inclusions with up to 69wt% NaCl eq, and Mark et al. (2005) found up to 55wt% NaCl eq.

As the BC10 group show a systematic REE depletion from BC10a to BC10b, with no apparent preference for LREE fractionation, an alternative explanation is required for this type of metasomatism. The sharp reaction front between the parent (BC10a) and product (BC10b) phases, as well as their close spatial relationships are characteristic of dissolution re-precipitation reactions (Putnis, 2009). As there is no evidence for preferential LREE mobility, and the brecciating fluids are interpreted as post-peak mineralization (see Section 5.4), it is interpreted that the metasomatic fluids were relatively enriched in S, showing no preference towards the mobility of LREE or HREE (Migdisov et al., 2016). Evidence for this is seen in Figure 5b, which shows the sample site for some BC10b samples brecciated by a later calcite generation (see section 5.4) containing proximal sulphide mineralization. Therefore, it is possible that the fluids responsible for this type of alteration may have been 'contaminated' by earlier sulphide mineralization, resulting in a relatively high S content.

The BC00 apatite samples also display textures consistent with dissolution re-precipitation reactions (Putnis, 2009). These samples also possess a minor enrichment in the HREE's Tm, Yb and Lu, which in previous studies has been attributed to a combination of preferential LREE mobility and coupled-dissolution re-precipitation reactions (Broom-Fendley, Styles, Appleton, Gunn, & Wall, 2016). Furthermore, Liu et al. (2017) has already proposed the idea of a coupled dissolution re-precipitation mechanism for the ore-stage apatite to explain the presence of As^{3+} rich cores and As^{4+} rich rims. The high concentration of As (up to ~3wt%: Figure 12 a & b) is comparable to a study by Borg, Liu, Pearce, Cleverley, and MacRae (2014), who demonstrate that the dissolution of calcite with a arsenate-phosphate solution can cause significantly enriched As rims of apatite (up to 8x the fluid bulk composition) to occur. A similar mechanism may be proposed for the dissolution of apatite by a Ca rich solution, explaining the As rich rims seen in the BC00 samples. As the rims/intermediate zones of the BC00 apatite grains appear to represent an incorporation of As into the apatite, and arsenopyrite (representative of As fluids) only appears alongside the ore-stage assemblage (Mark et al., 2006), the interpretation can be made that the fluid responsible for the deposition of the ore-stage assemblage may also be responsible for the dissolution re-precipitation reactions of the BC00 apatite. This is consistent with the age of the BC00 apatite, which correlates with dates proposed for Cu-Au mineralization (Twyerould, 1997). Here, it is suggested that the addition of a new fluid (possibly ore-bearing) caused a dissolution re-precipitation reaction in the Ernest Henry orebody apatite, producing a relative enrichment of REE's and As in the intermediate zone/rims of the ore-stage apatite (as seen in Figure 12 a & b).

5.4 Calcite Trace Element Analysis

SOURCE OF CALCITE

The source of the calcite can provide insight into the fluids responsible for multiple alteration events. Figures 16a and 16b suggest that calcite from this study shares geochemical similarities with magmatic calcite, calcite from greisen type deposits and calcite from hydrothermally altered granites. These results agree with the interpretations of Fuss (2014), that the ore-stage calcite analysed in this study was likely derived from a magmatic/metamorphic fluid that has diffused through the heavily altered Mount-Fort Constantine host rocks before deposition. Furthermore, a similar genesis is interpreted for the E1 and BC10 calcite samples, which also share a similarity to altered granites and calcite from greisen type deposits, possibly also the result of magmatic/hydrothermal fluid diffusion through heavily Ca-Na altered rocks.

IMPLICATIONS FOR REE COMPOSITIONS

Geochemical similarities between the two calcite populations suggest they possess a similar genesis. However, cross cutting relationships present in the ore-stage and veining calcite samples imply that the veining calcite post-dates the ore stage calcite, requiring further explanation regarding their geochemical similarities. Previous research identified the late veining as having a dominantly meteoric isotopic signature, whilst the ore-stage calcite was sourced from metamorphic fluids (Fuss, 2014). Therefore, it could be suggested that the samples from this study were not representable of calcite described by Fuss (2014), or the geochemical similarities between two calcite generations are the result of REE diffusion from one calcite generation to another. The later hypothesis would require sufficient energy to allow diffusion to occur, with experimental values for the closure temperature of Nd and Yb in calcite ranging from 500°C to 700°C for grains with an effective diffusion radius from 0.1 to 1cm (Cherniak, 1998). This is consistent with the upper homogenization temperature from fluid inclusion data within the ore-stage assemblage which ranges from 350-500°C (Kendrick et al., 2007; Mark et al., 2005) and would further suggest the orebody was still hot, or reheated during, or after the emplacement of the veining calcite.

The E1 calcite sample used in this study is from a vein that cross-cuts fluorite mineralization, and is therefore representable of a post-ore hydrothermal event (Lilly et al., 2017; M. Williams et al., 2015). As the paragenesis of the E1 deposit and Ernest Henry deposit are directly comparable (Lilly et al., 2017), and the trace element composition of the BC10 and E1 calcite samples are very similar, it can be inferred that the calcite from the BC10 sample was deposited post- Cu-Au mineralization in the Ernest Henry deposit. This would also suggest that the effective range of late hydrothermal fluids in the region extends at least 6km. The association between the E1 and BC10 samples is not obvious from any textural relationships, unlike the ore-stage and veining calcite, which possess similar twinning and interference colours. This study provides the first evidence that the REE composition of calcite can be used to geochemically link paragenetic sequences from nearby deposits.

5.5 Series of Events

From evidence given in Section 4.1– 4.6, and discussed in Section 5.1– 5.4, Figure 21 (a-d) illustrates the sequence of events interpreted to have occurred in the Ernest Henry orebody.

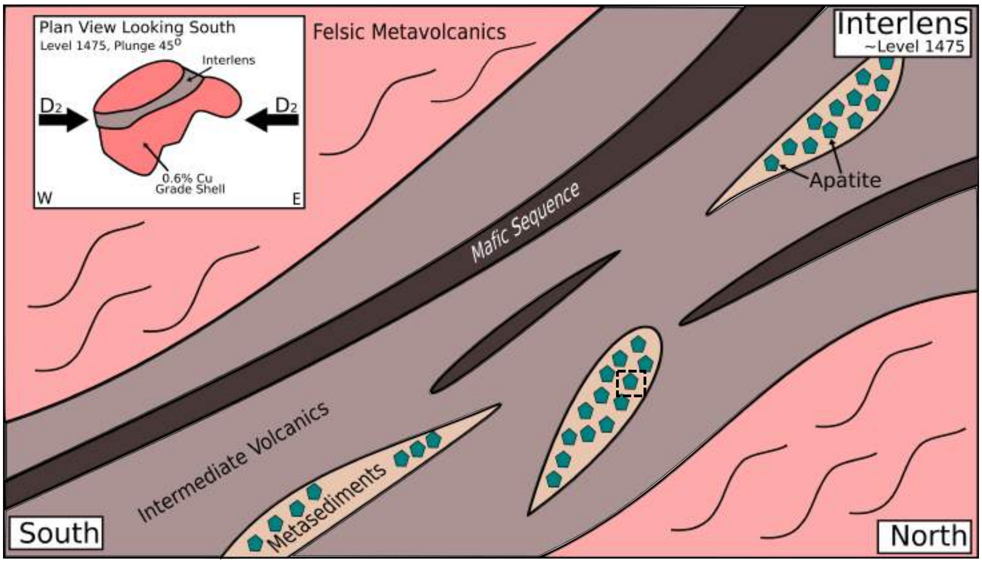

~1581 ± 16 Ma

a

-Peak metamorphic conditions.
-D2 deformation (1595–1575 Ma).
-Metamorphism of metasediments.
-Formation of coarse-grained apatite.

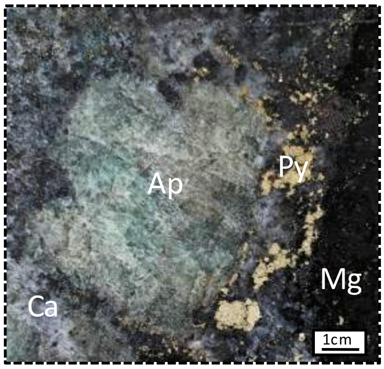

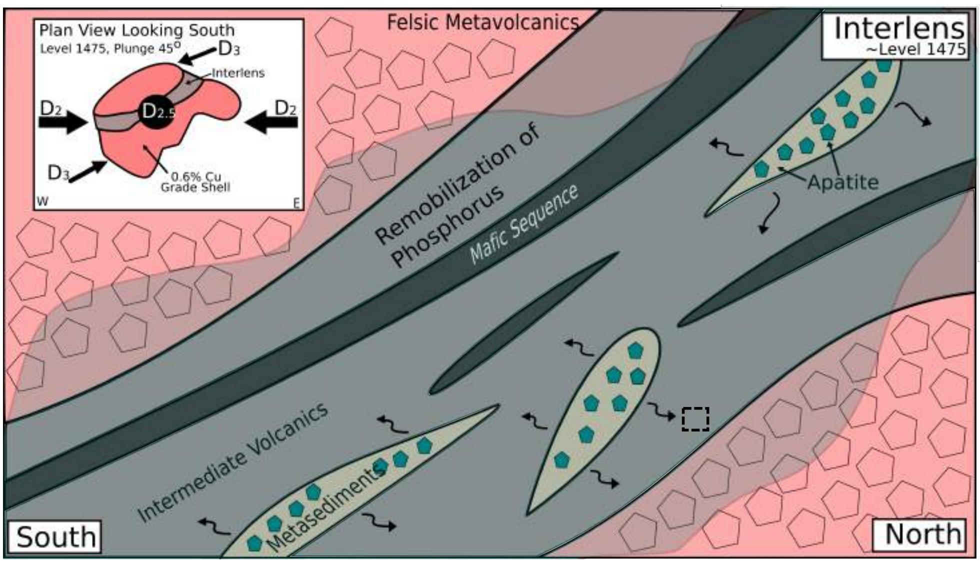

~1557 ± 23 Ma

b

-Retrograde metamorphic conditions.
-D2 deformation.
-D2.5 deformation?
-Onset of D3 deformation.
-Infiltration of Na, Ca and Cl rich fluids.
-Remobilization of phosphorus.
-Alteration of BC22 apatite.

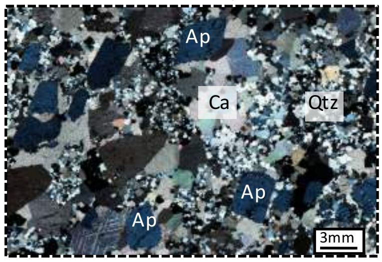

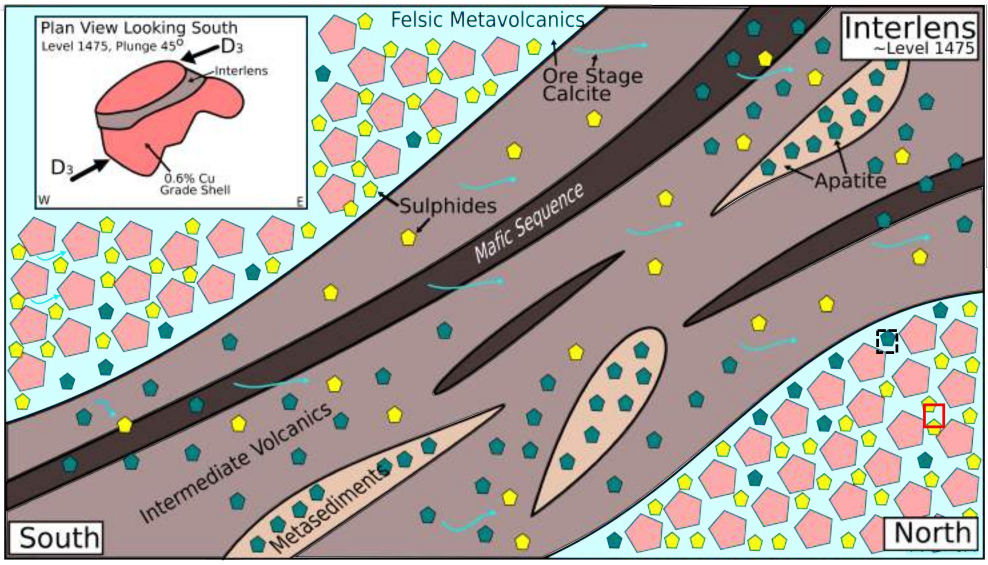

~1529 ± 39 Ma

c

-Retrograde metamorphic conditions.
-D3 deformation (1532–1480 Ma).
-Infiltration of Na, Ca and Cl rich fluids.
-Alteration of ore-stage apatite.
-Ore stage calcite.
-Cu-Au mineralization.
-Mount Margaret granite (1530 ± 8 Ma).

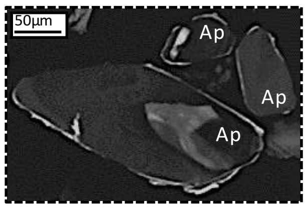

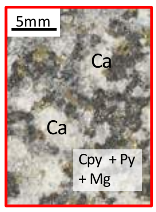

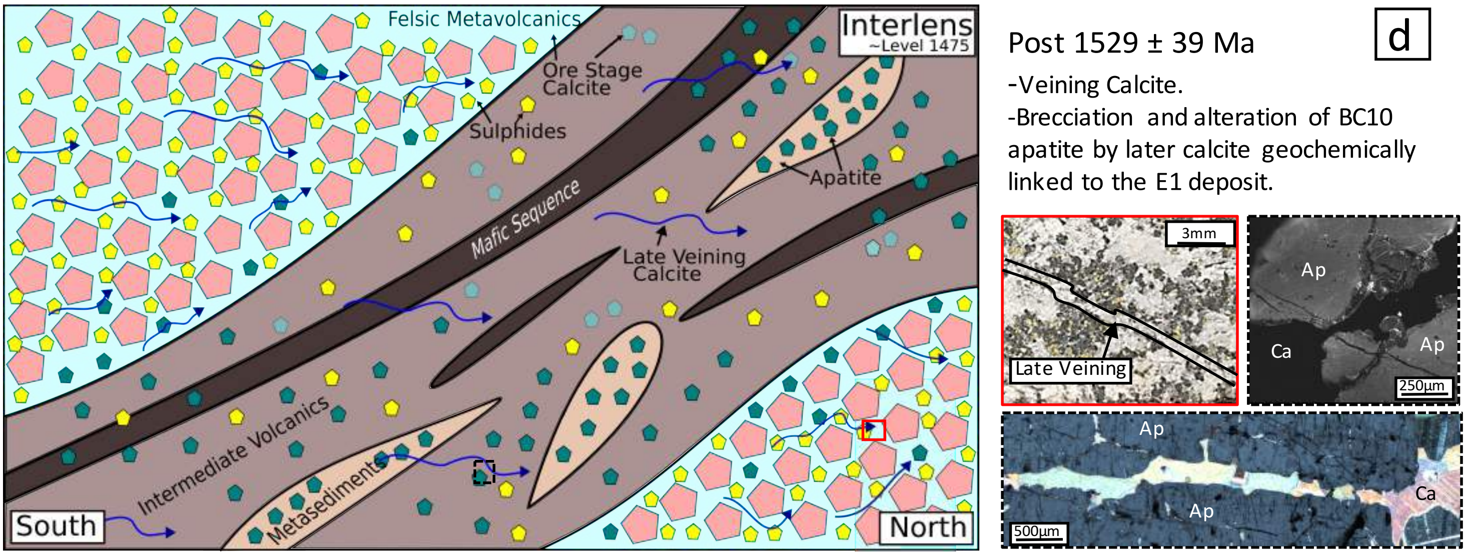

Figure 21: A schematic diagram illustrating the series of events interpreted to have occurred from the data presented in this study. Diagrams are facing east. Inserts located in the top left of the diagrams indicate the relative stress on the deposit from a plan view of the orebody at level 1475. This also shows the interpreted deformation event associated with each stress regime. The dot points state the events interpreted from this study. The images in the bottom right of each diagram show the evidence associated with each interpretation made. The coloured outline of each image corresponds to its relative location on the diagram.

6. CONCLUSIONS

- Coarse-grained apatite formed in the Interlens at 1581 ± 16Ma, likely a result of D_2 deformation during regional peak metamorphism.
- Apatite from the Interlens also records a later age of 1557 ± 23Ma, possibly a result of D_2, $D_{2.5}$ or D_3 deformation.
- The 1529 ± 39 Ma age of the apatite from the orebody likely represents the influx of ore-bearing fluids.
- The metasomatized regions of apatite from the Interlens did not produce a statistically significant age to unaltered regions.
- Apatite sourced from the Interlens and the orebody have REE compositions consistent with a hydrothermal/magmatic source.
- In all cases, the alteration of apatite occurred under the influence of Ca and/or Na rich fluids, with varying amounts of S and Cl.

- The U-Pb calcite dating technique proved successful on standards of a known age.
- Calcite from the Ernest Henry deposit is not suitable for U-Pb geochronology.
- Two populations of calcite are identified at the Ernest Henry based on their trace element composition.
- Calcite from the E1 and Ernest Henry deposits can be geochemically linked.

ACKNOWLEDGMENTS

Firstly, I would like to thank Richard Lilly for all the help/advice throughout the year, this project would not have been possible without your help. I would also like to thank Cassie Lintvelt and James Hewett from team AWESOME for making this year great, alongside the rest of the honours cohort. Furthermore, Brad Miller, Dan Ashton, Jack Gurney, Vanessa Sexton and Chloe Hawtin for their great hospitality during our stay at the Ernest Henry Mine. I would also like to thank Dave Kelsey and Sarah Gilbert from Adelaide Microscopy for going out of their way to help me on the SEM and LA-ICP-MS. I would also like to thank Jack Gillipse for his support in the development of the calcite dating method and Stijn Glorie for acquiring the WC-1 standard. Furthermore, Jack Gillipse, Gilby Jepson, James Hall and Stijn Glorie for helping me with the apatite dating technique. Lastly, I would like to thank Alec Walsh for helping me throughout the year with a variety of things. I would also like to thank Mount Isa Mines for funding such an exciting project.

REFERENCES

Babo, J., Spandler, C., Oliver, N., Brown, M., Rubenach, M., & Creaser, R. (2017). The High-Grade Mo-Re Merlin Deposit, Cloncurry District, Australia: Paragenesis and Geochronology of Hydrothermal Alteration and Ore Formation. *Economic Geology, 112*(2), 397-422.

Baker, T., Mustard, R., Fu, B., Williams, P., Dong, G., Fisher, L., . . . Ryan, C. (2008). Mixed messages in iron oxide–copper–gold systems of the Cloncurry district, Australia: insights from PIXE analysis of halogens and copper in fluid inclusions. *Mineralium Deposita, 43*(6), 599.

Baker, T., Perkins, C., Blake, K., & Williams, P. (2001). Radiogenic and stable isotope constraints on the genesis of the Eloise Cu-Au deposit, Cloncurry district, northwest Queensland. *Economic Geology, 96*(4), 723-742.

Bell, T., & Hickey, K. (1998). Multiple deformations with successive subvertical and subhorizontal axial planes in the Mount Isa region; their impact on geometric development and significance for mineralization and exploration. *Economic Geology, 93*(8), 1369-1389.

Belousova, E., Griffin, W., O'Reilly, S., & Fisher, N. (2002). Apatite as an indicator mineral for mineral exploration: trace-element compositions and their relationship to host rock type. *Journal of Geochemical Exploration, 76*(1), 45-69.

Belousova, E., Walters, S., Griffin, W., & O'Reilly, S. (2001). Trace-element signatures of apatites in granitoids from the Mt Isa Inlier, northwestern Queensland. *Australian Journal of Earth Sciences, 48*(4), 603-619.

Betts, P., Giles, D., Mark, G., Lister, G., Goleby, B., & Ailleres, L. (2006). Synthesis of the Proterozoic evolution of the Mt Isa Inlier. *Australian Journal of Earth Sciences, 53*(1), 187-211.

Borg, S., Liu, W., Pearce, M., Cleverley, J., & MacRae, C. (2014). Complex mineral zoning patterns caused by ultra-local equilibrium at reaction interfaces. *Geology, 42*(5), 415-418.

Broom-Fendley, S., Styles, M. T., Appleton, J. D., Gunn, G., & Wall, F. (2016). Evidence for dissolution-reprecipitation of apatite and preferential LREE mobility in carbonatite-derived late-stage hydrothermal processes. *American Mineralogist, 101*(3), 596-611.

Chew, D., Petrus, J., & Kamber, B. (2014). U–Pb LA–ICPMS dating using accessory mineral standards with variable common Pb. *Chemical Geology, 363*, 185-199.

Cleverley, J. (2006). Using the chemistry of apatite to track fluids in Fe-oxide Cu–Au systems. *Geochimica et Cosmochimica Acta, 70*(18), A105.

Connors, K., & Page, R. (1995). Relationships between magmatism, metamorphism and deformation in the western Mount Isa Inlier, Australia. *Precambrian Research, 71*(1-4), 131-153.

Coward, M. (2001). *Structural Controls on Ore Formation and Distribution at the Ernest Henry Cu-Au Deposit, NWQld.* (Bachelor of Science (Honours)), James Cook University.

Davis, B., Pollard, P., Lally, J., Blake, K., & Williams, P. (2001). Deformation history of the Naraku Batholith, Mt Isa Inlier, Australia: implications for pluton ages and geometries from structural study of the Dipvale Granodiorite and Levian Granite. *Australian Journal of Earth Sciences, 48*(1), 113-129.

Debruyne, D., Hulsbosch, N., & Muchez, P. (2016). Unraveling rare earth element signatures in hydrothermal carbonate minerals using a source–sink system. *Ore Geology Reviews, 72*, 232-252.

Dolníček, Z., Kropáč, K., Uher, P., & Polach, M. (2010). Mineralogical and geochemical evidence for multi-stage origin of mineral veins hosted by teschenites at Tichá, Outer Western Carpathians, Czech Republic. *Chemie der Erde-Geochemistry, 70*(3), 267-282.

Farkaš, J., Frýda, J., & Holmden, C. (2016). Calcium isotope constraints on the marine carbon cycle and CaCO 3 deposition during the late Silurian (Ludfordian) positive δ 13 C excursion. *Earth and Planetary Science Letters, 451*, 31-40.

Foster, A., Williams, P., & Ryan, C. (2007). Distribution of gold in hypogene ore at the Ernest Henry iron oxide copper-gold deposit, Cloncurry District, NW Queensland. *Exploration and Mining Geology, 16*(3-4), 125-143.

Foster, D., & Austin, J. (2008). The 1800–1610Ma stratigraphic and magmatic history of the Eastern Succession, Mount Isa Inlier, and correlations with adjacent Paleoproterozoic terranes. *Precambrian Research, 163*(1), 7-30.

Fuss, M. (2014). *Isotopic (87Sr/86Sr, δ13C and δ18O) indicators of fluid source from carbonates in the Ernest Henry deposit, Queensland, Australia: implications for genesis and exploration.* (Bachelor of Geology (Honours)), James Cook University.

Gauthier, L., Hall, G., Stein, H., & Schaltegger, U. (2001). The Osborne deposit, Cloncurry district: a 1595 Ma Cu–Au skarn deposit. *Contributions of the Economic Geology Research Unit, James Cook University, 59*, 58-59.

Giles, D., Ailléres, L., Jeffries, D., Betts, P., & Lister, G. (2006). Crustal architecture of basin inversion during the Proterozoic Isan Orogeny, Eastern Mount Isa Inlier, Australia. *Precambrian Research, 148*(1), 67-84.

Giles, D., Betts, P., Ailleres, L., Hulscher, B., Hough, M., & Lister, G. (2006). Evolution of the Isan Orogeny at the southeastern margin of the Mt Isa Inlier. *Australian Journal of Earth Sciences, 53*(1), 91-108.

Griffin, W., Belousova, E., Walters, S., & O'Reilly, S. (2006). Archaean and Proterozoic crustal evolution in the Eastern Succession of the Mt Isa district, Australia: U–Pb and Hf-isotope studies of detrital zircons. *Australian Journal of Earth Sciences, 53*(1), 125-149.

Haas, J., Shock, E., & Sassani, D. (1995). Rare earth elements in hydrothermal systems: estimates of standard partial molal thermodynamic properties of aqueous complexes of the rare earth elements at high pressures and temperatures. *Geochimica et Cosmochimica Acta, 59*(21), 4329-4350.

Harlov, D. (2015). Apatite: A fingerprint for metasomatic processes. *Elements, 11*(3), 171-176.

Harlov, D., Andersson, U., Förster, H., Nyström, J., Dulski, P., & Broman, C. (2002). Apatite–monazite relations in the Kiirunavaara magnetite–apatite ore, northern Sweden. *Chemical Geology, 191*(1), 47-72.

Harlov, D., & Förster, H. (2003). Fluid-induced nucleation of (Y+ REE)-phosphate minerals within apatite: Nature and experiment. Part II. Fluorapatite. *American Mineralogist, 88*(8-9), 1209-1229.

Harlov, D., Förster, H., & Nijland, T. (2002). Fluid-induced nucleation of (Y+ REE)-phosphate minerals within apatite: Nature and experiment. Part I. Chlorapatite. *American Mineralogist, 87*(2-3), 245-261.

Harlov, D., Wirth, R., & Förster, H. (2005). An experimental study of dissolution–reprecipitation in fluorapatite: fluid infiltration and the formation of monazite. *Contributions to Mineralogy and Petrology, 150*(3), 268-286.

Hewett, J. (2017). *Distribution of gold and its relation to pyrite trace element geochemistry at Ernest Henry Deposit, NW Queensland.* (Bachelor of Sciecne (Honours)), University of Adelaide.

Hughes, J., & Rakovan, J. (2015). Structurally robust, chemically diverse: apatite and apatite supergroup minerals. *Elements, 11*(3), 165-170.

Hutton, L., Denaro, T., Dhnaram, C., & Derrick, G. (2012). Mineral Systems in the Mount Isa Inlier. *Episodes, 35*(1), 120-130.

Ionov, D., & Harmer, R. (2002). Trace element distribution in calcite–dolomite carbonatites from Spitskop: inferences for differentiation of carbonatite magmas and the origin of carbonates in mantle xenoliths. *Earth and Planetary Science Letters, 198*(3), 495-510.

Jong, G., & Williams, P. (1995). Giant metasomatic system formed during exhumation of mid-crustal Proterozoic rocks in the vicinity of the Cloncurry Fault, northwest Queensland. *Australian Journal of Earth Sciences, 42*(3), 281-290.

Kendrick, M., Mark, G., & Phillips, D. (2007). Mid-crustal fluid mixing in a Proterozoic Fe oxide–Cu–Au deposit, Ernest Henry, Australia: evidence from Ar, Kr, Xe, Cl, Br, and I. *Earth and Planetary Science Letters, 256*(3), 328-343.

Kontonikas-Charos, A., Ciobanu, C., & Cook, N. (2014). Albitization and redistribution of REE and Y in IOCG systems: insights from Moonta-Wallaroo, Yorke Peninsula, South Australia. *Lithos, 208*, 178-201.

Krneta, S., Ciobanu, C. L., Cook, N. J., Ehrig, K., & Kontonikas-Charos, A. (2017). Rare Earth Element Behaviour in Apatite from the Olympic Dam Cu–U–Au–Ag Deposit, South Australia. *Minerals, 7*(8), 135.

Krneta, S., Cook, N. J., Ciobanu, C. L., Ehrig, K., & Kontonikas-Charos, A. (2017). The Wirrda Well and Acropolis prospects, Gawler Craton, South Australia: Insights into evolving fluid conditions through apatite chemistry. *Journal of Geochemical Exploration, 181*, 276-291.

Li, Q., Parrish, R., Horstwood, M., & McArthur, J. (2014). U–Pb dating of cements in Mesozoic ammonites. *Chemical Geology, 376*, 76-83.

Lilly, R., Case, G., & Miller, B. (2017). Ernest Henry iron oxide copper-gold deposit. *AusIMM Monograph, Australian Ore Deposits*(1), 1-6.

Liu, W., Mei, Y., Etschmann, B., Brugger, J., Pearce, M., Ryan, C., . . . Paterson, D. (2017). Arsenic in hydrothermal apatite: Oxidation state, mechanism of uptake, and comparison between experiments and nature. *Geochimica et Cosmochimica Acta, 196*, 144-159.

Ludwig, K. (2003). *User's manual for Isoplot 3.00: a geochronological toolkit for Microsoft Excel*: Kenneth R. Ludwig.

Machel, H., & Burton, E. (1991). Factors governing cathodoluminescence in calcite and dolomite, and their implications for studies of carbonate diagenesis.

Mark, G., & Crookes, R. (1999). Epigenetic alteration at the Ernest Henry Fe-oxide-(Cu-Au) deposit, Australia. *Mineral deposits: Processes to processing: Rotterdam, Balkema*, 185-188.

Mark, G., & Foster, D. (2000). Magmatic–hydrothermal albite–actinolite–apatite-rich rocks from the Cloncurry district, NW Queensland, Australia. *Lithos, 51*(3), 223-245.

Mark, G., Oliver, N., & Williams, P. (2006). Mineralogical and chemical evolution of the Ernest Henry Fe oxide–Cu–Au ore system, Cloncurry district, northwest Queensland, Australia. *Mineralium Deposita, 40*(8), 769.

Mark, G., Williams, P., Oliver, N., Ryan, C., & Mernagh, T. (2005). *Fluid inclusion and stable isotope geochemistry of the Ernest Henry Fe oxide-Cu-Au deposit, Queensland, Australia.* Paper presented at the Mineral Deposit Research: Meeting the Global Challenge.

Maughan, J. (2016). *Geochemistry of the Mafic Sequences in the Cloncurry District, Queensland: Implications for crustal accretion and prospectivity.* (Bachelor of Science (Honours)), University of Adelaide.

Migdisov, A., Williams-Jones, A., Brugger, J., & Caporuscio, F. (2016). Hydrothermal transport, deposition, and fractionation of the REE: Experimental data and thermodynamic calculations. *Chemical Geology, 439*, 13-42.

O'Brien, S. (2016). *Structural and Mineralogical Controls on the Formation of the 'Inter-lens' at the Ernest Henry Deposit, Queensland.* (Bachelor of Science (Honours)), University of Adelaide.

Oliver, N., Butera, K., Rubenach, M., Marshall, L., Cleverley, J., Mark, G., . . . Esser, D. (2008). The protracted hydrothermal evolution of the Mount Isa Eastern Succession: A review and tectonic implications. *Precambrian Research, 163*(1), 108-130.

Page, R., & Bell, T. (1986). Isotopic and structural responses of granite to successive deformation and metamorphism. *The Journal of Geology, 94*(3), 365-379.

Page, R., & Sun, S. (1998). Aspects of geochronology and crustal evolution in the Eastern Fold Belt, Mt Isa Inlier∗. *Australian Journal of Earth Sciences, 45*(3), 343-361.

Paton, C., Hellstrom, J., Paul, B., Woodhead, J., & Hergt, J. (2011). Iolite: Freeware for the visualisation and processing of mass spectrometric data. *Journal of Analytical Atomic Spectrometry, 26*(12), 2508-2518.

Perring, C., Pollard, P., & Nunn, A. (2001). Petrogenesis of the Squirrel Hills granite and associated magnetite-rich sill and vein complex: Lightning Creek prospect, Cloncurry district, northwest Queensland. *Precambrian Research, 106*(3), 213-238.

Pollard, P., & McNaughton, N. (1997). U/Pb geochronology and Sm/Nd isotope characterization of Proterozoic intrusive rocks in the Cloncurry district, Mount Isa inlier, Australia. *AMIRA P438 Cloncurry Base Metals and Gold Final Report, Section, 4*, 19.

Pollard, P., & Perkins, C. (1997). 40Ar/39Ar geochronology of alteration and Cu–Au–Co mineralization in the Cloncurry district, Mount Isa Inlier. *P438 Cloncurry Base Metals and Gold Final Report, Section, 3*.

Putnis, A. (2009). Mineral replacement reactions. *Reviews in Mineralogy and Geochemistry, 70*(1), 87-124.

Roberts, N., & Walker, R. (2016). U-Pb geochronology of calcite-mineralized faults: Absolute timing of rift-related fault events on the northeast Atlantic margin. *Geology, 44*(7), 531-534.

Rubenach, M., Foster, D., Evins, P., Blake, K., & Fanning, C. (2008). Age constraints on the tectonothermal evolution of the Selwyn Zone, Eastern fold belt, Mount Isa Inlier. *Precambrian Research, 163*(1), 81-107.

Rusk, B., Oliver, N., Cleverley, J., Blenkinsop, T., Zhang, D., Williams, P., & Habermann, P. (2010). Physical and chemical characteristics of the Ernest Henry iron oxide copper gold deposit, Australia; implications for IOGC genesis: PGC Publishing.

Schoene, B., Crowley, J., Condon, D., Schmitz, M., & Bowring, S. (2006). Reassessing the uranium decay constants for geochronology using ID-TIMS U–Pb data. *Geochimica et Cosmochimica Acta, 70*(2), 426-445.

Sharib, A., & Sanislav, I. (2013). Polymetamorphism accompanied switching in horizontal shortening during Isan Orogeny: Example from the Eastern Fold Belt, Mount Isa Inlier, Australia. *Tectonophysics, 587*, 146-167.

Shuang, Y., Bi, X., Hu, R., Peng, J., Li, H., Li, D., & Zhu, C. (2010). REE, Mn, Fe, Mg and C, O Isotopic Geochemistry of Calcites from Furong Tin Deposit, South China: Evidence for the Genesis of the Hydrothermal Ore-forming Fluids. *Resource geology, 60*(1), 18-34.

Sun, S., & McDonough, W. (1989). Chemical and isotopic systematics of oceanic basalts: implications for mantle composition and processes. *Geological Society, London, Special Publications, 42*(1), 313-345.

Taylor, R. (2017). Overview report concerning 10 samples from the 'inter-lens' zone of the Ernest Henry deposit, Queensland. Tasmania.

Twyerould, S. (1997). *The Geology and Genesis of the Ernest Henry Fe-Cu-Au Deposit, NW Queensland, Australia.* (Doctor of Philosophy Dissertation), University of Oregon.

Williams, M., Holwell, D., Lilly, R., Case, G., & McDonald, I. (2015). Mineralogical and fluid characteristics of the fluorite-rich Monakoff and E1 Cu–Au deposits, Cloncurry region, Queensland, Australia: Implications for regional F–Ba-rich IOCG mineralisation. *Ore Geology Reviews, 64*, 103-127.

Williams, P. (1998). Metalliferous economic geology of the Mt Isa eastern succession, Queensland. *Australian Journal of Earth Sciences, 45*(3), 329-341.

Williams, P., Barton, M., Johnson, D., Fontboté, L., De Haller, A., Mark, G., . . . Marschik, R. (2005). Iron oxide copper-gold deposits: Geology, space-time distribution, and possible modes of origin. *Economic Geology*, 371-405.

Wyborn, L. (1998). Younger ca 1500 Ma granites of the Williams and Naraku Batholiths, Cloncurry district, eastern Mt Isa Inlier: Geochemistry, origin, metallogenic significance and exploration indicators∗. *Australian Journal of Earth Sciences, 45*(3), 397-411.

APPENDIX A – LOGS OF THE DRILL CORES SAMPLED AT ERNEST HENRY MINE

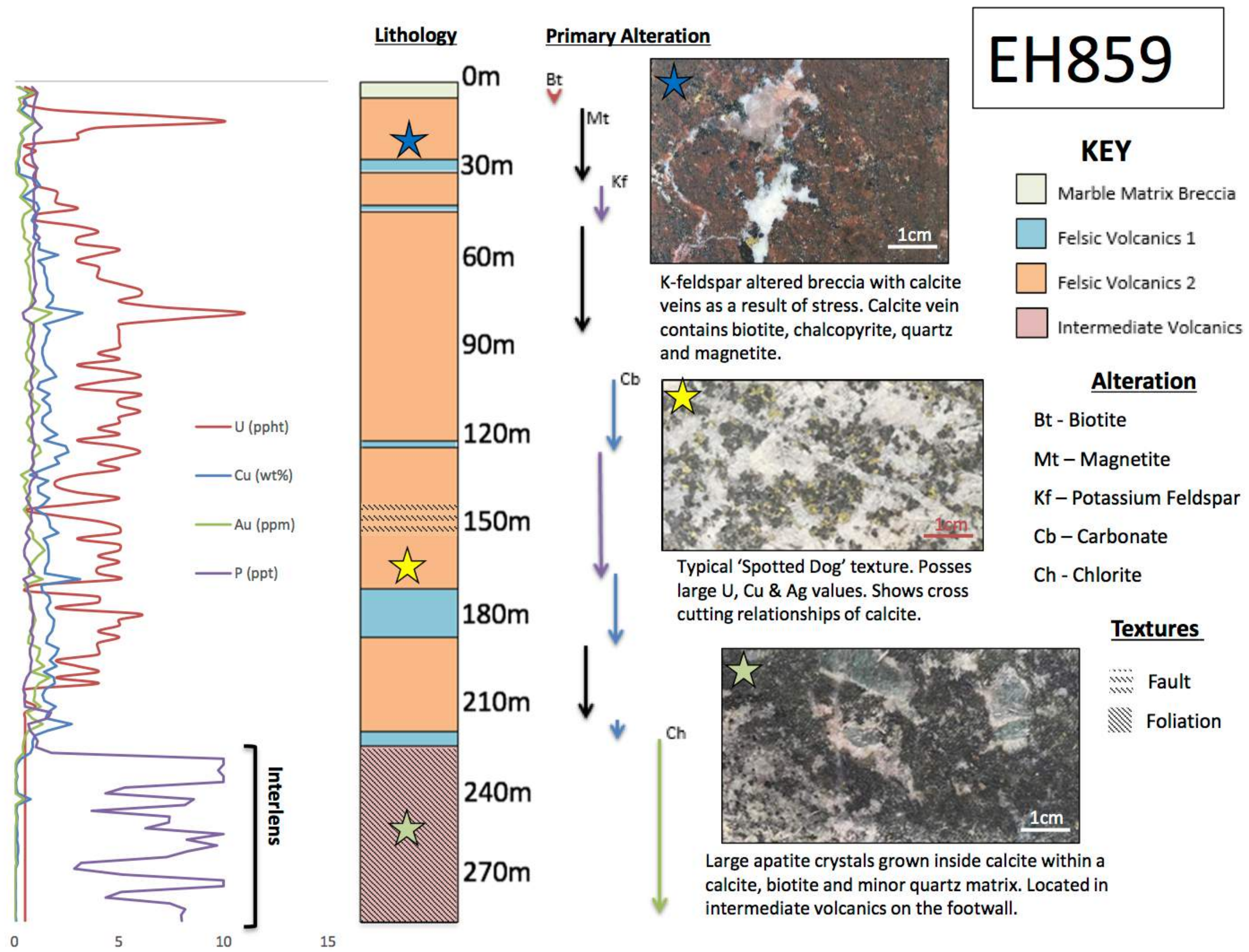

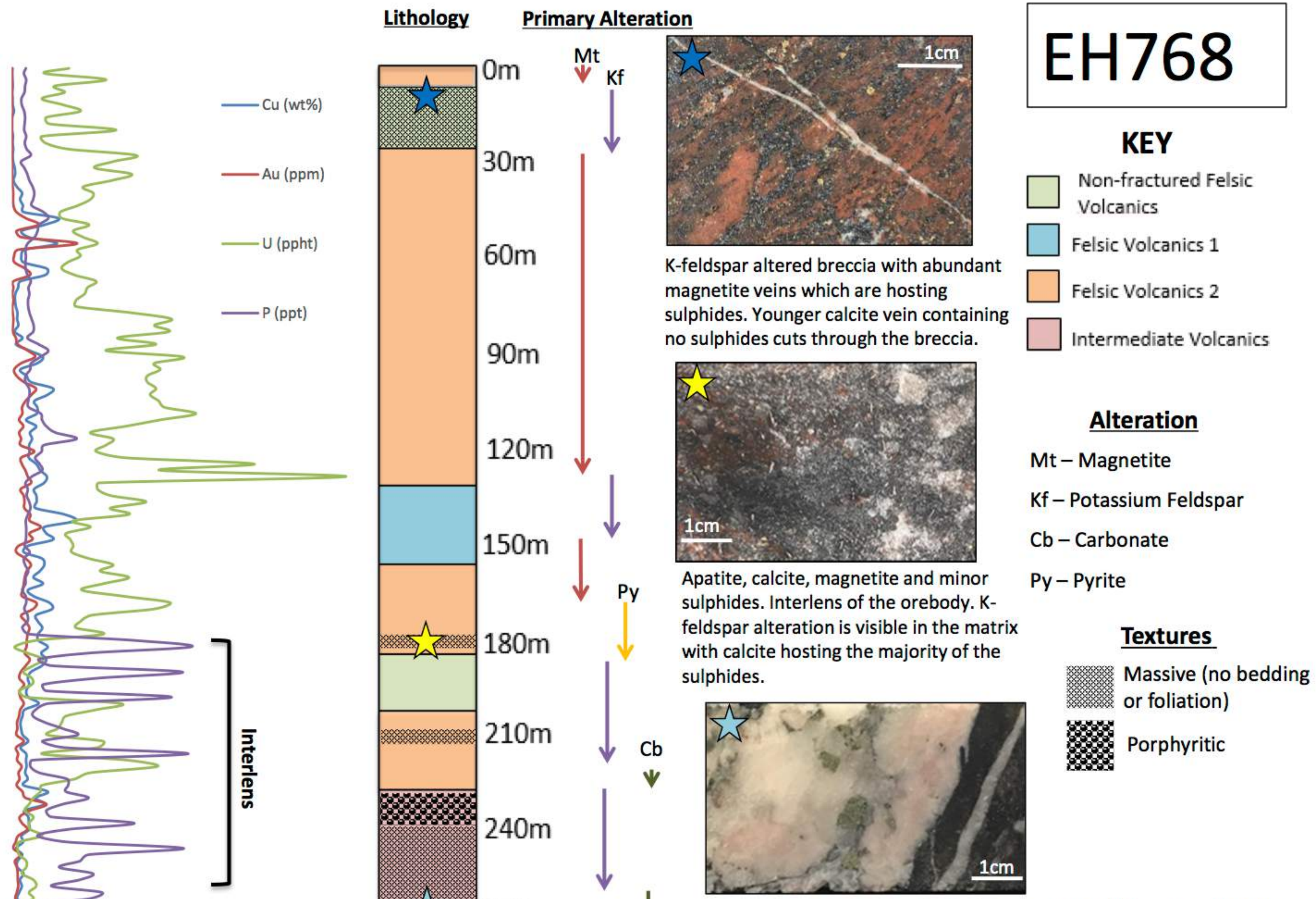

K-feldspar altered breccia with abundant magnetite veins which are hosting sulphides. Younger calcite vein containing no sulphides cuts through the breccia.

Apatite, calcite, magnetite and minor sulphides. Interlens of the orebody. K-feldspar alteration is visible in the matrix with calcite hosting the majority of the sulphides.

Large calcite vein cutting through a magnetite rich breccia containing minimal sulphides and apatite. This sample is located in the intermediate volcanics outside of economic mineralization

EH864

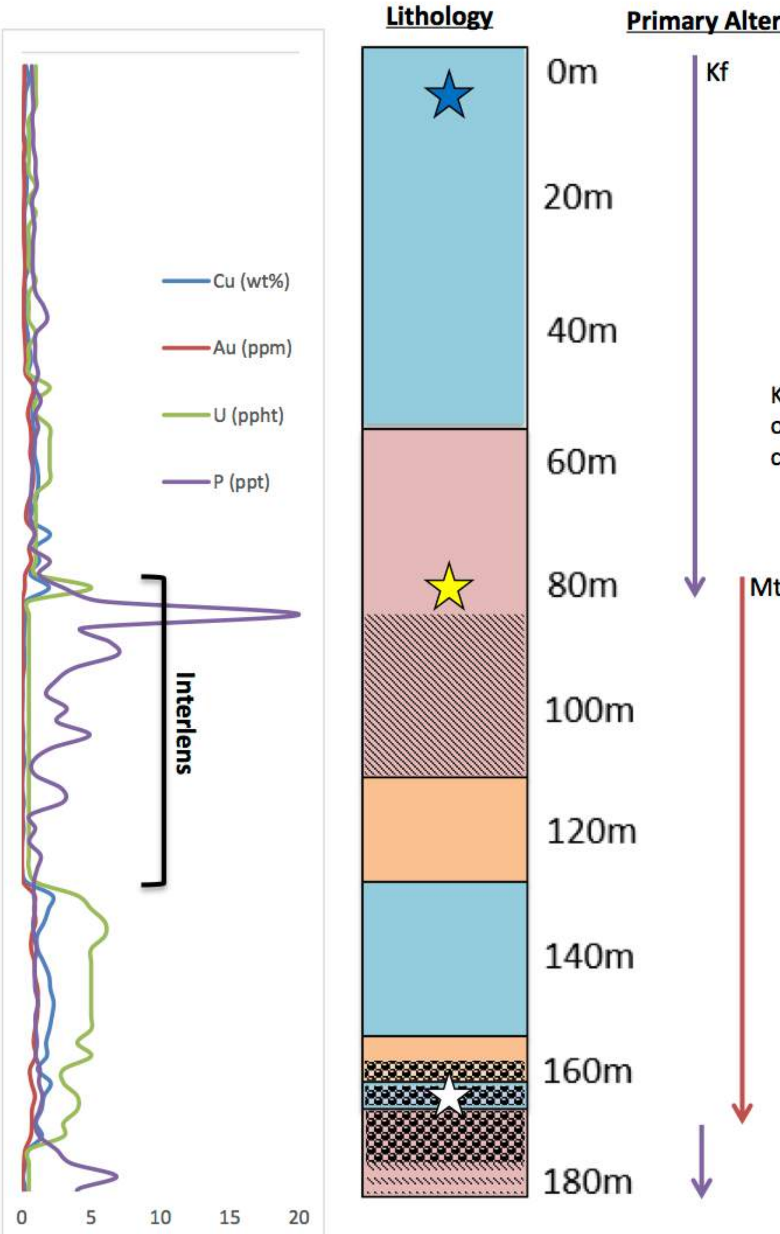

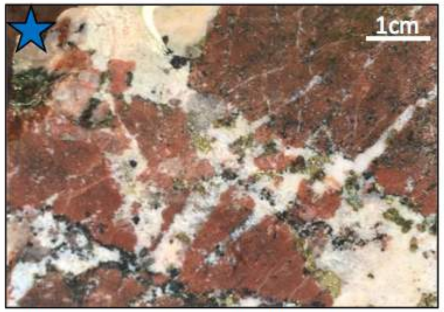

K-feldspar altered breccia with abundant veins of calcite containing magnetite, biotite, quartz, chalcopyrite and pyrite.

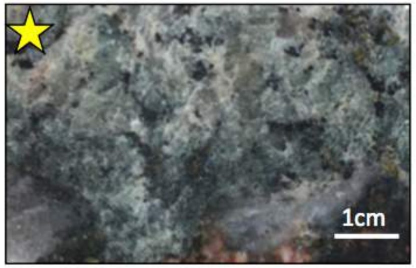

Apatite rich vein containing calcite, magnetite, quartz, chalcopyrite and pyrite. Located in the interlens.

Potassium feldspar altered breccia containing a high percent of magnetite and minimal sulphides. Calcite vein contains potassium feldspar and magnetite.

KEY

Felsic Volcanics 1

Felsic Volcanics 2

Intermediate Volcanics

Alteration

Mt – Magnetite

Kf – Potassium Feldspar

Textures

Fault

Foliation

Porphyritic

APPENDIX B – SAMPLE DESCRIPTIONS AND IMAGES

Sample Number	Depth (m)	Thin Section	Description
Drill Core - EH859			
BC00	170.2	Y	Typical 'Spotted Dog' feature. This was located in apart of the drill core which recorded the highest U, Cu & Ag percent. Also, shows calcite vein cutting through the spotted dog texture.
BC01	232.9	N	Shows very large euhedral and well developed apatite grains. This is located during the entrance of the footwall as you leave the orebody into the intermediate volcanics.
BC02	234.6	Y	Shows very large euhedral and well developed apatite grains. This is also located during the entrance of the footwall as you leave the orebody into the intermediate volcanics.
BC03	236.7	Y	Large, well developed euhedral apatite surrounded by calcite, quartz, magnetite and minor biotite. Located in footwall of mine, as you enter the intermediate volcanics.
BC04	239.2	Y	Large, well developed euhedral apatite surrounded by calcite, quartz, magnetite and minor biotite. Located in footwall of mine, as you enter the intermediate volcanics. Very similar as BC03.
BC05	243	N	Shows apatite, quartz, biotite, magnetite and RRA. Typical of intermediate volcanics texture. Also shows some medium grained apatite crystals.
BC06	246.7	Y	Abundant apatite, almost consists of an apatite vein. Also shows calcite and magnetite as other predominant minerals. Also found in intermediate volcanics within the footwall.
BC07	250.1	N	Shows apatite within a calcite vein. This also shows breccia made up from RRA and magnetite. Also typical of intermediate volcanics
BC08	251.6	Y	Abundant magnetite and calcite with large apatite crystals. Within intermediate volcanics on footwall side of mine. Minor to no sulphides.
BC09	260.2	Y	Large apatite crystals grown inside calcite within a calcite, biotite and minor quartz matrix. Located in intermediate volcanics on the footwall.
BC10	262.1	Y	Large euhedral apatite crystals which have grown within a calcite and magnetite matrix. Shows minor sulphides located in calcite surrounding the grains of apatite. Located in the footwall of the deposit, in the intermediate volcanics.
BC11	276.8	Y	Well-developed & large apatite veins within a magnetite and calcite matrix. Some sulphides are located throughout the matrix and around the apatite crystals. This is well into the footwall of the deposit into the intermediate volcanics.
BC12	281.5	N	Calcite, magnetite and sulphide rich sample. Also contains some apatite around the calcite vein(s). Intermediate volcanics.
BC13	289.8	N	Typical intermediate volcanics. Contains a high amount of sulphides and magnetite with a large calcite vein. Apatite throughout the calcite vein is also visible.
Drill Core - EH768			
BC14	183.1	Y	Apatite, calcite, magnetite and minor sulphides as you approach the interlense of the orebody. Economic mineralization is low. RRA is also visible within the matrix. Calcite hosts majority of the sulphides.
BC15	183.5	N	This shows apatite, calcite, magnetite and RRA. Minor sulphides are also located within the sample, predominantly within the magnetite and calcite rich areas.
BC16	255.1	N	This rocks shows a RRA, calcite and magnetite matric with some minor sulphides and apatite. This is typical of the intermediate volcanics sequence.
BC17	263	Y	Med grains of apatite within calcite, magnetite and minor qtz matrix. No visible sulphides. Interlense of deposit, no economic mineralization.
BC18	264.25	N	This is predominantly a magnetite dominated sample which also contains minor sulphides, with a medium amount of quartz and apatite. Intermediate Volcanics.
BC19	270.9	N	This sample is predominantly calcite and magnetite with some sulphides and apatite within the large calcite vein. This sample is located within the intermediate volcanics outside of the orebody.
Drill Core - EH864			
BC20	81.9	Y	Apatite rich sample with calcite, magnetite, quartz, magnetite, chalcopyrite and pyrite. Found in Interlens outside of economic rich mineralization.
BC21	83.5	Y	Apatite rich vein also containing magnetite, calcite, pyrite, chalcopyrite. Also found in Interlens of orebody, not in economically rich part of orebody.
BC22	88.2	Y	Apatite within calcit, magnetite and some RRE matrix. This also shows to have minimal sulphides. This is located in the interlense between Ernest Henry and Ernest Junior.
BC23	97.1	N	This is also located within the Interlens. This is predominantly made up of a RRA, calcite and magnetite matrix with minor sulphides distributed throughout. Apatite located within the carbonate phase. Also located in the Interlens.
BC24	99	N	This shows a heavily apatite rich vein which appears to be surrounded by calcite. Apatite only appears in calcite rich areas. Matrix is predominantly magnetite and RRA. This is also located in the Interlens.
BC25	101.2	N	This shows well developed apatite phenocrysts within a weathered matrix of RRA, calcite and magnetite. This is also located in the interlense.
BC26	170	N	High magnetite and RRE rich rock. Contains minimal sulphides, however does possess a large calcite vein containing RRE and magnetite.

Sample BC00

Sample BC01

Sample BC02

Sample BC03

Sample BC04

Sample BC05

Sample BC06

Sample BC07

Sample BC08

Sample BC09

Sample BC10

Sample BC11

Sample BC12

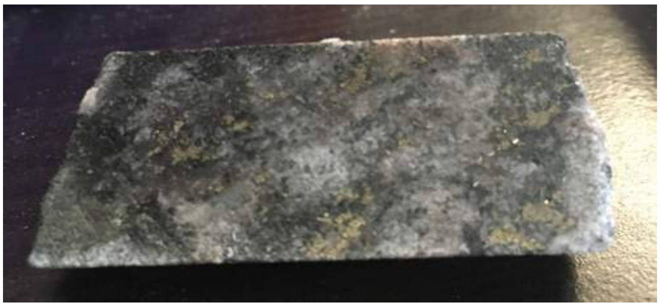

Sample BC13

Sample BC14

Sample BC15

Sample BC16

Sample BC17

Sample BC18

Sample BC19

Sample BC20

Sample BC21

Sample BC22

Sample BC23

Sample BC24

Sample BC25

Sample BC26

APPENDIX C – ELEMENTAL ACQUISITION PARAMETERS FOR LA-ICP-MS WORK

Apatite Maps		Calcite Geochronology		Apatite Geochronology		Calcite Trace Elements	
Mass/Element Name	IntegTime (s)	Mass/Element Name	IntegTime (s)	Mass/Element Name	IntegTime (s)	Mass/Element Name	IntegTime (s)
24 Mg	0.005	43 Ca	0.005	29 Si	0.005	24 Mg	0.01
29 Si	0.005	202 Hg	0.03	35 Cl	0.005	29 Si	0.005
31 P	0.005	204 Pb	0.03	43 Ca	0.005	43 Ca	0.005
35 Cl	0.005	206 Pb	0.05	51 V	0.005	51 V	0.02
43 Ca	0.005	207 Pb	0.05	55 Mn	0.005	55 Mn	0.05
51 V	0.01	208 Pb	0.01	88 Sr	0.005	75 As	0.02
55 Mn	0.005	232 Th	0.02	89 Y	0.005	88 Sr	0.02
75 As	0.01	238 U	0.03	90 Zr	0.005	89 Y	0.02
88 Sr	0.01			139 La	0.005	90 Zr	0.02
89 Y	0.01			140 Ce	0.005	139 La	0.02
90 Zr	0.01			141 Pr	0.005	140 Ce	0.02
139 La	0.01			146 Nd	0.005	141 Pr	0.02
140 Ce	0.01			147 Sm	0.005	146 Nd	0.02
141 Pr	0.01			153 Eu	0.005	147 Sm	0.02
146 Nd	0.01			157 Gd	0.005	153 Eu	0.02
147 Sm	0.01			159 Tb	0.005	157 Gd	0.02
153 Eu	0.01			163 Dy	0.005	159 Tb	0.02
157 Gd	0.01			165 Ho	0.005	163 Dy	0.02
159 Tb	0.01			166 Er	0.005	165 Ho	0.02
163 Dy	0.01			169 Tm	0.005	166 Er	0.02
165 Ho	0.01			172 Yb	0.005	169 Tm	0.02
166 Er	0.01			175 Lu	0.005	172 Yb	0.02
169 Tm	0.01			202 Hg	0.02	175 Lu	0.02
172 Yb	0.01			204 Pb	0.02	202 Hg	0.01
175 Lu	0.01			206 Pb	0.1	204 Pb	0.02
202 Hg	0.01			207 Pb	0.1	206 Pb	0.02
204 Pb	0.01			208 Pb	0.01	207 Pb	0.02
206 Pb	0.01			232 Th	0.02	208 Pb	0.02
207 Pb	0.01			238 U	0.03	232 Th	0.02
208 Pb	0.01					238 U	0.02
232 Th	0.01						
238 U	0.01						

APPENDIX D – ADDITIONAL PETROGRAPHY

Petrography – Sample BC00

This sample consists of ~80% calcite with cpy, py, mg, bt, qtz and minor ap. Cl and Epd in some cases, is seen rimming sulphides. Most the calcite is very coarse-grained with profound twinning. A second calcite generation is visible which cross cuts the ore-stage calcite. Evidence shows the later calcite "spilling" into first generation calcite (based on twinning planes and reflective index, image below). In some cases, ca has grown around qtz, and the calcite also shows to be brecciating the sulphides. Sulphide rich sample, is representable of the locally termed "Spotted Dog" texture.

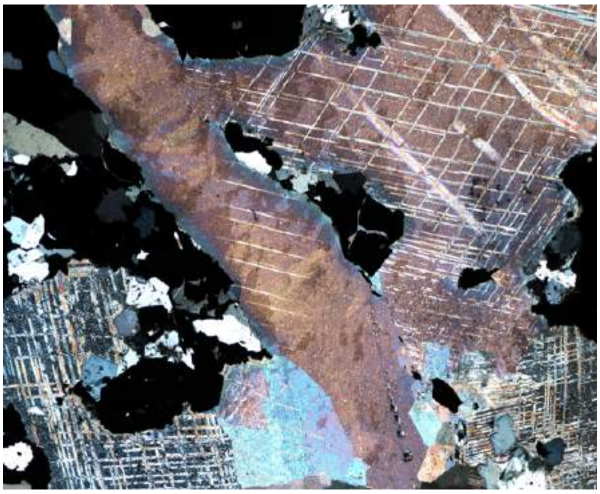

Petrography – Sample BC02

This sample depicts coarse-grained apatite brecciated by ca, bt, qtz with minimal sulphides. Ap is large, and shows a spatial relationship to coarse-grained ca. Reaction fronts between the ca and ap is visible, characterised by a high order biofringence. Cl is also visible throughout samples, mainly confined to smaller vein like structures. Throughout sample, it is shown that qtz ranges from coarse- to fine-grained.

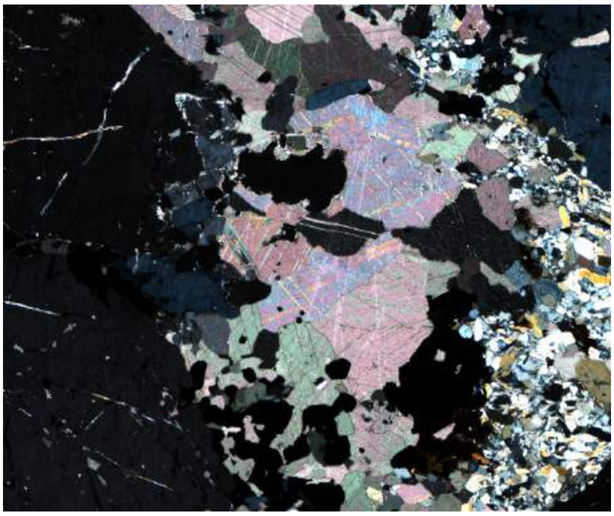

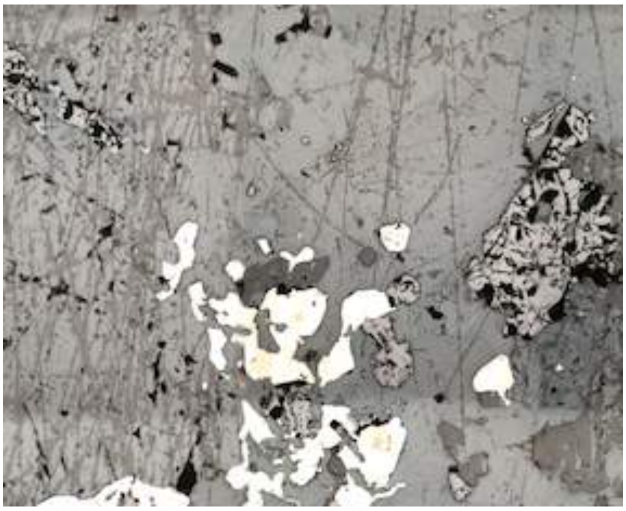

Petrography – Sample BC03

This sample shows very coarse grained apatite brecciated by a groundmass of coarse-grained Ca with minor sulphides, biotite, qtz and cl. A later Ap2 generation is visible and is characterized by smaller and rounded apatite grains distributed in cracks and proximal to large ap grains. Reaction fronts seen between coarse-grained apatite and coarse-grained calcite grains. Large apatite is relatively intact (little reworking?). Sulphide mineralization and biotite only located in distinct vein regions throughout the sample. Mg is also the abundant sulphide throughout the sample.

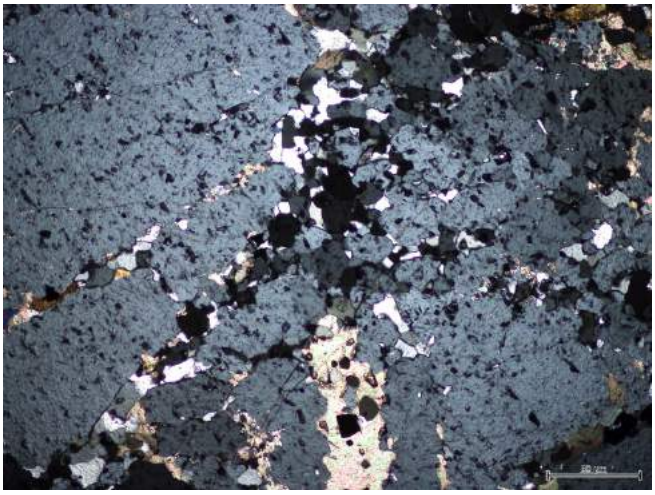

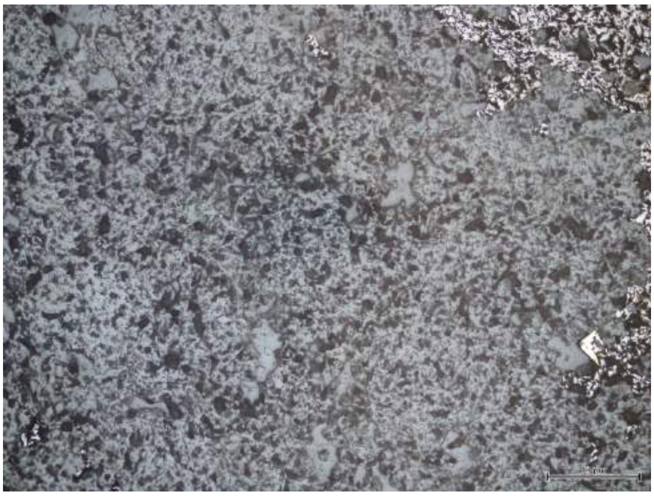

Petrography – Sample BC04
Shows coarse-grained apatite brecciated by a mineralogy of bt, mg, sulphides, hbl and coarse-grained calcite. Ca, qtz and bt range from fine- to coarse-grained. Minimal, however heavily altered and replaced st is visible. A large reaction front is visible showing high order interference colours between large ca and ap grains.

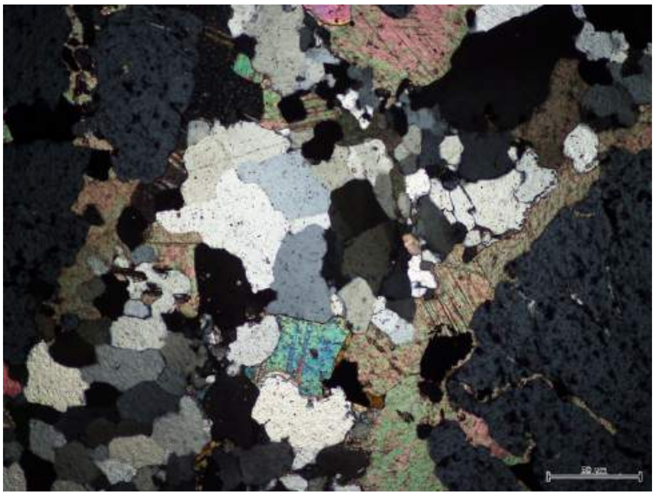

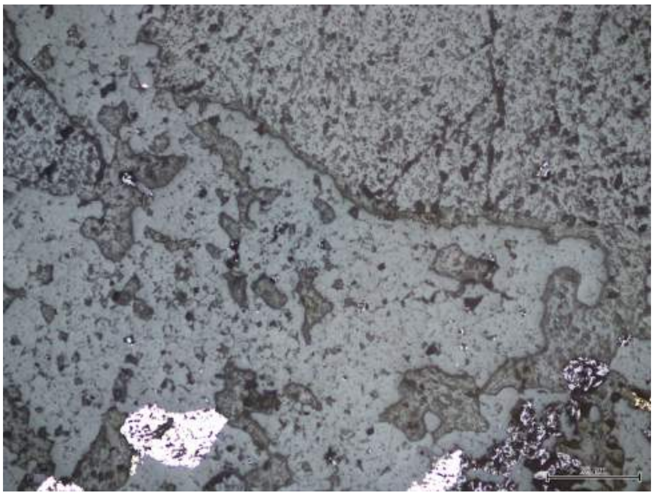

Petrography – Sample BC06
A visible shearing texture is present throughout the sample. This texture seems to have displaced? The coarse-grained apatite. Apatite is less fractures than previous samples. Groundmass of ca, qtz, bt, mg with very minor sulphides. Calcite is found throughout sample, however most prominent brecciating apatite grains. Again, heavily replaced st is visible ad replaced by the groundmass. coarse-grained biotite is only located within distinctive veins alongside some sulphides.

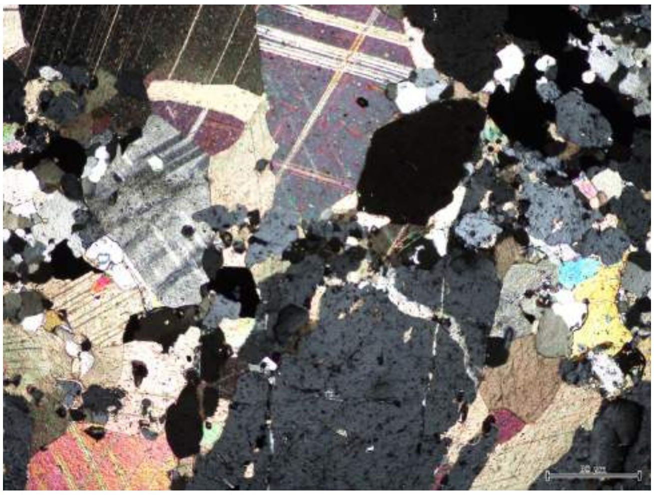

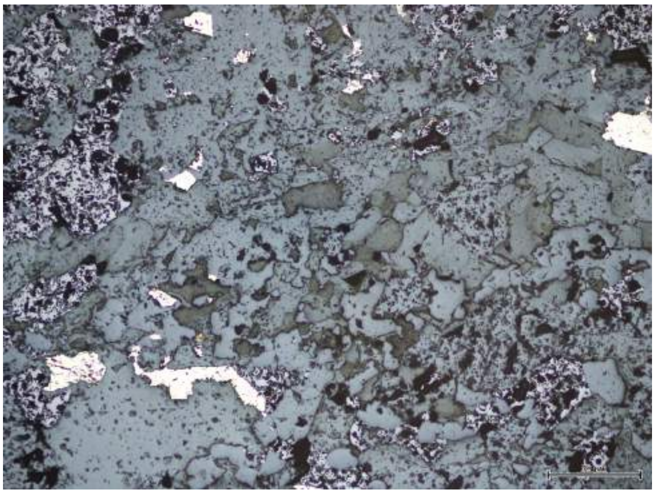

Petrography – Sample BC08
A dominant shearing texture is present throughout this sample. Apatite is medium-grained with some coarse-grained apatite visible. Groundmass is predominantly fine-grained qtz, with coarse-grained calcite located around large apatite grains. Some minor bt, mg, mcv visible. No sulphides are present in this sample. Heavy reaction textures between apatite and calcite are visible (high order interference colurs).

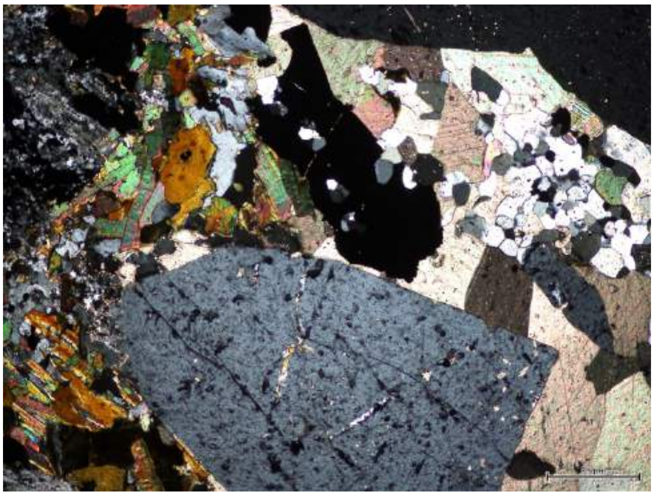

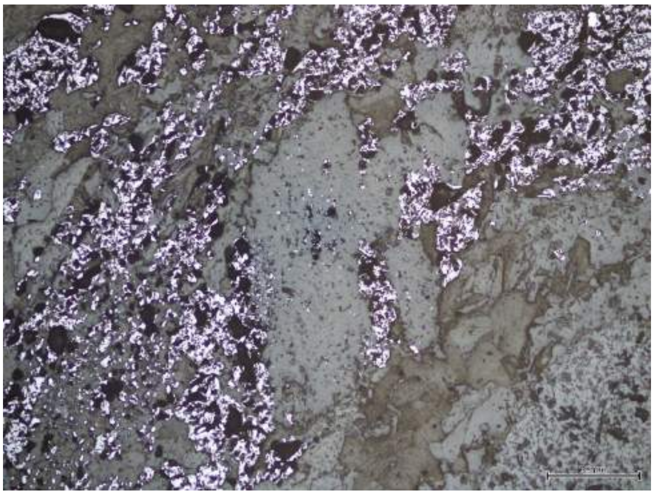

Petrography – Sample BC09
This sample shows coarse-grained apatites brecciated by a ground mass of predominantly coarse-grained calcite with minor qtz, mg, bt, hbl, cl and py. Very minor sulphides are visible in this sample. The apatites are relatively intact, maybe due to minimal reworking. Reaction front between ap and ca grains are also visible

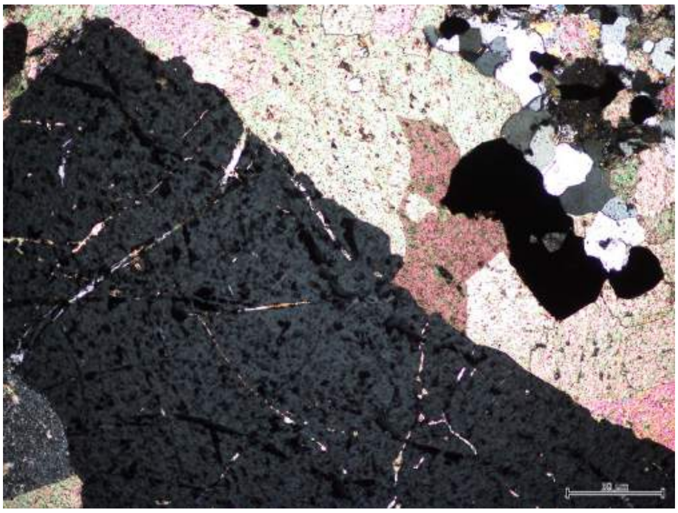

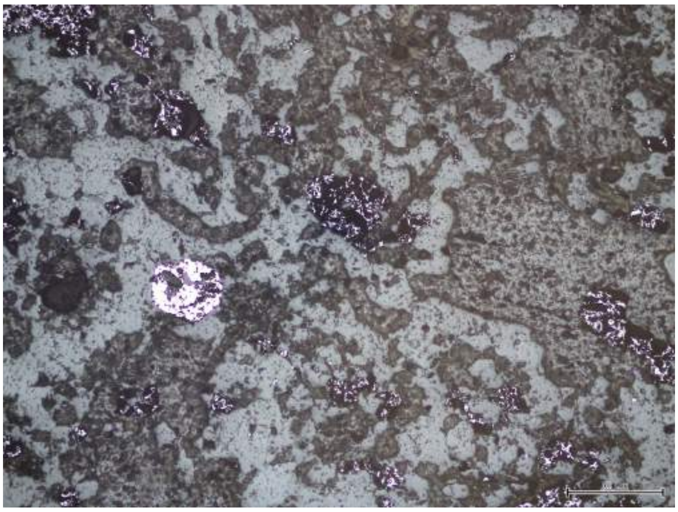

Petrography – Sample BC10
This sample shows coarse-grained apatite brecciated by coarse-grained calcite. Minor sulphides are present in the groundmass, with Mg visible around large ap grains. Typical reaction fronts visible between ca and ap. Groundmass is made up of fine-grained qtz, ca, bt and hbl with minor cl and sulphides. In some areas, sulphides are visible within the ca brecciating the apatite. Ap2 generation is also visible, occupying space in fractures and around the large Ap grains. Very large apatites (cm) scale throughout sample.

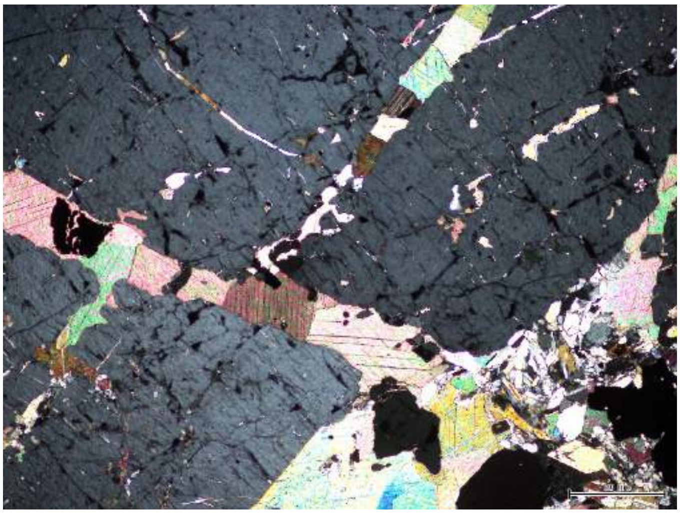

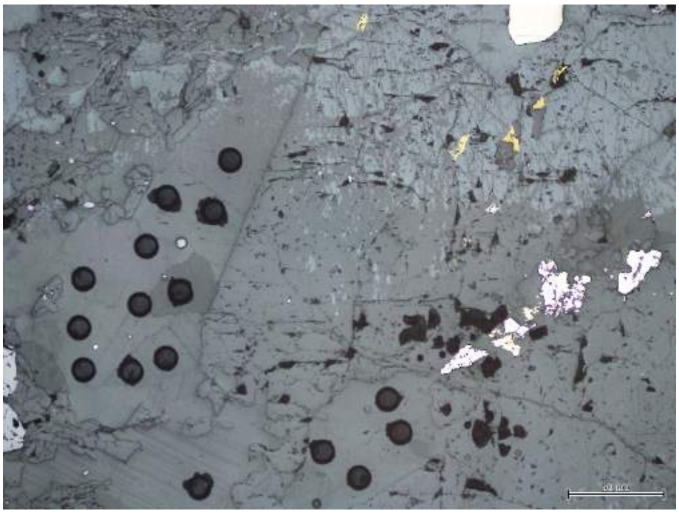

Petrography – Sample BC11
Apatite ranges from coarse-grained to fine-grained. Minor py and cpy confined to areas of calcite. High amount of mg present in the groundmass of qtz, ca and bt. Ca is also very abundant throughout sample. Common reaction front between ca and ap visible. Coarse-grained ca found around areas of coarse-grained apatite, and predominantly brecciates the apatite (only minimal). Mg visible within the groundmass as a minor component.

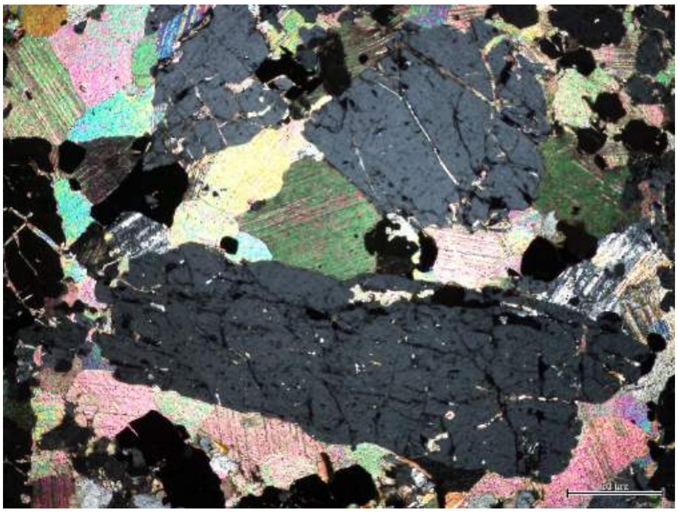

Petrography – Sample BC14
This sample looks more like typical ore-grade breccia rather than typical samples found within the Interlens. Apatite from this sample is relatively small and ranges from heavily brecciated to not brecciated at all. Brecciating minerals are predominantly qtz and ca. Minor sulphides and red rock alteration present. Ca and mg are both abundant along fine-grained qtz and ca. Sulphides are only located within ca. Mg shows to possess inclusions of qtz.

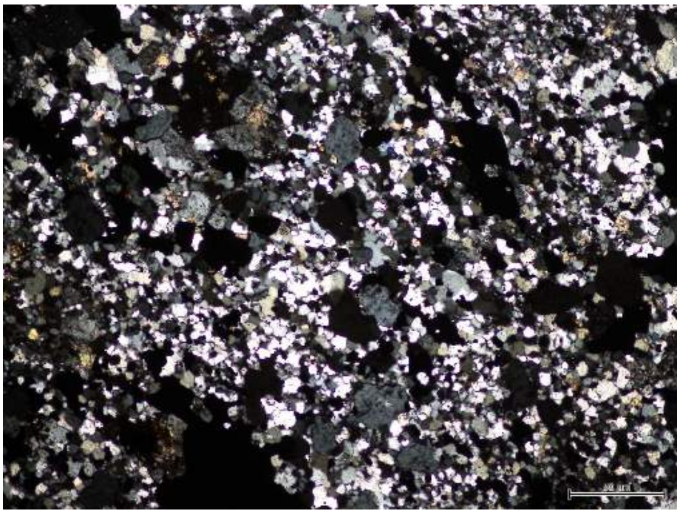

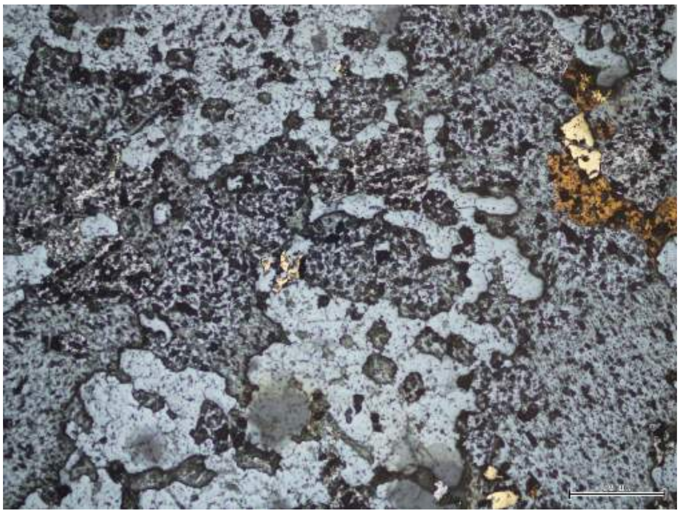

Petrography – Sample RML (E1 deposit)
Calcite vein is very-coarse grained (up to cm scale) and is predominantly calcite (99%), also, calcite inclusions within large calcite veins. Large amount of zonation is resent around the edge of the calcite towards the ore-grade assemblage. Calcite cross cuts ore-stage assemblage, which consists of sulphides, bt, qtz, dark rocks. Ore-stage mineralization is a very fine grained assemblage, very heavily brecciated and very messy.

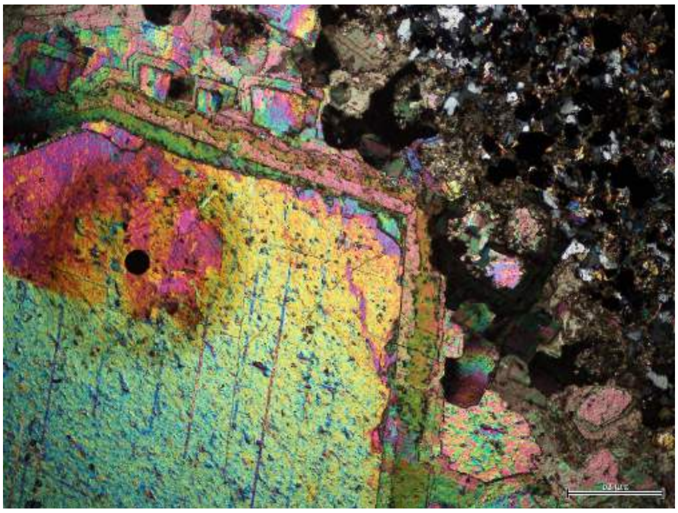

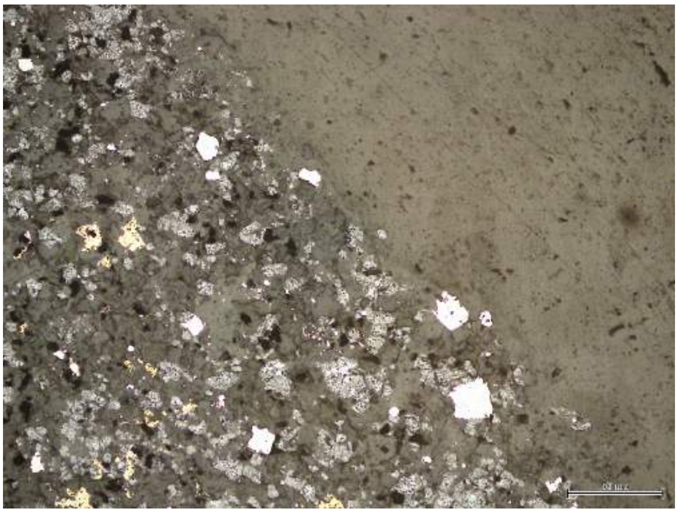

Petrography – Sample BC17
This sample is predominantly groundmass (90%), with a small abundance of Ap. The fine-grained groundmass consists of qtz, ca, mg, feldspar? Mg with no sulphides visible. Ap is relatively un-brecciated, and generally surrounded by fine to coarse-grained calcite. Mg visible throughout, which is sometimes brecciated by calcite.

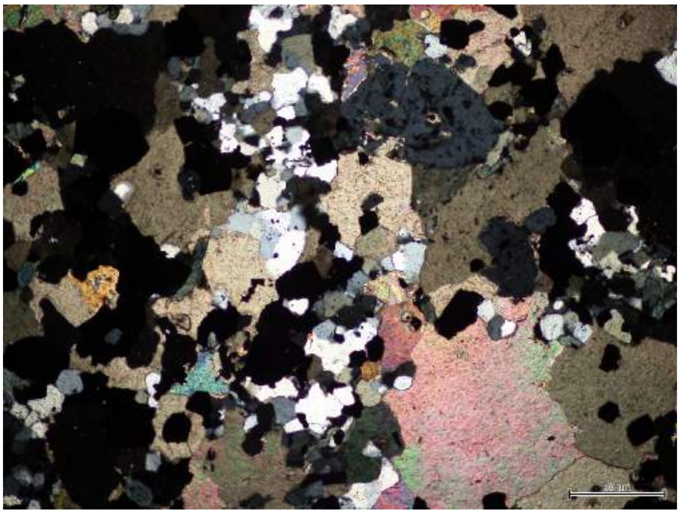

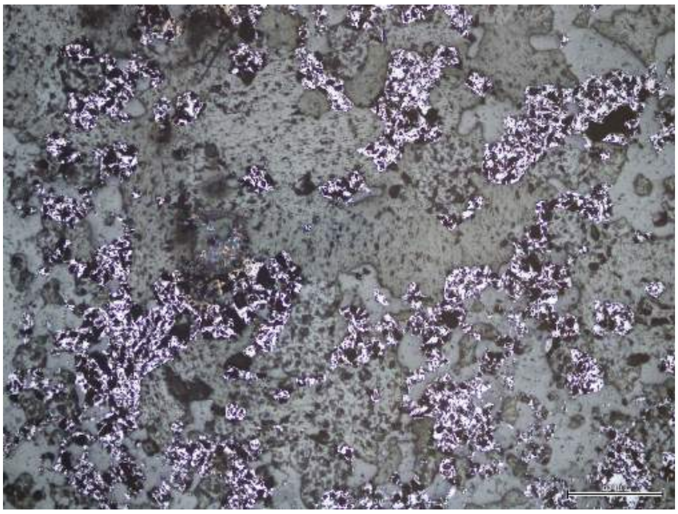

Petrography – Sample BC20
Coarse-grained apatite common, often highly brecciated by ca and qtz. High amount of sulphides in this sample, up to ~5% groundmass. Ca and qtz range from fine- to coarse grained. Actinolite found in veins with fine-grained qtz, mg and bt throughout sample, somewhat comparable to the ore-stage breccia associated with the RML sample. Reaction fronts between Ca and ap visible. Ap 2 is very common throughout this sample, visible throughout the groundmass.

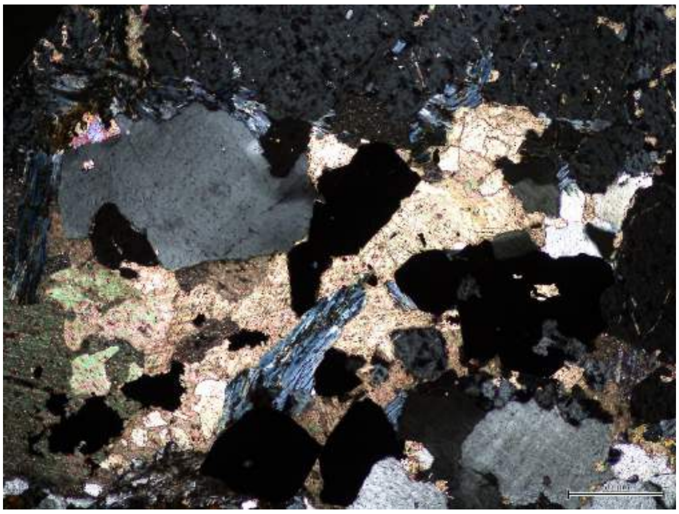

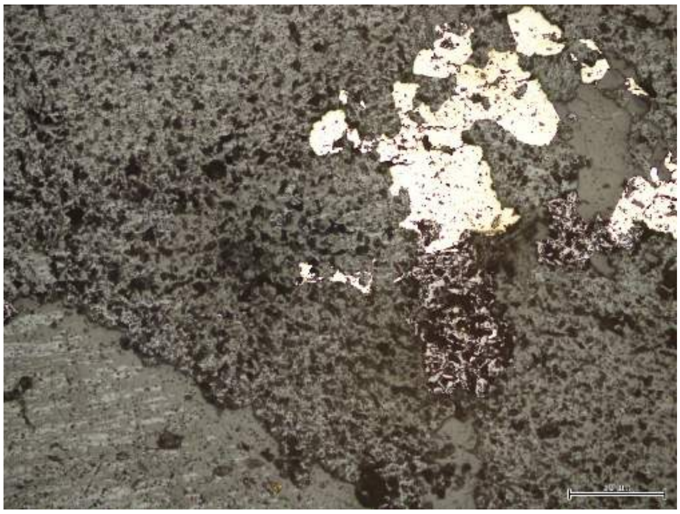

Petrography – Sample BC21
One very large euhedral apatite grain is visible, which is brecciated predominantly by ca. Again, coarse-grained calcite is found proximal to apatite. Groundmass contains ~5% sulphides, with some Mg, ca, qtz, with biotite ranging from coarse-grained to fine-grained. Qtz is predominantly fine-grained. Sulphides are generally spatially associated with Ca, and in some cases brecciated Ca. Large coarse-grained calcite is often brecciated by the fine-grained groundmass.

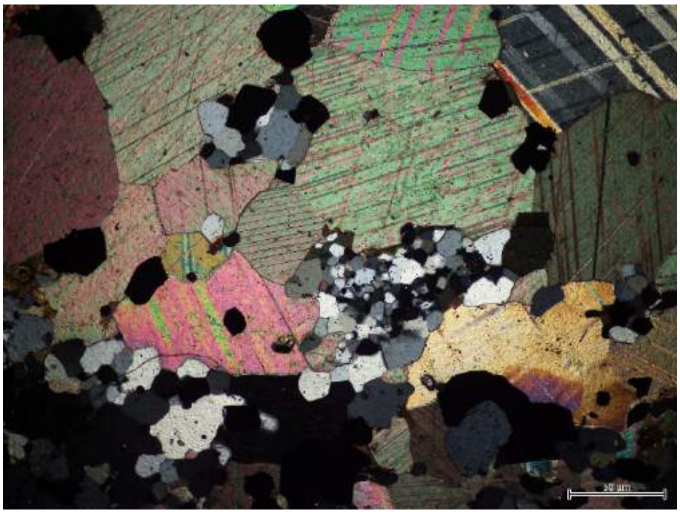

Petrography – Sample BC22

Apatite ranges from coarse-grained to relatively fine-grained. A distinct shearing texture is visible and shown by a fin-grained mineralogy of ca, qtz and bt. Coarse-grained ca is associated located proximal to coarse-grained apatite. Sulphides show to brecciate the apatite and form around it, however the dominant brecciating mineral is calcite. Groundmass is relatively mg rich, with minor sulphides. This sample is dominated by groundmass, commonly fine to medium -grained.

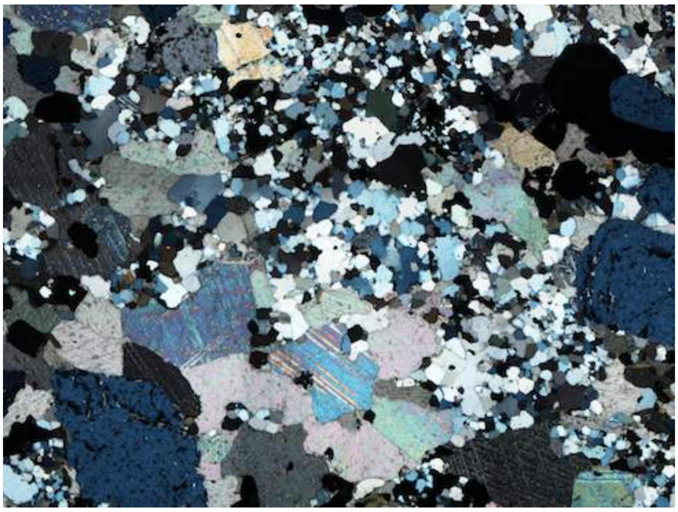

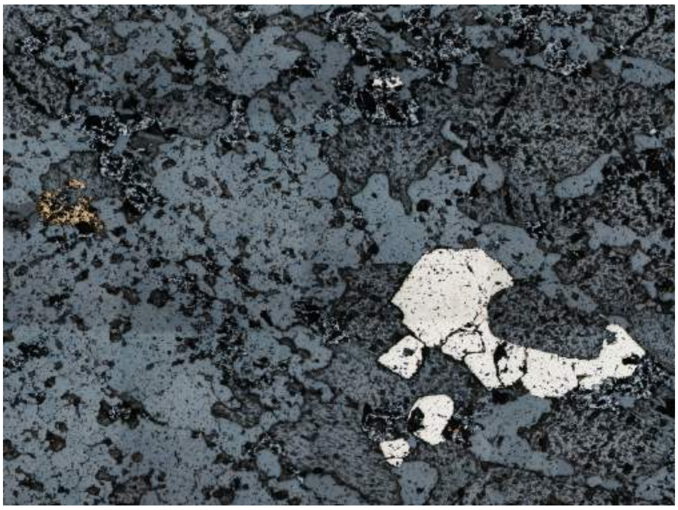

APPENDIX E – APATITE U-PB GEOCHRONOLOGY DATA

Sample	238U/206Pb Final	238U/206Pb Propagated Error	Pb207/Pb206 Final	207Pb/206Pb Propagated Error	238U/206Pb vs 207Pb/206Pb Error Correlation	Final 207Pb Age	Final 207Pb Age Propagated Error	238U (ppm)	206Pb (ppm)
BC00_1	1.776199	0.1640539	0.331	0.016	0.025393	1490	160	1.25	2.37
BC00_2	2.03666	0.1576234	0.328	0.022	-0.39597	1450	150	1.6	2.54
BC00_3	2.212389	0.132156	0.299	0.014	0.21914	1465	130	1.584	2.511
BC00_4	2.55102	0.2082466	0.237	0.017	-0.44794	1584	110	2.6	3.38
BC00_5	2.347418	0.1322489	0.281	0.014	0.0091816	1479	140	1.838	2.68
BC00_6	1.680672	0.1525316	0.341	0.015	-0.45668	1650	140	1.559	2.83
BC00_7	1.724138	0.1426873	0.369	0.027	0.46597	1350	230	0.745	1.55
BC00_8	1.727116	0.1163342	0.348	0.018	0.25615	1530	210	1.28	2.317
BC00_9	1.582278	0.1226767	0.367	0.023	0.085505	1440	240	0.927	1.84
BC00_10	1.821494	0.1161244	0.366	0.021	0.27777	1470	210	0.915	1.681
BC00_11	1.872659	0.1087124	0.332	0.017	0.25826	1580	220	1.132	2.041
BC00_12	2.016129	0.1382024	0.321	0.028	0.16793	1580	230	1.04	1.88
BC00_13	2.702703	0.1899196	0.211	0.015	-0.11114	1609	120	1.96	2.26
BC00_14	2.994012	0.170318	0.1912	0.0092	-0.092478	1522	100	3.42	3.847
BC10A_1	2.754821	0.1517808	0.213	0.014	-0.23571	1716	140	5.85	7.2
BC10A_2	2.86533	0.1642023	0.243	0.015	0.40758	1567	130	4.448	5.33
BC10A_3	2.857143	0.1795918	0.246	0.014	0.095539	1562	120	4.64	5.61
BC10A_4	2.915452	0.1699972	0.252	0.014	-0.21323	1521	130	5.11	5.97

BC10A_5	2.853881	0.1547481	0.256	0.013	0.33715	1500	120	5.4	6.6
BC10A_6	2.816901	0.1666336	0.242	0.011	0.40532	1562	100	5.51	6.96
BC10A_7	1.901141	0.1409591	0.411	0.018	0.10617	1543	130	2.31	3.96
BC10A_8	1.988072	0.1462399	0.44	0.03	-0.013363	1370	170	1.66	2.93
BC10A_9	2.469136	0.1646091	0.247	0.012	0.18403	1772	130	4.48	6.12
BC10A_10	2.849003	0.1704532	0.241	0.013	0.57432	1543	150	5.32	6.55
BC10A_11	2.617801	0.1439105	0.308	0.015	0.2794	1476	150	3.32	4.32
BC10A_12	3.082614	0.1710452	0.216	0.012	0.51921	1506	140	4.907	5.4
BC10A_13	2.610966	0.1704286	0.303	0.019	0.43737	1470	150	2.128	2.77
BC10A_14	1.996008	0.1354576	0.394	0.021	0.61538	1580	210	1.808	3.05
BC10A_15	2.493766	0.1492528	0.28	0.014	0.15526	1654	130	3.36	4.5
BC10A_16	2.320186	0.1561146	0.266	0.015	0.3097	1830	200	3.93	6.05
BC10A_17	2.840909	0.1614153	0.249	0.012	0.43195	1543	120	5.86	6.88
BC10A_18	2.793296	0.1716551	0.247	0.016	-0.22278	1577	110	5.68	6.73
BC10A_19	2.493766	0.1554717	0.299	0.022	-0.087238	1585	150	3.52	4.82
BC10A_20	2.192982	0.1346568	0.328	0.019	0.19036	1689	160	5.26	7.75
BC10A_21	1.968504	0.1666253	0.321	0.02	-0.12358	1790	140	1.98	3.51
BC10A_22	2.777778	0.2160494	0.255	0.027	-0.25244	1550	130	4.4	6.02
BC10A_23	2.475248	0.1531713	0.32	0.018	-0.155	1532	140	2.72	3.89
BC10A_24	3.134796	0.2161928	0.2	0.013	-0.6307	1579	92	5.35	5.6
BC10A_25	2.475248	0.1715518	0.326	0.019	0.21383	1610	130	2.41	3.12
BC10A_26	2.770083	0.1764873	0.264	0.013	0.14763	1633	130	3.72	4.48
BC10A_27	2.873563	0.1981768	0.243	0.014	-0.13735	1577	90	4.4	5.17
BC10A_28	3.019324	0.1640937	0.222	0.012	-0.17753	1605	110	4.41	5.05
BC10A_29	2.624672	0.1860004	0.274	0.016	0.042591	1621	110	3.31	4.09
BC10A_30	2.222222	0.1728395	0.386	0.029	-0.012312	1630	170	1.813	2.667
BC10A_31	2.375297	0.1466929	0.338	0.019	0.38666	1690	170	2.088	2.9
BC10A_32	2.80112	0.1726181	0.288	0.02	-0.25734	1511	110	3.2	3.81

BC10A_33	2.923977	0.1709928	0.25	0.012	-0.037815	1559	100	4.953	5.63
BC10A_34	3.067485	0.1787798	0.217	0.013	-0.23775	1565	99	5.03	5.54
BC10A_35	2.994012	0.170318	0.231	0.012	-0.069411	1592	92	4.46	5.04
BC10A_36	2.994909	0.1704201	0.225	0.012	-0.093454	1618	120	4.06	4.51
BC10A_37	3.039514	0.1940115	0.24	0.014	-0.24592	1534	110	4.28	4.65
BC10A_38	2.915452	0.1869969	0.257	0.014	-0.069755	1604	110	3.651	4.15
BC10A_39	2.770851	0.1535523	0.279	0.011	-0.027119	1603	110	7.34	9.18
BC10A_40	2.923977	0.1966417	0.2347	0.0098	-0.45134	1583	88	7.51	8.46
BC10A_41	2.840909	0.1694861	0.285	0.02	-0.39399	1535	73	7.38	8.79
BC10A_42	3.11042	0.1644701	0.236	0.01	0.036958	1508	96	7.06	7.55
BC10A_43	2.88517	0.1581599	0.237	0.01	0.16949	1631	120	6.02	6.91
BC10A_44	2.80112	0.2118494	0.239	0.017	-0.58135	1609	68	6.73	7.61
BC10A_45	2.898551	0.2016383	0.234	0.012	0.10935	1576	89	6.25	6.88
BC10A_46	2.994012	0.1792822	0.247	0.012	-0.38666	1581	110	6.58	7.28
BC10A_47	2.857143	0.1959184	0.24	0.011	-0.39548	1632	100	5.85	6.52
BC10A_48	2.985075	0.1693027	0.247	0.01	0.056014	1565	120	6.49	7.25
BC10A_49	2.898551	0.1680319	0.25	0.011	-0.083863	1595	100	6.85	8
BC10A_50	2.518892	0.2157237	0.268	0.019	-0.31608	1760	120	3.6	4.38
BC10A_51	2.906977	0.1774608	0.293	0.015	0.0079641	1486	100	3.64	3.99
BC10A_52	3.184713	0.202848	0.1958	0.0064	0.061147	1563	98	6.19	6.61
BC10A_53	3.030303	0.2662994	0.245	0.02	0.3376	1550	160	8	7.96
BC10A_54	2.832861	0.2728535	0.222	0.011	-0.35037	1575	63	5.42	6.08
BC10A_55	2.97619	0.212585	0.231	0.012	-0.47315	1577	95	7.33	7.82
BC10A_56	1.692047	0.117384	0.496	0.036	0.4964	1380	320	1.095	2.21
BC10A_57	2.247191	0.2019947	0.35	0.024	0.15289	1500	170	2.14	3.44
BC10A_58	2.597403	0.2091415	0.287	0.018	-0.40589	1550	130	3.65	4.58
BC10A_59	2.747253	0.2037797	0.263	0.022	-0.46537	1626	76	4.45	6.02
BC10A_60	2.873563	0.2312062	0.233	0.011	-0.37374	1567	110	7.71	8.49

BC10A_61	2.624672	0.1791115	0.2809	0.0074	0.13093	1539	86	6.85	8.3
BC10B_1	3.012048	0.2177384	0.247	0.021	-0.32742	1550	110	3.83	4.08
BC10B_2	2.890173	0.1754151	0.252	0.015	0.075651	1589	130	3.554	4.26
BC10B_3	1.109878	0.10101	0.629	0.041	-0.33284	1550	290	3.01	8.18
BC10B_4	3.003003	0.1803605	0.229	0.013	0.5881	1579	120	3.8	4.4
BC10B_5	2.739726	0.1651342	0.287	0.018	0.40268	1572	130	3.51	6.22
BC10B_6	2.935134	0.1636852	0.2347	0.0087	0.44473	1580	120	4.59	7.9
BC10B_7	2.9274	0.1628238	0.248	0.013	0.61282	1589	120	4.76	5.58
BC10B_8	1.992032	0.1904732	0.47	0.045	0.31498	1480	260	0.64	1.64
BC10B_9	2.369668	0.1628445	0.377	0.017	-0.18595	1543	130	2.35	3.8
BC10B_10	2.915452	0.1699972	0.256	0.02	0.39121	1568	150	4.09	4.76
BC10B_11	3.012048	0.2358833	0.21	0.015	0.19306	1610	140	5.82	6.18
BC22A_1	3.076923	0.2366864	0.171	0.014	-0.90487	1568	46	6.91	7.79
BC22A_2	2.915452	0.2294962	0.207	0.022	-0.91859	1589	42	6.495	7.63
BC22A_3	2.03252	0.2726552	0.4	0.06	-0.80537	1550	120	4.73	8.3
BC22A_4	1.666667	0.3888889	0.397	0.072	-0.34148	1540	130	5.75	11.9
BC22A_5	3.10559	0.1928938	0.198	0.023	-0.79522	1577	68	6.6	7.16
BC22A_6	2.932551	0.2665956	0.223	0.031	-0.85623	1530	47	7.91	9.16
BC22A_7	2.506266	0.3015056	0.268	0.046	-0.76088	1600	120	6	8.15
BC22A_8	2.202643	0.4317957	0.288	0.058	-0.50569	1658	89	6.86	10.1
BC22A_9	3.30033	0.1960592	0.158	0.012	-0.7843	1558	74	7.03	7.27
BC22A_10	2.710027	0.2717371	0.247	0.041	-0.48677	1585	87	6.51	7.93
BC22A_11	2.754821	0.3111506	0.278	0.055	-0.30641	1527	100	6.61	8.08
BC22A_12	2.849003	0.3084391	0.258	0.054	-0.75648	1455	83	6.98	8.6
BC22A_13	2.932551	0.2665956	0.223	0.031	-0.85623	1530	47	7.91	9.16
BC22A_14	1.333333	0.4266667	0.383	0.07	-0.94022	1530	130	5.79	12.7

BC22A_15	1.449275	0.3780718	0.405	0.074	-0.90755	1440	200	4.34	10.4
BC22B_1	2.824859	0.2872738	0.222	0.03	-0.8019	1587	73	3.99	5.08
BC22B_2	1.686341	0.2729995	0.508	0.076	-0.14069	1370	260	1.308	2.57
BC22B_3	3.215434	0.2894925	0.241	0.035	0.015488	1414	93	1.84	2.47
BC22B_4	1.190476	0.297619	0.568	0.068	-0.2757	1620	250	0.766	2.9
BC22B_5	2.457002	0.2475113	0.249	0.039	-0.53885	1648	93	3.37	5.3
BC22B_6	2.680965	0.2443775	0.279	0.035	-0.67696	1606	100	2.78	3.48
BC22B_7	2.673797	0.3574595	0.4	0.14	0.073235	1480	160	4.554	5.78
BC22B_8	2.985075	0.2316774	0.243	0.058	-0.25367	1590	130	4.12	5.49
BC22B_9	3.021148	0.2373107	0.238	0.04	-0.71561	1477	96	5.58	7.5
BC22B_10	1.893939	0.2690255	0.429	0.058	-0.31769	1660	140	1.28	2.59
BC22B_11	1.515152	0.5050505	0.368	0.067	-0.37205	1650	130	2.52	5.3
BC22B_12	1.587302	0.3275384	0.462	0.057	-0.5613	1440	210	1.847	3.67
BC22B_13	1.886792	0.4271983	0.385	0.061	-0.37286	1750	150	1.313	2.38
BC22B_14	2.673797	0.3574595	0.4	0.14	0.073235	1480	160	4.554	5.78
BC22C_1	0.007692308	0.009467456	1.042	0.06	0.060449	N/A	N/A	1.51	162
BC22C_2	0.4524887	0.1228476	0.658	0.072	0.13802	N/A	N/A	0.642	5
BC22C_3	0.3030303	0.1101928	0.801	0.08	-0.27195	N/A	N/A	0.759	8.6
BC22C_4	0.1515152	0.06887052	0.731	0.06	-0.10209	N/A	N/A	0.587	11.2
BC22C_5	0.3448276	0.1664685	0.82	0.15	0.036251	N/A	N/A	0.591	5.3
BC22C_6	0.06289308	0.0249199	0.807	0.052	-0.15908	N/A	N/A	0.566	29
BC22C_7	0.1666667	0.06388889	0.821	0.084	-0.13855	N/A	N/A	0.567	14.6
BC22C_8	0.5050505	0.1606979	0.728	0.081	-0.26503	N/A	N/A	1.296	9.5

APPENDIX F – CALCITE U-PB GEOCHRONOLOGY DATA

Source file	Final 238/206	238/206 Propagated Error	Final 207/206	Final 207/206 Propagated Error	238/206 vs 207/206 Error Correlation	Corrected 238/206	Corrected 207/206	U (ppm)	Pb (ppm)
NIST614 - 1.d	1.26183	0.06528	0.878	0.0077	0.46131	1.337843	0.828112	0.8616	2.412
NIST614 - 2.d	1.25094	0.06572	0.8658	0.007	0.47019	1.326296	0.816605	0.8572	2.39
NIST614 - 3.d	1.25850	0.06494	0.8698	0.0076	0.49735	1.334308	0.820378	0.8232	2.286
NIST614 - 4.d	1.26279	0.06538	0.8773	0.0071	0.42548	1.338857	0.827452	0.8167	2.242
NIST614 - 5.d	1.26119	0.06521	0.8656	0.0072	0.32314	1.337169	0.816417	0.8209	2.25
NIST614 - 6.d	1.20686	0.06263	0.8728	0.0072	0.40664	1.279557	0.823208	0.8294	2.396
NIST614 - 7.d	1.19503	0.06284	0.8645	0.0075	0.49658	1.267018	0.815379	0.853	2.482
NIST614 - 8.d	1.16809	0.06140	0.8683	0.0077	0.5226	1.238455	0.818963	0.813	2.402
NIST614 - 9.d	1.27470	0.06662	0.8763	0.0073	0.50219	1.351486	0.826509	0.836	2.292
NIST614 - 10.d	1.25565	0.06464	0.8692	0.0075	0.54692	1.331292	0.819812	0.8338	2.319
NIST614 - 11.d	1.24673	0.06528	0.878	0.0071	0.43204	1.321831	0.828112	0.836	2.34
NIST614 - 12.d	1.24984	0.06561	0.8688	0.007	0.52814	1.325136	0.819435	0.8159	2.261
NIST614 - 13.d	1.19119	0.06243	0.8714	0.0078	0.57362	1.262943	0.821887	0.7468	2.163
NIST614 - 14.d	1.21330	0.06330	0.8659	0.008	0.46125	1.286388	0.816700	0.7706	2.206
NIST614 - 15.d	1.25597	0.06468	0.8704	0.0072	0.59405	1.331626	0.820944	0.819	2.27
NIST614 - 16.d	1.25628	0.06629	0.8732	0.0078	0.40929	1.331961	0.823585	0.839	2.325
NIST614 - 17.d	1.22324	0.06434	0.8758	0.0086	0.54626	1.296931	0.826037	0.855	2.437
NIST614 - 18.d	1.18779	0.06208	0.8689	0.0079	0.48012	1.259343	0.819529	0.854	2.505
NIST614 - 19.d	1.18106	0.06138	0.8685	0.0076	0.6007	1.252204	0.819152	0.848	2.499
NIST614 - 20.d	1.17938	0.06120	0.8712	0.0075	0.38854	1.250432	0.821698	0.842	2.491
NIST614 - 21.d	1.23244	0.06379	0.8716	0.0082	0.71511	1.306681	0.822076	0.829	2.345
NIST614 - 22.d	1.18977	0.06228	0.8705	0.0073	0.49049	1.261441	0.821038	0.84	2.458

NIST614 - 23.d	1.20875	0.06283	0.8707	0.0077	0.3705	1.281568	0.821227	0.842	2.386
NIST614 - 24.d	1.23350	0.06390	0.8728	0.0081	0.55533	1.307809	0.823208	0.847	2.383
NIST614 - 25.d	1.25016	0.06564	0.8711	0.0077	0.46059	1.325467	0.821604	0.832	2.333
NIST614 - 26.d	1.24611	0.06522	0.8681	0.0077	0.42132	1.321173	0.818775	0.8343	2.321
NIST614 - 27.d	1.26839	0.06596	0.8683	0.008	0.51704	1.344801	0.818963	0.838	2.307
NIST614 - 28.d	1.24487	0.06509	0.8713	0.0077	0.48875	1.319857	0.821793	0.833	2.33
NIST614 - 29.d	1.25644	0.06472	0.872	0.0075	0.34127	1.332128	0.822453	0.8221	2.27
NIST614 - 30.d	1.26711	0.06583	0.8742	0.0077	0.42778	1.343438	0.824528	0.8221	2.296
NIST612 - 1.d	3.52423	0.18630	0.9065	0.0056	0.45637	3.736532	0.854993	40.23	40.43
NIST612 - 2.d	3.63928	0.18542	0.9067	0.0055	0.5419	3.858508	0.855181	39.93	39.58
NIST612 - 3.d	3.69727	0.19138	0.9092	0.0056	0.4454	3.919995	0.857539	37.37	36.44
NIST612 - 4.d	3.45925	0.17950	0.9071	0.0056	0.4303	3.667639	0.855559	37.51	38.81
NIST612 - 5.d	3.42325	0.17578	0.9086	0.0055	0.39589	3.629471	0.856973	39.67	41.22
NIST612 - 6.d	3.46849	0.18046	0.9098	0.0055	0.49392	3.677434	0.858105	40.97	42.04
NIST612 - 7.d	3.59661	0.18110	0.9075	0.0055	0.62566	3.813268	0.855936	42.12	41.66
NIST612 - 8.d	3.59144	0.18058	0.9075	0.0055	0.40379	3.807790	0.855936	41.38	41.24
NIST612 - 9.d	3.63703	0.18519	0.9081	0.0054	0.40729	3.856123	0.856502	40.82	40.21
NIST612 - 10.d	3.63941	0.18543	0.9067	0.0054	0.54703	3.858649	0.855181	40.8	40.24
NIST612 - 11.d	3.42936	0.17641	0.9056	0.0055	0.68788	3.635943	0.854144	37.44	39.31
NIST612 - 12.d	3.46813	0.18042	0.9062	0.0054	0.34852	3.677051	0.854710	37.14	38.66
NIST612 - 13.d	3.43548	0.17704	0.9074	0.0055	0.4218	3.642438	0.855842	35.8	37.47
NIST612 - 14.d	3.42994	0.17647	0.9069	0.0055	0.45011	3.636567	0.855370	34.96	36.66
NIST612 - 15.d	3.46861	0.18047	0.9062	0.0068	0.33535	3.677561	0.854710	38.23	39.23
NIST612 - 16.d	3.48189	0.18185	0.9073	0.0066	0.45619	3.691647	0.855747	37.16	38.27
NIST612 - 17.d	3.40368	0.17378	0.9033	0.0063	0.44545	3.608717	0.851974	36.27	38.23
NIST612 - 18.d	3.42349	0.17580	0.9071	0.0061	0.45385	3.629719	0.855559	36.13	37.69

NIST612 - 19.d	3.50976	0.18478	0.9047	0.0056	0.43546	3.721188	0.853295	37.85	38.87
NIST612 - 20.d	3.60270	0.18171	0.9064	0.0057	0.26544	3.819725	0.854898	39.95	39.72
NIST612 - 21.d	3.57117	0.19130	0.9053	0.0055	0.55321	3.786304	0.853861	39.87	40.09
NIST612 - 22.d	3.60737	0.18218	0.9081	0.0056	0.45331	3.824685	0.856502	39.3	39.2
NIST612 - 23.d	3.49614	0.18334	0.9055	0.0055	0.19648	3.706747	0.854049	38.35	39.4
NIST612 - 24.d	3.53107	0.18703	0.9065	0.006	0.33013	3.743789	0.854993	39.48	39.92
NIST612 - 25.d	3.46705	0.18031	0.9065	0.0056	0.49463	3.675904	0.854993	36.05	37.29
NIST612 - 26.d	3.47633	0.18127	0.904	0.0056	0.43465	3.685743	0.852635	35.86	36.98
NIST612 - 27.d	3.45423	0.17898	0.9074	0.006	0.42132	3.662318	0.855842	36.95	38.73
NIST612 - 28.d	3.45901	0.17947	0.903	0.006	0.41798	3.667385	0.851692	36.1	37.31
NIST612 - 29.d	3.44471	0.17799	0.9055	0.0061	0.26395	3.652225	0.854049	36.16	37.77
NIST612 - 30.d	3.41064	0.17449	0.9057	0.0061	0.52144	3.616102	0.854238	35.47	37.11
WC1 - 1.d	21.89621	1.15067	0.1175	0.003	0.087097	23.215261	0.110824	5.97	0.0756
WC1 - 2.d	21.49613	1.10900	0.118	0.0033	0.1719	22.791078	0.111295	6.419	0.0865
WC1 - 3.d	22.05558	1.16748	0.0956	0.0035	-0.38336	23.384229	0.090168	6.141	0.0536
WC1 - 4.d	22.13369	1.17576	0.0994	0.003	-0.20407	23.467042	0.093752	5.592	0.0505
WC1 - 5.d	22.41650	1.15575	0.0968	0.003	0.36408	23.766890	0.091300	6.275	0.0484
WC1 - 6.d	21.72496	1.13274	0.1018	0.0029	0.058297	23.033695	0.096016	5.287	0.0543
WC1 - 7.d	20.56767	1.14218	0.1425	0.0056	-0.8577	21.806684	0.134403	5.252	0.0951
WC1 - 8.d	21.63098	1.12296	0.1282	0.0024	0.2201	22.934046	0.120916	7.305	0.1125
WC1 - 9.d	21.71081	1.13126	0.1252	0.002	0.087196	23.018692	0.118086	6.723	0.095
WC1 - 10.d	21.36296	1.09530	0.1284	0.0024	0.12632	22.649882	0.121104	6.661	0.1002
WC1 - 11.d	21.74859	1.13520	0.1165	0.0027	0.24599	23.058742	0.109880	4.459	0.0595
WC1 - 12.d	22.33140	1.14699	0.12	0.0025	0.25681	23.676663	0.113182	6.428	0.0845
WC1 - 13.d	21.79124	1.13966	0.1296	0.0025	0.082197	23.103965	0.122236	7.418	0.1175
WC1 - 14.d	20.85941	1.08779	0.1371	0.0025	0.22449	22.115998	0.129310	5.8	0.1021

WC1 - 15.d	21.51000	1.15670	0.1322	0.005	-0.80486	22.805785	0.124688	5.84	0.0967
WC1 - 16.d	20.91613	1.13746	0.1317	0.0058	-0.76543	22.176134	0.124217	5.318	0.0882
WC1 - 17.d	21.25399	1.12933	0.1305	0.0025	0.42597	22.534346	0.123085	6.631	0.1033
WC1 - 18.d	21.25399	1.12933	0.1313	0.0025	0.24002	22.534346	0.123840	6.128	0.0974
WC1 - 19.d	22.15330	1.17785	0.0894	0.0025	0.1198	23.487837	0.084320	5.3	0.0362
WC1 - 20.d	21.68257	1.12832	0.1059	0.0024	0.29874	22.988746	0.099883	5.353	0.0598
WC1 - 21.d	20.85941	1.08779	0.1136	0.0034	0.037636	22.115998	0.107145	5.13	0.0686
WC1 - 22.d	21.44082	1.14927	0.1105	0.0041	-0.4204	22.732439	0.104221	7.03	0.0843
WC1 - 23.d	21.81501	1.14215	0.1035	0.0026	0.20894	23.129166	0.097619	4.914	0.0532
WC1 - 24.d	21.28565	1.13270	0.1285	0.0025	0.26842	22.567922	0.121199	5.757	0.0878
WC1 - 25.d	21.96354	1.15775	0.1134	0.0022	0.36622	23.286645	0.106957	6.888	0.0885
WC1 - 26.d	21.07038	1.10990	0.1204	0.0023	0.50556	22.339675	0.113559	7.108	0.0997
WC1 - 27.d	21.20891	1.12454	0.1131	0.0049	-0.080399	22.486553	0.106674	5.098	0.0643
WC1 - 28.d	22.30649	1.19419	0.0866	0.0026	0.18921	23.650256	0.081679	5.235	0.0354
WC1 - 29.d	21.72024	1.13225	0.1043	0.0045	-0.67636	23.028692	0.098374	5.386	0.052
WC1 - 30.d	21.30379	1.13463	0.1029	0.0028	0.15059	22.587153	0.097053	4.746	0.0491
WC1 - 31.d	21.29925	1.13415	0.1034	0.0066	-0.89275	22.582342	0.097525	5.808	0.064
WC1 - 32.d	21.06150	1.10897	0.1258	0.0027	0.062491	22.330265	0.118652	6.065	0.0899
WC1 - 33.d	21.33106	1.13754	0.1105	0.0031	0.31655	22.616062	0.104221	5.539	0.0679
WC1 - 34.d	21.12825	1.11601	0.1115	0.0031	-0.035113	22.401035	0.105165	5.167	0.0627
WC1 - 35.d	20.96436	1.09876	0.1358	0.0031	0.29175	22.227274	0.128084	5.447	0.0935
WC1 - 36.d	20.74258	1.07564	0.1308	0.0027	-0.024196	21.992138	0.123368	6.573	0.1044
WC1 - 37.d	20.82899	1.08462	0.1331	0.003	0.078005	22.083753	0.125537	5.803	0.0957
WC1 - 38.d	20.79434	1.08101	0.1298	0.0032	0.24721	22.047015	0.122425	5.53	0.0978
WC1 - 39.d	21.04820	1.10757	0.1335	0.0027	0.0052796	22.316164	0.125915	5.421	0.0906
WC1 - 40.d	21.39495	1.09859	0.12	0.0025	0.17959	22.683803	0.113182	6.505	0.0905
WC1 - 41.d	21.44082	1.10330	0.1155	0.0026	0.38394	22.732439	0.108937	6.539	0.0899
WC1 - 42.d	20.30869	1.07235	0.1326	0.0025	0.35712	21.532107	0.125066	6.339	0.1089

WC1 - 43.d	21.57497	1.11715	0.102	0.0027	0.20556	22.874670	0.096204	5.077	0.0498
WC1 - 44.d	21.57963	1.11763	0.1098	0.003	-0.20701	22.879606	0.103561	5.971	0.068
WC1 - 45.d	21.51463	1.11091	0.118	0.0021	0.36658	22.810692	0.111295	7.32	0.0974
WC1 - 46.d	21.27207	1.13125	0.1189	0.0024	0.059186	22.553520	0.112144	6.425	0.0908
WC1 - 47.d	20.90738	1.09280	0.1285	0.0026	0.1702	22.166861	0.121199	5.537	0.092
WC1 - 48.d	21.79124	1.13966	0.1191	0.0025	0.2693	23.103965	0.112333	6.406	0.0895
WC1 - 49.d	20.55498	1.05627	0.1408	0.0024	0.28166	21.793237	0.132800	6.581	0.1208
WC1 - 50.d	21.25399	1.17450	0.124	0.0039	0.096135	22.534346	0.116954	7.75	0.1086
WC1 - 51.d	20.84636	1.08643	0.1226	0.0022	0.24618	22.102167	0.115634	7.032	0.1012
WC1 - 52.d	20.03606	1.08390	0.1364	0.003	-0.17401	21.243057	0.128650	5.755	0.1081
WC1 - 53.d	21.25850	1.12981	0.124	0.0025	0.26134	22.539136	0.116954	6.99	0.1072
WC1 - 54.d	20.05616	1.04585	0.1399	0.0029	0.30534	21.264359	0.131951	5.049	0.0979
WC1 - 55.d	20.87683	1.08961	0.127	0.0036	-0.27474	22.134467	0.119784	7.114	0.1089
WC1 - 56.d	21.04377	1.10710	0.1083	0.0027	0.14896	22.311468	0.102146	5.284	0.0625
WC1 - 57.d	21.41328	1.10047	0.1026	0.0025	-0.011623	22.703233	0.096770	5.79	0.063
WC1 - 58.d	22.17295	1.17994	0.11	0.0031	0.17293	23.508669	0.103750	5.353	0.0608
BC00CAL4 - 1.d	0.37622	0.01982	0.8288	0.0079	-0.59893	0.398887	0.781708	0.359	3.273
BC00CAL4 - 2.d	0.37850	0.02006	0.8325	0.007	0.024278	0.401302	0.785197	0.3686	3.304
BC00CAL4 - 3.d	0.38730	0.02100	0.8408	0.0069	-0.36941	0.410628	0.793026	0.3798	3.36
BC00CAL4 - 4.d	0.39793	0.02059	0.8362	0.0071	-0.19665	0.421902	0.788687	0.3981	3.455
BC00CAL4 - 5.d	0.38745	0.02102	0.8424	0.0066	-0.023318	0.410787	0.794535	0.4032	3.59
BC00CAL4 - 6.d	0.38139	0.02036	0.8282	0.0079	-0.54408	0.404363	0.781142	0.3761	3.337
BC00CAL4 - 7.d	0.39093	0.01987	0.8315	0.008	-0.24379	0.414480	0.784254	0.3832	3.352
BC00CAL4 - 8.d	0.39541	0.02033	0.8265	0.0091	-0.68973	0.419233	0.779538	0.4006	3.493
BC00CAL4 - 9.d	0.39714	0.02050	0.8283	0.0071	-0.47412	0.421065	0.781236	0.4198	3.582
BC00CAL4 - 10.d	0.39093	0.01987	0.8358	0.0075	-0.4288	0.414480	0.788310	0.3993	3.511

BC00CAL4 - 11.d	0.37327	0.01951	0.8394	0.007	0.40559	0.395760	0.791705	0.3474	3.198
BC00CAL4 - 12.d	0.39809	0.02060	0.8361	0.008	0.17001	0.422070	0.788593	0.4319	3.696
BC00CAL4 - 13.d	0.39683	0.02205	0.8386	0.0077	0.19217	0.420731	0.790951	0.4087	3.557
BC00CAL4 - 14.d	0.38820	0.02110	0.8432	0.0078	-0.46324	0.411584	0.795289	0.4109	3.675
BC00CAL4 - 15.d	0.38640	0.02090	0.8408	0.0078	0.079498	0.409676	0.793026	0.409	3.61
BC00CAL4 - 16.d	0.37893	0.02010	0.8238	0.011	-0.30479	0.401759	0.776992	0.4139	3.642
BC00CAL4 - 17.d	0.39920	0.02231	0.824	0.012	-0.83656	0.423250	0.777180	0.45	3.477
BC00CAL4 - 18.d	0.38926	0.02121	0.8391	0.0079	-0.33278	0.412706	0.791422	0.3964	3.518
BC00CAL4 - 19.d	0.38986	0.02128	0.8387	0.0079	-0.19264	0.413349	0.791045	0.3925	3.51
BC00CAL4 - 20.d	0.39417	0.02175	0.8405	0.0075	-0.22289	0.417911	0.792743	0.4044	3.489
BC00CAL4 - 21.d	0.39510	0.02185	0.8336	0.0077	-0.68931	0.418902	0.786235	0.459	3.576
BC00CAL4 - 22.d	0.39730	0.02052	0.838	0.0069	-0.10053	0.421232	0.790385	0.4204	3.613
BC00CAL4 - 23.d	0.40800	0.02330	0.8373	0.0076	0.080184	0.432575	0.789725	0.437	3.637
BC00CAL4 - 24.d	0.38700	0.02097	0.844	0.007	-0.1341	0.410310	0.796044	0.4134	3.669
BC00CAL4 - 25.d	0.38476	0.02073	0.841	0.0072	0.28071	0.407942	0.793214	0.4112	3.652
BC00CAL4 - 26.d	0.39573	0.02192	0.8402	0.0076	0.39252	0.419565	0.792460	0.4202	3.659
BC00CAL4 - 27.d	0.38895	0.02118	0.837	0.0081	0.43315	0.412385	0.789442	0.408	3.622
BC00CAL4 - 28.d	0.39078	0.01985	0.8401	0.0068	0.014013	0.414318	0.792366	0.4003	3.505
BC00CAL4 - 29.d	0.38285	0.02052	0.8419	0.0071	0.049605	0.405912	0.794063	0.3952	3.581
BC00CAL4 - 30.d	0.38212	0.02044	0.8402	0.0068	0.35286	0.405136	0.792460	0.3948	3.529
BC00CAL3 - 1.d	0.38226	0.02046	0.8382	0.0074	-0.87119	0.405291	0.790573	0.3642	3.294
BC00CAL3 - 2.d	0.38358	0.02060	0.835	0.0065	-0.89487	0.406690	0.787555	0.3653	3.271
BC00CAL3 - 3.d	0.39888	0.02228	0.8364	0.0068	-0.84447	0.422912	0.788876	0.3827	3.277
BC00CAL3 - 4.d	0.38655	0.02092	0.8383	0.0077	-0.80185	0.409834	0.790668	0.3784	3.361
BC00CAL3 - 5.d	0.40241	0.02105	0.8392	0.0077	-0.74089	0.426656	0.791517	0.406	3.481
BC00CAL3 - 6.d	0.40833	0.02168	0.8371	0.0071	-0.43078	0.432928	0.789536	0.4152	3.491

BC00CAL3 - 7.d	0.39432	0.02021	0.8364	0.0086	0.037235	0.418076	0.788876	0.3974	3.489
BC00CAL3 - 8.d	0.38700	0.02097	0.8337	0.0069	0.0038853	0.410310	0.786329	0.4023	3.513
BC00CAL3 - 9.d	0.39557	0.02034	0.8378	0.0074	0.10898	0.419399	0.790196	0.4036	3.503
BC00CAL3 - 10.d	0.37722	0.01992	0.838	0.007	0.18323	0.399940	0.790385	0.3905	3.548
BC00CAL3 - 11.d	0.39216	0.02153	0.825	0.0072	-0.29093	0.415781	0.778124	0.4	3.483
BC00CAL3 - 12.d	0.37313	0.01949	0.8308	0.0068	0.26697	0.395612	0.783594	0.374	3.39
BC00CAL3 - 13.d	0.38110	0.02033	0.8314	0.0072	-0.52635	0.404055	0.784160	0.3824	3.412
BC00CAL3 - 14.d	0.39078	0.01985	0.8384	0.0071	-0.65782	0.414318	0.790762	0.3865	3.403
BC00CAL3 - 15.d	0.38986	0.02128	0.8389	0.0071	-0.30109	0.413349	0.791234	0.4083	3.555
BC00CAL3 - 16.d	0.38580	0.02084	0.835	0.0073	-0.2423	0.409044	0.787555	0.4197	3.695
BC00CAL3 - 17.d	0.38926	0.01970	0.834	0.0075	-0.041003	0.412706	0.786612	0.4266	3.733
BC00CAL3 - 18.d	0.39108	0.01988	0.8426	0.0067	0.2385	0.414643	0.794723	0.4163	3.676
BC00CAL3 - 19.d	0.38805	0.02108	0.8374	0.008	-0.064197	0.411425	0.789819	0.4142	3.615
BC00CAL3 - 20.d	0.39200	0.01998	0.8399	0.0071	-0.045638	0.415618	0.792177	0.4153	3.636
BC00CAL3 - 21.d	0.39154	0.02146	0.8388	0.0074	-0.12813	0.415130	0.791139	0.4251	3.718
BC00CAL3 - 22.d	0.38820	0.02110	0.8307	0.0066	0.065995	0.411584	0.783500	0.4092	3.599
BC00CAL3 - 23.d	0.38715	0.02098	0.8337	0.0073	0.010732	0.410469	0.786329	0.4239	3.724
BC00CAL3 - 24.d	0.39339	0.02167	0.8271	0.0072	-0.25184	0.417089	0.780104	0.4212	3.583
BC00CAL3 - 25.d	0.38805	0.02108	0.8333	0.0086	-0.37737	0.411425	0.785952	0.4138	3.648
BC00CAL3 - 26.d	0.39588	0.02194	0.8393	0.0068	-0.017739	0.419731	0.791611	0.4174	3.638
BC00CAL3 - 27.d	0.39557	0.02191	0.8328	0.0079	-0.39938	0.419399	0.785480	0.4196	3.663
BC00CAL3 - 28.d	0.39635	0.02042	0.8345	0.008	-0.52936	0.420230	0.787084	0.4154	3.582
BC00CAL3 - 29.d	0.39841	0.02222	0.833	0.0077	-0.56014	0.422407	0.785669	0.4233	3.652
BC00CAL3 - 30.d	0.40225	0.02103	0.8312	0.0071	0.084813	0.426485	0.783971	0.4185	3.577
BC00CAL1 - 1.d	0.38110	0.02033	0.8409	0.0064	0.18993	0.404055	0.793120	0.4192	3.778
BC00CAL1 - 2.d	0.38300	0.02054	0.8376	0.0066	0.48828	0.406067	0.790008	0.4058	3.644

BC00CAL1 - 3.d	0.38226	0.02046	0.8385	0.0068	0.32479	0.405291	0.790856	0.3942	3.544
BC00CAL1 - 4.d	0.38402	0.02065	0.8386	0.0061	0.2218	0.407159	0.790951	0.393	3.525
BC00CAL1 - 5.d	0.38775	0.01955	0.8433	0.0065	0.43108	0.411105	0.795384	0.3909	3.491
BC00CAL1 - 6.d	0.38986	0.01976	0.8416	0.0067	0.38804	0.413349	0.793780	0.396	3.514
BC00CAL1 - 7.d	0.38388	0.02063	0.8354	0.0069	0.35321	0.407002	0.787933	0.3969	3.554
BC00CAL1 - 8.d	0.38506	0.02076	0.845	0.0068	0.25041	0.408256	0.796987	0.398	3.581
BC00CAL1 - 9.d	0.37608	0.01980	0.8353	0.0068	0.14393	0.398737	0.787838	0.3993	3.589
BC00CAL1 - 10.d	0.37965	0.02018	0.8424	0.0075	0.42589	0.402521	0.794535	0.4013	3.596
BC00CAL1 - 11.d	0.38388	0.02063	0.84	0.0069	0.3873	0.407002	0.792271	0.3963	3.533
BC00CAL1 - 12.d	0.39730	0.02052	0.8384	0.007	0.47845	0.421232	0.790762	0.408	3.531
BC00CAL1 - 13.d	0.39308	0.02009	0.8417	0.0065	0.44289	0.416761	0.793875	0.4053	3.53
BC00CAL1 - 14.d	0.39746	0.02054	0.8386	0.0062	0.21553	0.421399	0.790951	0.4183	3.624
BC00CAL1 - 15.d	0.39588	0.02037	0.8382	0.0062	0.33595	0.419731	0.790573	0.4161	3.601
BC00CAL1 - 16.d	0.39002	0.02130	0.8395	0.0067	0.14124	0.413511	0.791800	0.446	3.839
BC00CAL1 - 17.d	0.38760	0.01953	0.8409	0.007	0.15071	0.410946	0.793120	0.4223	3.789
BC00CAL1 - 18.d	0.39063	0.01984	0.8442	0.0076	0.34174	0.414157	0.796233	0.4188	3.714
BC00CAL1 - 19.d	0.39002	0.01977	0.8386	0.0074	0.29446	0.413511	0.790951	0.427	3.756
BC00CAL1 - 20.d	0.38285	0.02052	0.8372	0.0075	0.33401	0.405912	0.789630	0.4171	3.792
BC00CAL1 - 21.d	0.38760	0.02103	0.838	0.0072	0.43782	0.410946	0.790385	0.4122	3.643
BC00CAL1 - 22.d	0.39432	0.02021	0.8381	0.0066	0.39737	0.418076	0.790479	0.4044	3.532
BC00CAL1 - 23.d	0.40048	0.02085	0.8399	0.0063	0.45288	0.424606	0.792177	0.412	3.528
BC00CAL1 - 24.d	0.38745	0.01951	0.8409	0.0068	0.32988	0.410787	0.793120	0.4191	3.701
BC00CAL1 - 25.d	0.38895	0.01967	0.8364	0.0067	0.23831	0.412385	0.788876	0.4235	3.671
BC00CAL1 - 26.d	0.38941	0.01971	0.8371	0.0068	0.5475	0.412866	0.789536	0.4255	3.701
BC00CAL1 - 27.d	0.38986	0.01976	0.8355	0.0069	0.3925	0.413349	0.788027	0.4354	3.806
BC00CAL1 - 28.d	0.39401	0.02018	0.8402	0.0068	0.38562	0.417747	0.792460	0.4466	3.879
BC00CAL1 - 29.d	0.38521	0.02077	0.8394	0.0075	0.44917	0.408413	0.791705	0.4325	3.848
BC00CAL1 - 30.d	0.38685	0.02095	0.8326	0.0068	0.097506	0.410151	0.785292	0.4228	3.718

BC00CAL5 - 1.d	0.37078	0.01925	0.8386	0.0065	0.37288	0.393119	0.790951	0.3682	3.407
BC00CAL5 - 2.d	0.37064	0.01923	0.8357	0.0066	0.35374	0.392973	0.788216	0.3663	3.379
BC00CAL5 - 3.d	0.38168	0.02040	0.8346	0.0066	0.28219	0.404672	0.787178	0.3674	3.288
BC00CAL5 - 4.d	0.38911	0.02120	0.8421	0.0066	0.077481	0.412545	0.794252	0.373	3.288
BC00CAL5 - 5.d	0.37722	0.01992	0.8405	0.0068	0.39672	0.399940	0.792743	0.3728	3.405
BC00CAL5 - 6.d	0.38685	0.02095	0.8405	0.0067	0.1041	0.410151	0.792743	0.3859	3.414
BC00CAL5 - 7.d	0.38358	0.02060	0.8365	0.0064	0.38891	0.406690	0.788970	0.3873	3.474
BC00CAL5 - 8.d	0.38820	0.01959	0.8417	0.0068	0.25117	0.411584	0.793875	0.383	3.382
BC00CAL5 - 9.d	0.39277	0.02006	0.8409	0.0063	0.241	0.416434	0.793120	0.3792	3.326
BC00CAL5 - 10.d	0.39277	0.02006	0.8362	0.0073	0.26469	0.416434	0.788687	0.4006	3.484
BC00CAL5 - 11.d	0.39185	0.01996	0.8361	0.0076	0.32617	0.415455	0.788593	0.4084	3.533
BC00CAL5 - 12.d	0.39154	0.01993	0.8355	0.0074	0.24283	0.415130	0.788027	0.4012	3.51
BC00CAL5 - 13.d	0.40617	0.02145	0.8409	0.0065	0.45515	0.430642	0.793120	0.4183	3.486
BC00CAL5 - 14.d	0.41597	0.02249	0.836	0.0071	0.091462	0.441032	0.788498	0.4406	3.578
BC00CAL5 - 15.d	0.40634	0.02146	0.8365	0.0073	0.20353	0.430817	0.788970	0.437	3.622
BC00CAL5 - 16.d	0.40469	0.02129	0.8343	0.0073	-0.056646	0.429074	0.786895	0.4468	3.693
BC00CAL5 - 17.d	0.38926	0.02121	0.8374	0.0076	-0.028017	0.412706	0.789819	0.4203	3.751
BC00CAL5 - 18.d	0.38506	0.02076	0.8298	0.0071	0.086007	0.408256	0.782651	0.4197	3.708
BC00CAL5 - 19.d	0.39047	0.01982	0.8436	0.0066	0.088115	0.413995	0.795667	0.4123	3.629
BC00CAL5 - 20.d	0.38895	0.01967	0.8401	0.0067	0.03338	0.412385	0.792366	0.4213	3.691
BC00CAL5 - 21.d	0.39124	0.01990	0.836	0.0076	-0.041132	0.414805	0.788498	0.4121	3.644
BC00CAL5 - 22.d	0.38640	0.02090	0.8396	0.0074	0.22951	0.409676	0.791894	0.4348	3.828
BC00CAL5 - 23.d	0.38388	0.02063	0.8333	0.0071	0.014322	0.407002	0.785952	0.4202	3.705
BC00CAL5 - 24.d	0.38640	0.02090	0.8373	0.0072	-0.074517	0.409676	0.789725	0.4182	3.693
BC00CAL5 - 25.d	0.38670	0.02093	0.8358	0.0066	0.17671	0.409993	0.788310	0.433	3.773

BC00CAL5 - 26.d	0.39432	0.02021	0.8385	0.0069	-0.0059533	0.418076	0.790856	0.4282	3.76
BC00CAL5 - 27.d	0.38595	0.02085	0.8392	0.0071	0.28102	0.409201	0.791517	0.4331	3.835
BC00CAL5 - 28.d	0.38565	0.02082	0.827	0.0068	0.022358	0.408886	0.780010	0.4377	3.831
BC00CAL5 - 29.d	0.38506	0.02076	0.8362	0.0064	-0.04337	0.408256	0.788687	0.4261	3.774
BC00CAL5 - 30.d	0.37864	0.02007	0.837	0.007	-0.017641	0.401454	0.789442	0.4114	3.716
BC14CAL1 - 1.d	0.11905	0.02268	0.8752	0.0097	-0.32573	0.126219	0.825471	0.3387	7.52
BC14CAL1 - 2.d	0.12500	0.02656	0.8643	0.0083	-0.38906	0.132530	0.815190	0.3394	7.38
BC14CAL1 - 3.d	0.12195	0.04313	0.8552	0.0087	-0.054929	0.129298	0.806608	0.339	6.5
BC14CAL1 - 4.d	0.10417	0.02170	0.8667	0.011	-0.18819	0.110442	0.817454	0.3583	9.75
BC14CAL1 - 5.d	0.14368	0.01259	0.851	0.018	-0.05319	0.152333	0.802646	0.367	8.47
BC14CAL1 - 6.d	0.12547	0.01732	0.866	0.013	-0.16661	0.133029	0.816794	0.3669	9.08
BC14CAL1 - 7.d	0.11628	0.01893	0.875	0.014	-0.04947	0.123284	0.825283	0.3611	9.73
BC14CAL1 - 8.d	0.13298	0.01432	0.856	0.013	-0.11804	0.140989	0.807362	0.3564	8.44
BC14CAL1 - 9.d	0.13812	0.01793	0.866	0.012	-0.027627	0.146442	0.816794	0.358	8.11
BC14CAL1 - 10.d	0.14368	0.01982	0.868	0.014	-0.31079	0.152333	0.818680	0.3688	7.88
BC14CAL1 - 11.d	0.13369	0.01716	0.875	0.014	-0.12807	0.141743	0.825283	0.3663	8.79
BC14CAL1 - 12.d	0.14245	0.01562	0.871	0.015	-0.22016	0.151031	0.821510	0.3612	8.02
BC14CAL1 - 13.d	0.13947	0.01828	0.864	0.014	-0.10893	0.147872	0.814908	0.3578	7.71
BC14CAL1 - 14.d	0.14409	0.01910	0.87	0.017	-0.094339	0.152772	0.820567	0.3624	7.27
BC14CAL1 - 15.d	0.12346	0.02134	0.882	0.015	-0.18034	0.130894	0.831885	0.3621	8.32
BC14CAL1 - 16.d	0.13333	0.01564	0.884	0.015	-0.11622	0.141365	0.833771	0.408	10.31
BC14CAL1 - 17.d	0.16155	0.01540	0.851	0.011	-0.19387	0.171283	0.802646	0.3783	7.58
BC14CAL1 - 18.d	0.14124	0.02194	0.868	0.011	-0.34445	0.149752	0.818680	0.381	8.54
BC14CAL1 - 19.d	0.12953	0.01678	0.865	0.012	-0.23637	0.137337	0.815851	0.3748	9.01
BC14CAL1 - 20.d	0.13947	0.01867	0.866	0.012	-0.2614	0.147872	0.816794	0.374	8.17

BC14CAL1 - 21.d	0.13123	0.01894	0.883	0.015	-0.15779	0.139139	0.832828	0.3874	9.13
BC14CAL1 - 22.d	0.11628	0.01622	0.887	0.014	-0.20114	0.123284	0.836601	0.3766	9.41
BC14CAL1 - 23.d	0.13661	0.01530	0.878	0.016	-0.20613	0.144842	0.828112	0.3772	9.73
BC14CAL1 - 24.d	0.13072	0.01504	0.879	0.016	-0.16412	0.138594	0.829055	0.3724	9.99
BC14CAL1 - 25.d	0.12937	0.01841	0.879	0.014	-0.25302	0.137159	0.829055	0.3742	9.17
BC14CAL1 - 26.d	0.11111	0.01605	0.877	0.013	-0.15451	0.117805	0.827169	0.3821	11.8
BC14CAL1 - 27.d	0.13193	0.01914	0.885	0.013	-0.41866	0.139873	0.834714	0.3811	9.61
BC14CAL1 - 28.d	0.15129	0.01602	0.857	0.013	-0.20908	0.160400	0.808305	0.3861	8.34
BC14CAL1 - 29.d	0.14577	0.01764	0.879	0.012	-0.20841	0.154554	0.829055	0.3869	8.91
BC14CAL1 - 30.d	0.12195	0.02231	0.879	0.014	-0.084137	0.129298	0.829055	0.3782	9.61
BC10CAL1 - 1.d	0.29394	0.01555	0.8395	0.0064	-0.06881	0.311652	0.791800	0.3177	3.697
BC10CAL1 - 2.d	0.30377	0.01569	0.8382	0.0064	0.11544	0.322066	0.790573	0.3223	3.6
BC10CAL1 - 3.d	0.30340	0.01565	0.8435	0.0066	-0.11614	0.321675	0.795572	0.3311	3.724
BC10CAL1 - 4.d	0.30826	0.01615	0.8475	0.0063	0.13631	0.326831	0.799345	0.3296	3.667
BC10CAL1 - 5.d	0.29976	0.01528	0.8363	0.0069	0.16836	0.317818	0.788781	0.3344	3.786
BC10CAL1 - 6.d	0.30826	0.01615	0.8385	0.0063	0.1408	0.326831	0.790856	0.345	3.799
BC10CAL1 - 7.d	0.30432	0.01574	0.8433	0.0074	0.16421	0.322654	0.795384	0.3312	3.704
BC10CAL1 - 8.d	0.29490	0.01565	0.8361	0.0066	-0.1998	0.312663	0.788593	0.3295	3.731
BC10CAL1 - 9.d	0.30684	0.01601	0.8424	0.0083	-0.075146	0.325327	0.794535	0.3401	3.778
BC10CAL1 - 10.d	0.30423	0.01573	0.8387	0.0063	-0.039425	0.322556	0.791045	0.334	3.751
BC10CAL1 - 11.d	0.30331	0.01564	0.8345	0.0067	-0.55174	0.321577	0.787084	0.333	3.731
BC10CAL1 - 12.d	0.30021	0.01622	0.8426	0.0068	-0.14507	0.318295	0.794723	0.3243	3.686
BC10CAL1 - 13.d	0.30093	0.01540	0.8341	0.0074	0.28091	0.319061	0.786706	0.3284	3.726
BC10CAL1 - 14.d	0.30285	0.01651	0.8416	0.0078	-0.010575	0.321091	0.793780	0.3486	3.839
BC10CAL1 - 15.d	0.31368	0.01673	0.8366	0.0071	0.16852	0.332572	0.789064	0.3627	3.97
BC10CAL1 - 16.d	0.30637	0.01596	0.8367	0.0063	0.042606	0.324829	0.789159	0.3481	3.895

BC10CAL1 - 17.d	0.31104	0.01645	0.8392	0.0065	0.3378	0.329779	0.791517	0.3537	3.88
BC10CAL1 - 18.d	0.30404	0.01572	0.8366	0.0064	0.083419	0.322360	0.789064	0.3524	3.944
BC10CAL1 - 19.d	0.31008	0.01635	0.8339	0.0077	0.4537	0.328757	0.786518	0.3658	4.005
BC10CAL1 - 20.d	0.31486	0.01685	0.8356	0.0066	0.30934	0.333829	0.788121	0.3653	3.951
BC10CAL1 - 21.d	0.31726	0.01610	0.8402	0.0071	0.47678	0.336371	0.792460	0.3612	3.898
BC10CAL1 - 22.d	0.31456	0.01682	0.8349	0.0069	0.47173	0.333514	0.787461	0.3704	4.043
BC10CAL1 - 23.d	0.31546	0.01692	0.8386	0.0064	0.27842	0.334461	0.790951	0.3737	4.049
BC10CAL1 - 24.d	0.31847	0.01623	0.8422	0.0077	0.41171	0.337656	0.794346	0.3809	4.107
BC10CAL1 - 25.d	0.31095	0.01644	0.8356	0.0072	0.45245	0.329677	0.788121	0.383	4.235
BC10CAL1 - 26.d	0.30618	0.01594	0.8435	0.0066	0.27737	0.324630	0.795572	0.3635	4.073
BC10CAL1 - 27.d	0.30826	0.01615	0.8492	0.0067	0.04995	0.326831	0.800948	0.3683	4.09
BC10CAL1 - 28.d	0.30817	0.01614	0.8388	0.0066	0.23185	0.326731	0.791139	0.3614	4.014
BC10CAL1 - 29.d	0.30826	0.01615	0.8394	0.0064	0.32805	0.326831	0.791705	0.3792	4.18
BC10CAL1 - 30.d	0.30836	0.01616	0.8417	0.0068	0.39282	0.326932	0.793875	0.3626	4.028
BC10CAL2 - 1.d	0.29300	0.01545	0.839	0.0066	-0.2591	0.310648	0.791328	0.3062	3.559
BC10CAL2 - 2.d	0.29577	0.01575	0.8422	0.007	-0.28736	0.313588	0.794346	0.3066	3.494
BC10CAL2 - 3.d	0.29958	0.01615	0.8425	0.0066	-0.068649	0.317628	0.794629	0.3137	3.593
BC10CAL2 - 4.d	0.29967	0.01616	0.8406	0.0066	0.10291	0.317723	0.792837	0.3272	3.708
BC10CAL2 - 5.d	0.30874	0.01716	0.8409	0.0074	-0.19638	0.327336	0.793120	0.329	3.62
BC10CAL2 - 6.d	0.30432	0.01574	0.8401	0.0067	-0.033096	0.322654	0.792366	0.3278	3.665
BC10CAL2 - 7.d	0.30276	0.01558	0.8438	0.0072	0.1985	0.320993	0.795855	0.3274	3.707
BC10CAL2 - 8.d	0.29771	0.01595	0.8382	0.0075	-0.098056	0.315642	0.790573	0.3241	3.666
BC10CAL2 - 9.d	0.30003	0.01620	0.8387	0.0073	0.043798	0.318104	0.791045	0.3318	3.77
BC10CAL2 - 10.d	0.30303	0.01653	0.8417	0.007	-0.40145	0.321285	0.793875	0.3204	3.601
BC10CAL2 - 11.d	0.31037	0.01638	0.8386	0.0069	0.092318	0.329063	0.790951	0.3346	3.697
BC10CAL2 - 12.d	0.31626	0.01700	0.8379	0.0066	0.26031	0.335307	0.790291	0.3382	3.657

BC10CAL2 - 13.d	0.31959	0.01736	0.8439	0.007	-0.10051	0.338843	0.795950	0.3516	3.778
BC10CAL2 - 14.d	0.31556	0.01693	0.8405	0.007	0.037992	0.334566	0.792743	0.352	3.84
BC10CAL2 - 15.d	0.30423	0.01573	0.8435	0.007	0.32103	0.322556	0.795572	0.2991	3.383
BC10CAL2 - 16.d	0.31143	0.01649	0.8401	0.0067	0.14928	0.330190	0.792366	0.3728	4.112
BC10CAL2 - 17.d	0.29481	0.01564	0.8406	0.0078	0.44014	0.312571	0.792837	0.3609	4.144
BC10CAL2 - 18.d	0.29967	0.01616	0.8453	0.007	0.036214	0.317723	0.797270	0.3435	3.922
BC10CAL2 - 19.d	0.29886	0.01608	0.8381	0.0074	-0.22072	0.316868	0.790479	0.3472	3.963
BC10CAL2 - 20.d	0.29240	0.01795	0.8396	0.0073	-0.1263	0.310012	0.791894	0.3392	3.816
BC10CAL2 - 21.d	0.29214	0.01622	0.8428	0.0073	-0.17409	0.309740	0.794912	0.3213	3.767
BC10CAL2 - 22.d	0.29326	0.01720	0.8444	0.0078	-0.50789	0.310921	0.796421	0.3234	3.735
BC10CAL2 - 23.d	0.32258	0.02081	0.8436	0.007	0.086526	0.342013	0.795667	0.354	3.883
BC10CAL2 - 24.d	0.30248	0.01738	0.8402	0.0071	-0.36943	0.320702	0.792460	0.337	3.744
BC10CAL2 - 25.d	0.31143	0.01649	0.8413	0.0073	0.078421	0.330190	0.793497	0.3462	3.823
BC10CAL2 - 26.d	0.30479	0.01579	0.8365	0.0078	-0.025627	0.323146	0.788970	0.3519	3.91
BC10CAL2 - 27.d	0.30694	0.01602	0.8432	0.0077	0.092219	0.325427	0.795289	0.3534	3.961
BC10CAL2 - 28.d	0.30257	0.01648	0.8451	0.0066	-0.29862	0.320799	0.797081	0.3349	3.755
BC10CAL2 - 29.d	0.30893	0.01622	0.8418	0.0066	-0.2444	0.327538	0.793969	0.3447	3.832
BC10CAL2 - 30.d	0.30874	0.01620	0.8457	0.0068	0.3314	0.327336	0.797647	0.3525	3.917
js1 - 1.d	4.60830	0.50967	0.561	0.026	-0.63175	4.885903	0.529124	0.662	0.358
js1 - 2.d	3.54610	0.32695	0.652	0.016	-0.81506	3.759720	0.614953	0.706	0.553
JS1 - 3.d	6.75676	0.59350	0.476	0.032	-0.16663	7.163790	0.448954	0.3254	0.09
JS1 - 4.d	5.74713	0.39635	0.512	0.022	-0.89933	6.093339	0.482908	1.062	0.394
js1 - 5.d	5.84795	0.71817	0.508	0.04	-0.61314	6.200240	0.479135	0.191	0.0604
js1 - 6.d	1.74216	0.16390	0.741	0.012	-0.82501	1.847110	0.698896	0.8278	1.48
JS1 - 7.d	1.43885	0.08902	0.7592	0.0077	-0.35833	1.525527	0.716062	0.483	1.077
JS1 - 8.d	3.18471	0.24342	0.656	0.016	-0.84019	3.376564	0.618726	0.767	0.627

APPENDIX G – ADDITIONAL ELEMENTAL MAPS

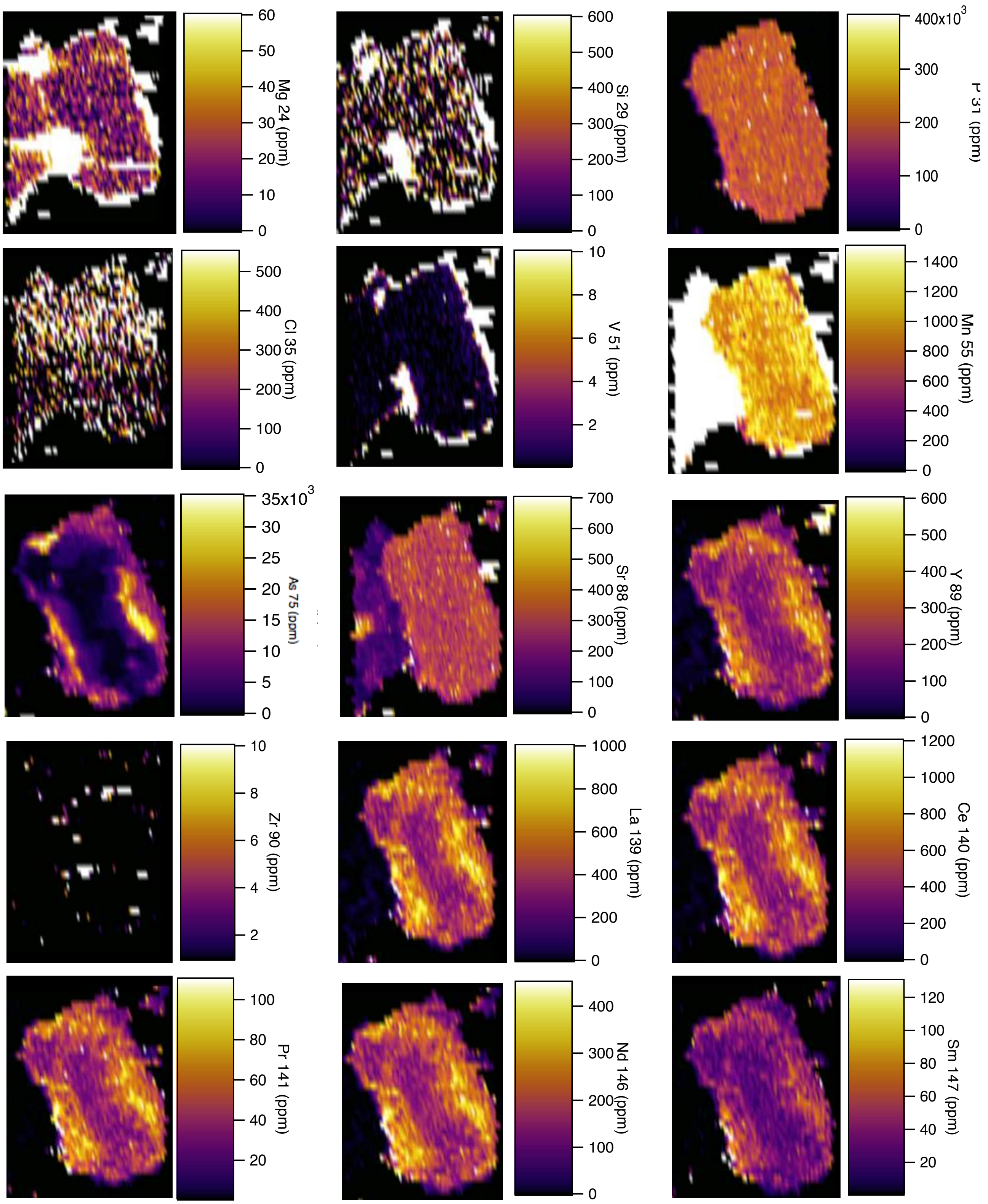

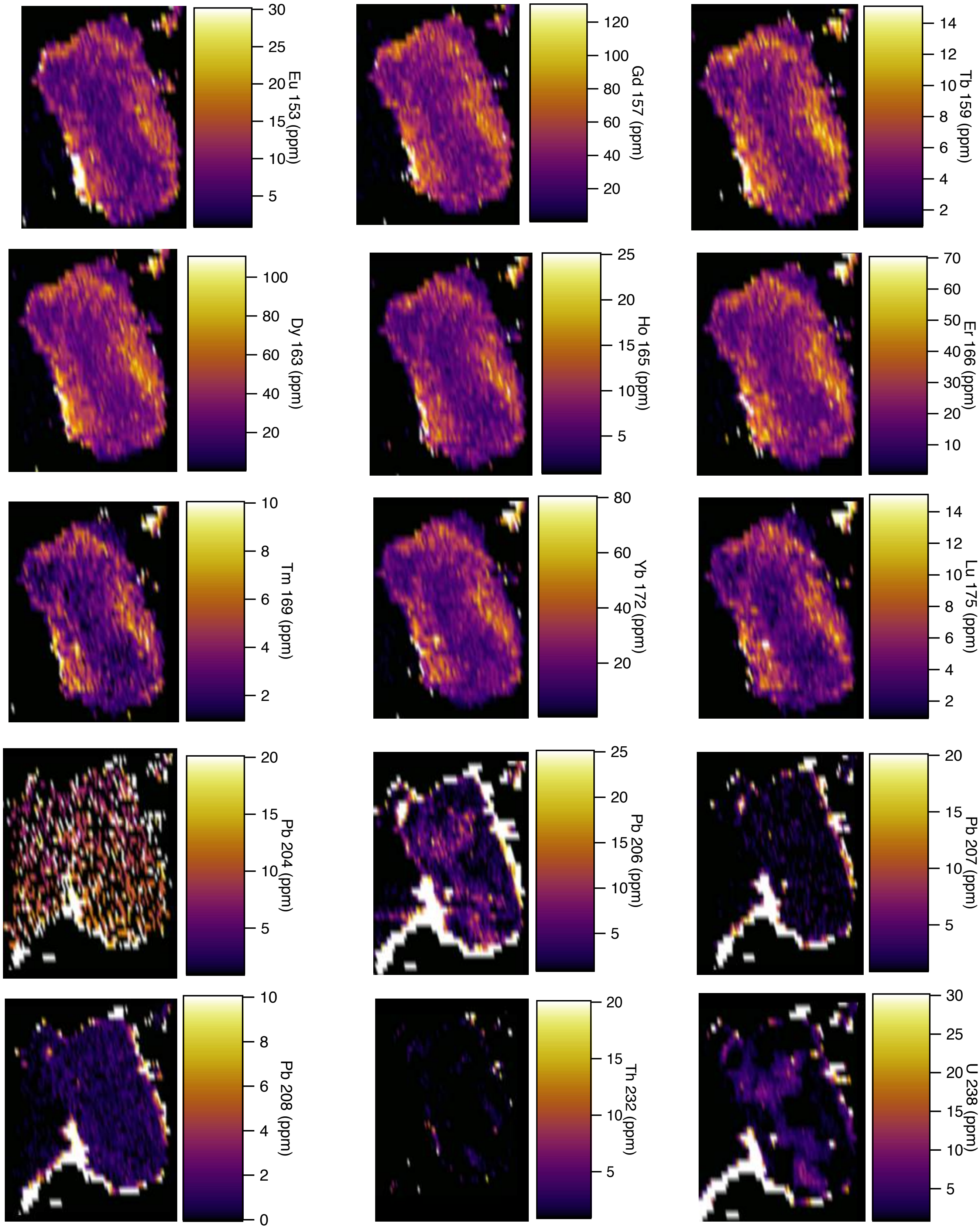
Eu 153 (ppm)
5 10 15 20 25 30
Gd 157 (ppm)
20 40 60 80 100 120
Tb 159 (ppm)
2 4 6 8 10 12 14
Dy 163 (ppm)
20 40 60 80 100
Ho 165 (ppm)
5 10 15 20 25
Er 166 (ppm)
10 20 30 40 50 60 70
Tm 169 (ppm)
2 4 6 8 10
Yb 172 (ppm)
20 40 60 80
Lu 175 (ppm)
2 4 6 8 10 12 14
Pb 204 (ppm)
5 10 15 20
Pb 206 (ppm)
5 10 15 20 25
Pb 207 (ppm)
5 10 15 20
Pb 208 (ppm)
0 2 4 6 8 10
Th 232 (ppm)
5 10 15 20
U 238 (ppm)
5 10 15 20 25 30

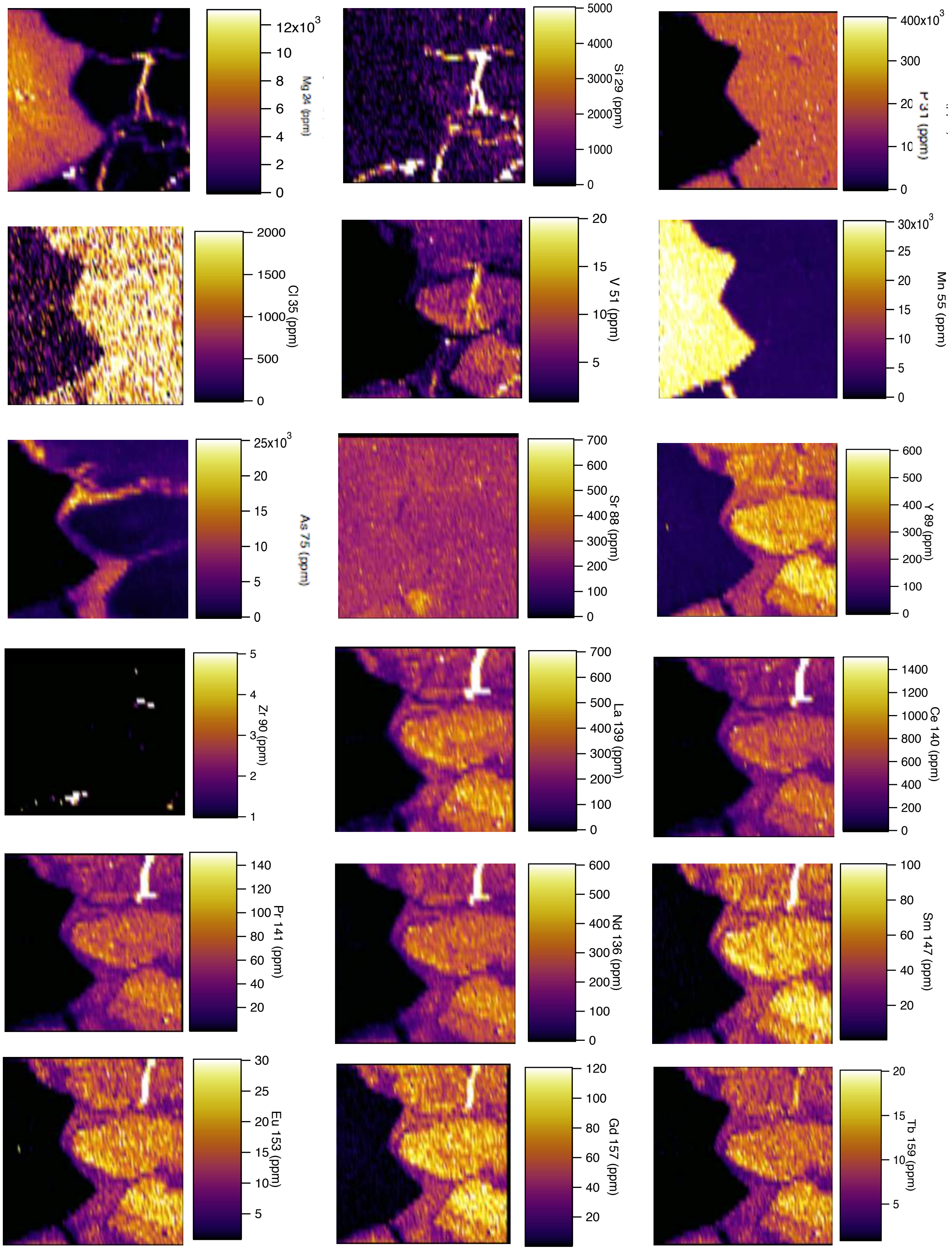
12x10^3
10
8
6
4
2
0
Mg 24 (ppm)
5000
4000
3000
2000
1000
0
Si 29 (ppm)
400x10^3
300
P 31 (ppm)
0
2000
1500
1000
500
0
Cl 35 (ppm)
20
15
10
5
V 51 (ppm)
30x10^3
25
20
15
10
5
0
Mn 55 (ppm)
25x10^3
20
15
10
5
0
As 75 (ppm)
700
600
500
400
300
200
100
0
Sr 88 (ppm)
600
500
400
300
200
100
0
Y 89 (ppm)
5
4
3
2
1
Zr 90 (ppm)
700
600
500
400
300
200
100
0
La 139 (ppm)
1400
1200
1000
800
600
400
200
0
Ce 140 (ppm)
140
120
100
80
60
40
20
Pr 141 (ppm)
600
500
400
300
200
100
0
Nd 136 (ppm)
100
80
60
40
20
Sm 147 (ppm)
30
25
20
15
10
5
Eu 153 (ppm)
120
100
80
60
40
20
Gd 157 (ppm)
20
15
10
5
Tb 159 (ppm)

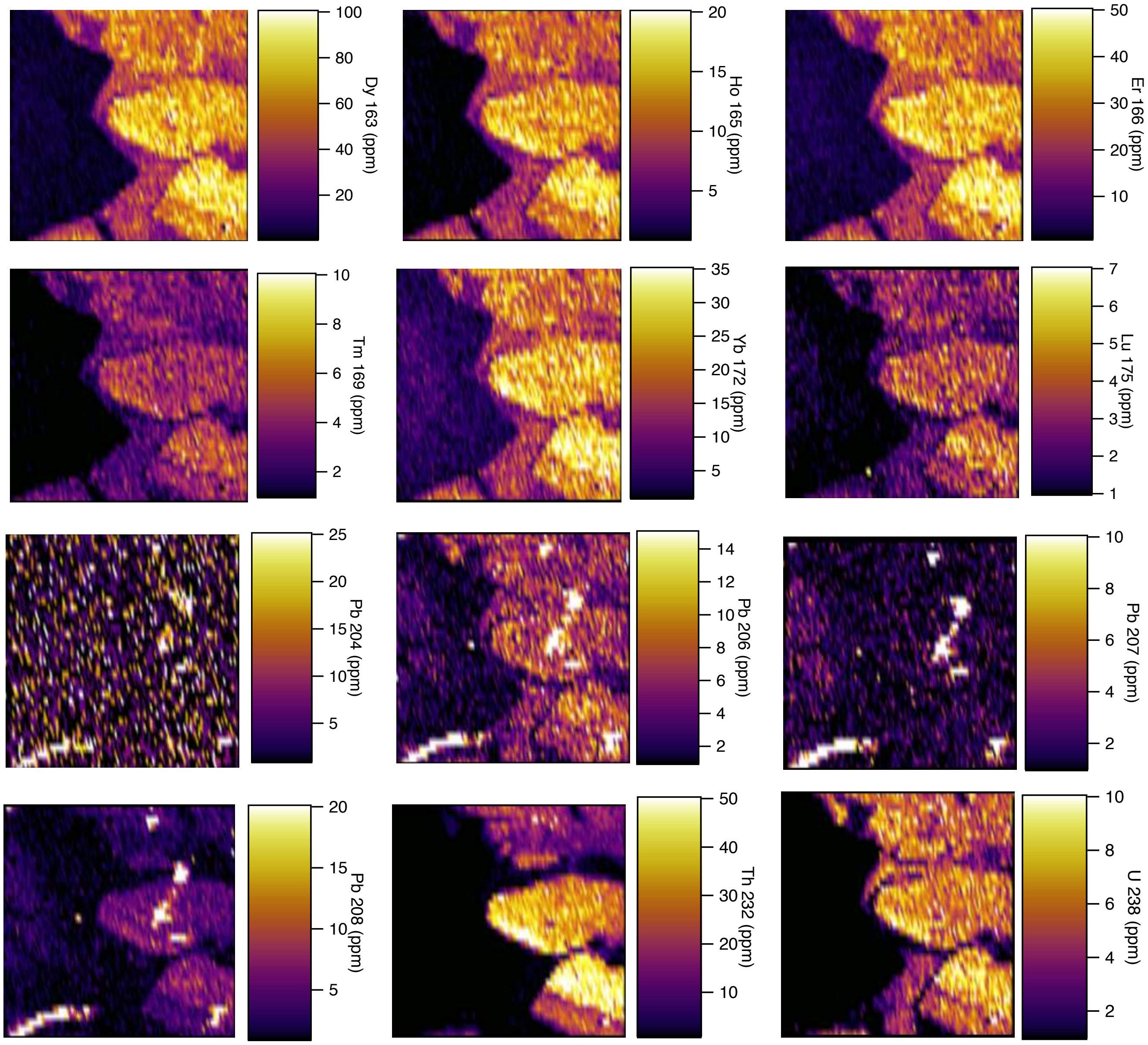
Dy 163 (ppm)
Ho 165 (ppm)
Er 166 (ppm)
Tm 169 (ppm)
Yb 172 (ppm)
Lu 175 (ppm)
Pb 204 (ppm)
Pb 206 (ppm)
Pb 207 (ppm)
Pb 208 (ppm)
Th 232 (ppm)
U 238 (ppm)

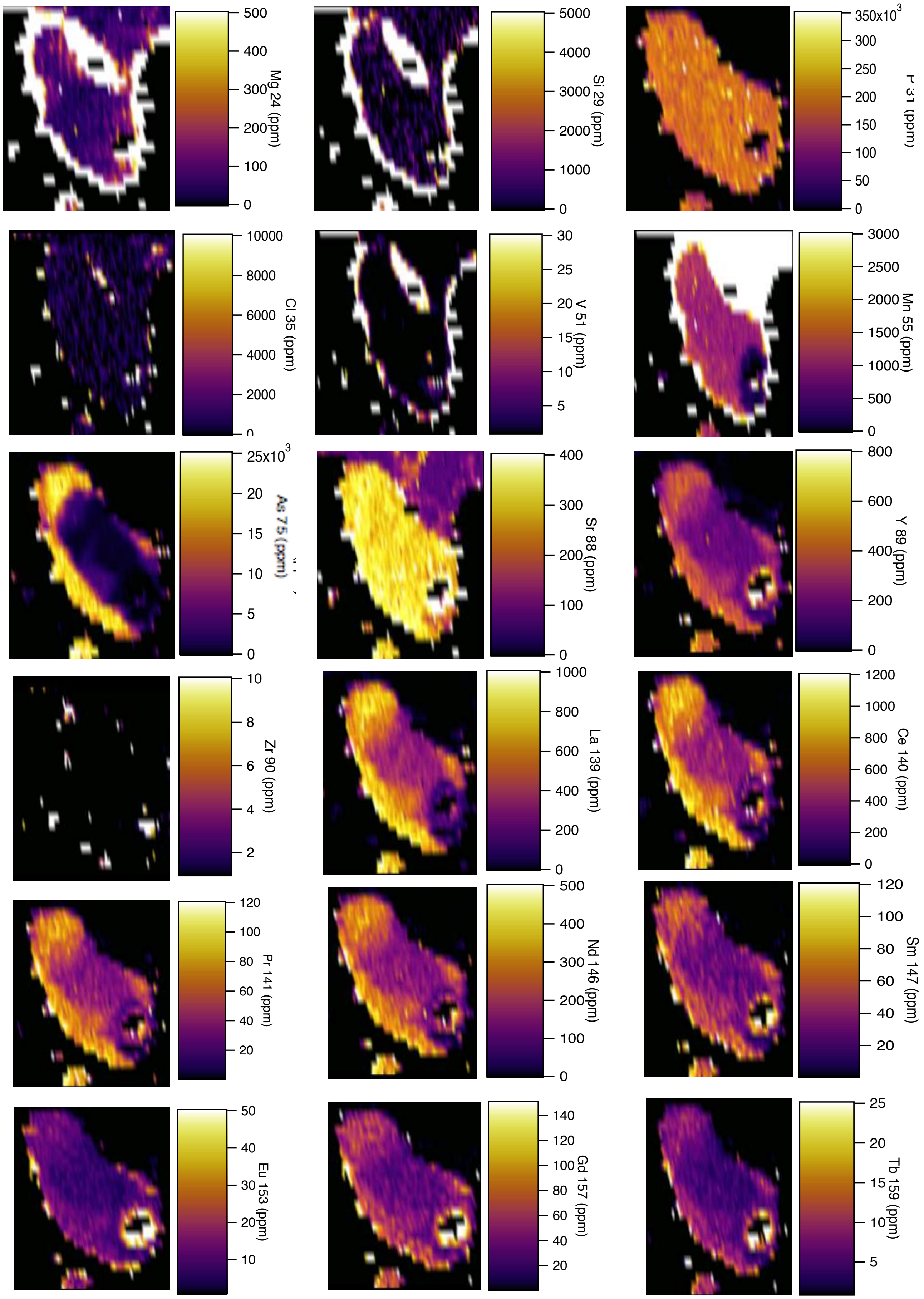
Mg 24 (ppm)
500 400 300 200 100 0
Si 29 (ppm)
5000 4000 3000 2000 1000 0
P 31 (ppm)
350x10^3 300 250 200 150 100 50 0
Cl 35 (ppm)
10000 8000 6000 4000 2000 0
V 51 (ppm)
30 25 20 15 10 5
Mn 55 (ppm)
3000 2500 2000 1500 1000 500 0
As 75 (ppm)
25x10^3 20 15 10 5 0
Sr 88 (ppm)
400 300 200 100 0
Y 89 (ppm)
800 600 400 200 0
Zr 90 (ppm)
10 8 6 4 2
La 139 (ppm)
1000 800 600 400 200 0
Ce 140 (ppm)
1200 1000 800 600 400 200 0
Pr 141 (ppm)
120 100 80 60 40 20
Nd 146 (ppm)
500 400 300 200 100 0
Sm 147 (ppm)
120 100 80 60 40 20
Eu 153 (ppm)
50 40 30 20 10
Gd 157 (ppm)
140 120 100 80 60 40 20
Tb 159 (ppm)
25 20 15 10 5

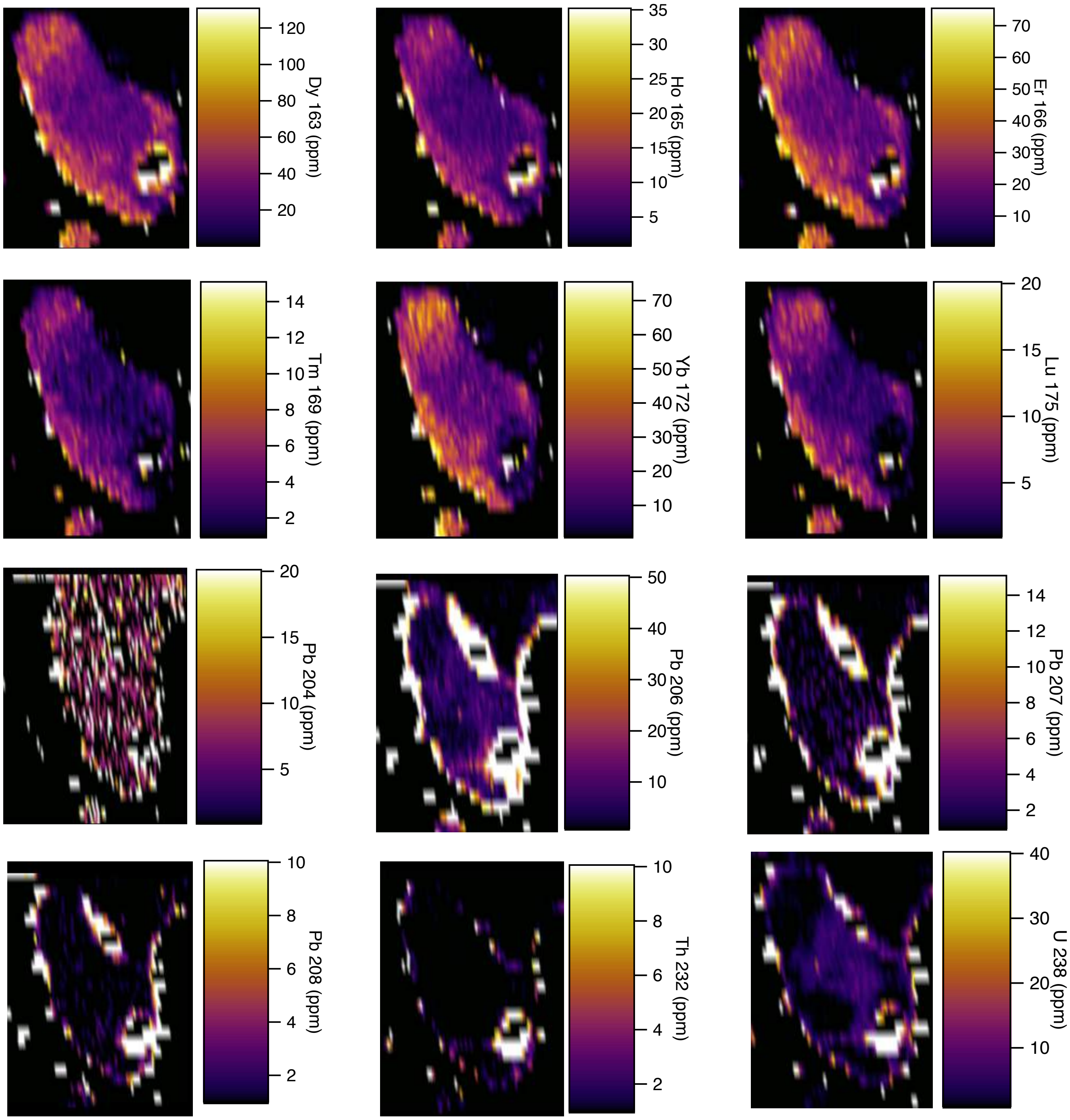
Dy 163 (ppm)
Ho 165 (ppm)
Er 166 (ppm)
Tm 169 (ppm)
Yb 172 (ppm)
Lu 175 (ppm)
Pb 204 (ppm)
Pb 206 (ppm)
Pb 207 (ppm)
Pb 208 (ppm)
Th 232 (ppm)
U 238 (ppm)

APPENDIX H – APATITE TRACE ELEMENT DATA

Sample	La	Ce	Pr	Nd	Sm	Eu	Gd	Tb	Dy	Y	Ho	Er	Tm	Yb	Lu	V	Mn	Sr	Pb206	Pb207	Pb208	Th 232	U238
BC00_1	756	801	72.8	295.4	52.4	12.42	62.2	8.32	50.7	363.9	11.07	32.73	4.51	33.8	7.52	Below LOD	1350	327.6	2.37	0.841	0.731	0.478	1.25
BC00_2	849	883	79.4	311.6	53.7	13.41	60.4	8.2	50.6	358.5	11.53	32.53	4.54	35.4	7.84	0.18	1328	325.4	2.54	0.871	0.799	0.77	1.6
BC00_3	811	861	76.5	312.6	59.5	13.32	62.4	8.71	53	383.8	11.91	35.37	4.88	37.9	8.15	Below LOD	1376	330.1	2.511	0.813	0.608	0.757	1.584
BC00_4	534.5	579.8	51.72	212.5	40.3	9.76	43.6	6.3	36.5	259.6	8.03	23.94	3.3	24.1	5.19	Below LOD	1185	310.8	3.38	0.841	0.545	0.241	2.6
BC00_5	399.7	436.5	39.82	159.8	30	7.73	33	4.65	26.04	198.8	5.79	16.75	2.25	16.41	3.51	Below LOD	1141	297.6	2.68	0.791	0.576	0.128	1.838
BC00_6	1411	1349	111.3	426	64.2	15.57	74.1	10.09	60.8	441.4	14.04	40.8	6.71	51.5	11.32	0.211	1466	334.8	2.83	1.024	0.85	1.184	1.559
BC00_7	694	739	65.7	262.4	49.1	12.3	54.8	7.43	46.9	335	10.43	29.9	4.44	31.9	7.29	Below LOD	1143	322	1.55	0.647	0.65	0.512	0.745
BC00_8	1023	1042	91.4	345.9	61.8	15.12	68.8	9.64	60	419.3	12.89	38.7	5.75	44.3	9.38	0.26	1379	336.1	2.317	0.888	0.686	0.895	1.28
BC00_9	792	858	75.8	297	54.6	14.06	65.8	8.93	53.6	375.2	11.68	34.1	5	37.4	7.74	0.26	1376	329.3	1.84	0.742	0.656	0.53	0.927
BC00_10	732.6	778	68.4	286.5	52.5	12.14	57.1	8.03	49.9	358.9	10.92	30.1	4.26	32	6.58	Below LOD	1278	317.4	1.681	0.649	0.568	0.58	0.915
BC00_11	717	747	65.1	275.8	51	12.04	58.1	8.2	48.8	356	11.1	30.96	4.41	30.63	6.38	0.27	1284	320.5	2.041	0.734	0.547	0.559	1.132
BC00_12	280.8	293.1	26.16	113.4	22.2	5.38	25.8	3.38	18.95	139.3	4.23	10.93	1.34	8.86	1.54	Below LOD	885	299.3	1.88	0.532	0.288	0.07	1.04
BC00_13	335.9	375.8	35.83	144.8	26	6.21	29	4.06	23.39	176.9	5.25	15.01	2.19	15.45	3.51	Below LOD	1019	303.7	2.26	0.505	0.345	0.162	1.96
BC00_14	357.5	395.1	36.96	151	27.4	6.48	31.3	4.17	25.4	184.9	5.48	16.32	2.29	16.51	3.8	Below LOD	1114	295.5	3.847	0.799	0.447	0.164	3.42
BC10A_1	405.1	685	70	301.5	59	16.12	66.5	9.45	55.5	323.3	10.93	27.3	3.25	20	3.09	7.11	2449	248.1	7.2	1.65	4.25	25.62	5.85
BC10A_2	419.5	681	66.6	281.7	53.3	13.64	60.3	8.05	45.9	271.5	9.47	23.01	3.03	17.85	2.56	5.32	2464	237.6	5.33	1.387	3.51	21.43	4.448

BC10A_3	432.2	717	71.5	300.3	55	13.56	59.8	7.94	44.9	275.1	9.23	23.11	3.03	17.16	2.64	6.36	2438	242.9	5.61	1.46	3.07	16.69	4.64
BC10A_4	662	991	91.9	365.8	58.5	14.42	66	8.49	50.4	298.2	9.89	25.69	3.34	18.7	2.97	8.61	2664	242	5.97	1.616	4.28	25.41	5.11
BC10A_5	681	1003	95.4	367.1	65.8	15.42	65.9	8.93	50.6	315	10.5	25.76	3.53	20.34	3.21	8.34	2768	249.1	6.6	1.9	5	27.14	5.4
BC10A_6	493.5	771	75.2	317.7	61.8	15.33	67.1	9.16	54.5	311.3	10.48	26.9	3.28	20.3	2.96	6.53	2562	236.1	6.96	1.806	7.66	34.2	5.51
BC10A_7	303	462	45.8	189.5	40.2	10.14	41.5	5.72	33.4	196.5	6.39	16.5	2.05	12.51	1.72	2.79	2558	233.3	3.96	1.764	3.19	12.7	2.31
BC10A_8	239.1	371.7	37.32	161.4	33	9.33	37.7	5.12	30.9	176.4	6.02	14.01	1.58	9.97	1.57	2.63	2534	244.5	2.93	1.35	1.71	4.17	1.66
BC10A_9	1070	1130	92.7	342	60.6	16.42	68.9	9.57	55.3	310.9	10.63	27.5	3.12	19.56	2.79	5.93	2404	251.3	6.12	1.672	4.57	24.9	4.48
BC10A_10	597.1	924	86.3	358.7	63.6	16.95	73.3	10.07	58.8	336.3	11.86	30.1	3.66	22.07	3.4	8.09	2749	247.9	6.55	1.665	4.6	28.28	5.32
BC10A_11	393.7	615.2	59.5	246.9	44.6	12.46	53.1	7.06	39.7	233.4	8.01	20.23	2.43	16.25	2.18	4	2631	240.1	4.32	1.4	3.02	15.94	3.32
BC10A_12	448.3	765	76.4	311	55.5	14.57	61.4	8.05	49.3	288.2	9.7	25.62	3.26	19.4	2.94	7.4	2335	252.7	5.4	1.316	3.2	18.96	4.907
BC10A_13	147.1	265.8	29.04	132.4	27.6	7.98	38.3	5.34	30.3	177.5	6.15	14.2	1.75	10.23	1.38	3.78	2409	261.5	2.77	0.883	0.75	0.797	2.128
BC10A_14	266.6	426.2	42.7	172.9	36.5	10.14	43.4	5.8	33.5	191.8	6.64	15.97	1.86	11.33	1.74	2.84	2596	245.4	3.05	1.284	1.8	5.89	1.808
BC10A_15	353.8	589	59.1	238.7	47.7	12.65	53.6	7.53	43.8	251.2	8.83	20.8	2.79	16.4	2.33	5.16	2428	244	4.5	1.332	2.56	13.92	3.36
BC10A_16	565	865	81.7	325.9	55.1	12.49	58.7	7.72	42.7	257.6	8.63	23.03	2.86	16.73	2.47	5.32	2496	245.7	6.05	1.75	4.16	22.32	3.93
BC10A_17	802	1172	105.9	411	63.4	13.93	67.8	8.98	50.7	308.7	10.25	26.7	3.38	21.1	3.2	8	2801	246.8	6.88	1.863	7.56	39.18	5.86
BC10A_18	493.6	813	81.5	329	60.1	15.81	68.5	9.22	53.8	312.9	10.69	27.1	3.43	21	3.18	6.19	2498	242.6	6.73	1.8	5.03	27.4	5.68
BC10A_19	376	590	56.7	227	42.6	10.87	43.9	6.09	32.9	202.8	6.58	16.71	2.24	13.1	1.83	4.78	2518	241.3	4.82	1.48	3.54	15.7	3.52
BC10A_20	790	1010	88	359	62	16.4	64	8.92	51.9	301.2	10.32	25.9	3.05	19.8	2.74	8.5	2716	246.5	7.75	2.7	5.97	28.2	5.26
BC10A_21	252.4	362	35.8	151.7	29.5	8.66	36.8	4.98	29.4	164.3	5.64	13.66	1.55	9.89	1.41	2.93	6010	200	3.51	1.32	2.38	7.19	1.98
BC10A_22	295.9	476	47.9	208	45.7	14.28	58.3	8.38	46	263.3	8.91	22.39	2.85	15.26	2.33	4.29	2617	236.2	6.02	1.87	3.87	18.1	4.4
BC10A_23	347.9	543	53.3	215	41.3	9.51	43.1	5.43	32.4	189.1	6.37	15.99	2.06	12.42	1.76	3.91	2528	237.3	3.89	1.364	2.65	11.1	2.72

BC10A_24	188.8	350	39.4	179.2	44.7	12.71	58.1	8.02	48.3	283.6	10.04	24.9	2.92	17.4	2.25	4.36	2018	270.7	5.6	1.212	1.76	7.79	5.35
BC10A_25	208.8	337.2	35.1	153.5	34.9	9.86	43.4	5.81	34.6	191.3	6.48	16.87	2.04	12.25	1.67	3.04	2286	257.3	3.12	1.113	1.27	3.63	2.41
BC10A_26	258.7	421	42.8	190	41.3	11.92	52.7	7.28	40.2	237.5	7.99	20.3	2.6	14.3	2.25	4.72	2338	253.5	4.48	1.306	1.77	7.45	3.72
BC10A_27	255.5	429.4	44.25	191.7	42.5	12.44	52.8	7.28	42.4	247.4	8.3	21.75	2.42	14.73	2.04	5.79	2308	248.7	5.17	1.35	1.6	7.9	4.4
BC10A_28	237.2	411.7	42.78	192.2	43.2	11.88	50.7	7.41	42.2	252.4	8.74	20.54	2.62	15.27	2.06	4.55	2359	258.2	5.05	1.25	1.73	7.45	4.41
BC10A_29	228.3	377.2	40	176.7	38.7	10.3	46.2	6.18	35.7	216.7	7.44	17.7	2.07	12.37	1.86	5.96	2394	254	4.09	1.22	1.7	4.72	3.31
BC10A_30	201.1	328.4	33.08	143.6	29	8.54	37.8	5.02	29	172	6	13.76	1.83	9.98	1.48	3.07	2412	249.5	2.667	1.043	1.12	1.93	1.813
BC10A_31	203.7	339.5	34.5	151	34	9.2	40.5	5.77	30.7	185.3	6.17	14.33	1.84	10.23	1.52	3.42	2369	246.7	2.9	1.08	1.32	2.88	2.088
BC10A_32	230	391	40.7	178.9	38	10.73	49.2	6.59	38.9	230	7.66	18.6	2.46	12.7	1.99	4.14	2258	247	3.81	1.216	1.81	7.6	3.2
BC10A_33	272.1	474.4	49.7	218	49.6	13.31	56.3	8.17	45.6	263.3	9.38	23.73	2.66	16.5	2.34	14.1	2320	253.3	5.63	1.514	2.39	11.17	4.953
BC10A_34	226.7	400.4	42.9	192.7	45.9	11.97	53.3	7.49	42.4	248.6	8.88	20.74	2.58	14.6	2.13	5.12	2242	252.7	5.54	1.288	1.46	5.57	5.03
BC10A_35	215.8	378.4	40.74	179.3	40.9	11.87	49.6	7.19	41.1	234.5	8.2	19.18	2.51	13.04	2.19	5.22	2222	251.9	5.04	1.284	1.46	4.4	4.46
BC10A_36	203.8	351.8	38.11	175.8	38.5	10.68	46.7	6.68	38.6	228.3	7.82	19.38	2.43	12.99	2.19	4.42	2176	255.3	4.51	1.076	1.25	4.24	4.06
BC10A_37	192.9	339.4	37.14	167.5	38.5	10.5	49.3	6.58	37.7	226.2	7.8	18.2	2.22	12.77	1.95	5.06	2115	258.7	4.65	1.172	1.19	4.24	4.28
BC10A_38	218.2	377.9	40.09	173.2	39.5	11.13	49.5	6.74	38.5	227.4	7.89	19.01	2.23	12.25	2.11	4.12	2216	246.2	4.15	1.138	1.53	6.14	3.651
BC10A_39	784	1004	91.9	360.6	75.6	21.2	86.9	12.98	73.9	409.4	14.8	36.7	4.65	26.5	3.98	8.05	2787	287.1	9.18	2.87	8.72	54.6	7.34
BC10A_40	1180	1315	111.2	397.1	73.3	18.36	79.3	10.66	62.7	370.2	12.47	32.4	4.16	24.98	3.99	8.66	2912	354.1	8.46	2.17	8.11	57.4	7.51
BC10A_41	962	1165	101.1	383.2	74.3	18.55	81.7	11.65	68.4	393.3	13.79	35	4.35	26.5	3.71	8.87	2854	322.8	8.79	2.82	8.8	56.6	7.38
BC10A_42	778	1002	93.2	359.9	73.2	19.75	86.7	12.71	69.3	401.9	13.98	35.4	4.19	24.7	3.93	8.06	2742	290.3	7.55	1.993	7.39	50.71	7.06
BC10A_43	550.1	780	76.6	315.3	67.4	19.87	83.2	11.89	67.8	369.6	12.94	33.4	4.21	24.3	3.82	7.39	2693	259.7	6.91	1.78	5.96	42.8	6.02
BC10A_44	429.1	671	68.9	301.1	69	20.05	88.1	12.42	73	402.6	14.45	36.6	4.3	25	3.84	7.66	2558	259.2	7.61	1.89	5.79	38.6	6.73

BC10A_45	494	738.9	74.6	319.7	71.2	21.42	91	12.78	73.9	411.2	14.34	36.8	4.65	26.6	3.98	6.75	2624	249.9	6.88	1.774	6.01	42.99	6.25
BC10A_46	463.2	721.4	74.1	309.5	72.4	21.33	92.7	13.12	73.8	415	14.88	37.8	4.62	25.9	3.89	7.22	2566	246.3	7.28	1.92	6.07	41.38	6.58
BC10A_47	428	638	65.4	279.3	63.4	18.69	77.9	11.25	67.1	372.3	13.07	33.2	3.94	22.9	3.7	6.56	2605	245.8	6.52	1.665	5.25	34.07	5.85
BC10A_48	675	919	84	349.3	70.8	20.44	84.9	12.32	73	400.7	13.91	35.3	4.31	25.8	3.77	7.66	2695	262.6	7.25	1.92	6.84	47.6	6.49
BC10A_49	690	939	87.7	352	73.4	20.71	84.4	12.56	72.7	424	14.67	35.7	4.64	27.1	4.04	8.91	2716	274.5	8	2.17	7.35	51.2	6.85
BC10A_50	244.1	427.2	43.1	204.2	46.7	12.51	53.9	7.75	43.5	262.7	8.67	21.5	2.44	14.93	2.28	4.57	2420	231.5	4.38	1.175	2.55	12.42	3.6
BC10A_51	303.1	506.3	51.1	235.2	49.5	14.94	64.1	9.2	52.4	313.2	10.63	26	3.02	18.3	3.01	6.44	2482	240.2	3.99	1.224	3.72	23.06	3.64
BC10A_52	294.5	524.8	54.4	246.4	55.3	15.77	67.8	10.04	56.6	339.3	11.31	27	3.31	20.15	3.05	5.15	2275	252.9	6.61	1.443	3.12	21.1	6.19
BC10A_53	426	669	68	310	65.8	18.97	81.4	11.72	70.6	393	13.34	34.1	4.05	24.2	3.45	7.7	2456	239.3	7.96	2.1	5.63	35.2	8
BC10A_54	309.8	526	54.9	244.5	55	15.72	68.2	9.49	56.5	314.4	10.93	27	3.15	19	2.78	5.34	2416	240.5	6.08	1.5	3.89	22.39	5.42
BC10A_55	428.7	708	71.2	315.2	71.5	20.89	83.1	12.5	69.9	401.5	13.9	33.6	4.28	25.8	3.52	7.52	2498	236.7	7.82	1.92	5.66	37.1	7.33
BC10A_56	179.5	279.5	28.28	120.9	24.2	8.02	33.6	4.36	25.9	148.2	5.42	12.51	1.39	8.48	1.25	3.72	2521	237	2.21	1.207	1.3	1.96	1.095
BC10A_57	186.6	302	30.57	140.9	31.9	9.29	41	5.66	32.4	182.4	6.23	15.03	1.62	10.29	1.59	4.49	2457	234.8	3.44	1.254	1.96	6.44	2.14
BC10A_58	261.6	428	43.8	197	47.3	13.01	58.8	7.76	45.8	255.8	8.77	21	2.41	14.5	2.39	4.84	2457	235.1	4.58	1.5	3.35	18.2	3.65
BC10A_59	325	531	54.4	241	56.6	16.1	69.1	9.68	55.5	314	10.9	26.1	3.04	17.4	2.76	6.24	2523	241.9	6.02	1.69	4.74	26.8	4.45
BC10A_60	439	715	71.8	317.8	72.4	21.9	90.2	12.33	73.6	407.7	14.47	35.5	4.2	25.16	3.86	8.22	2543	240.6	8.49	2.094	6.81	44	7.71
BC10A_61	494	747	71.5	311.8	70.4	19.9	83.9	11.99	68.9	385	14.24	32.7	3.99	23.8	3.62	7.84	2653	244.9	8.3	2.525	6.79	37.8	6.85
BC10B_1	208.5	336.4	35.67	162	42.1	11.81	54.5	8.02	45.1	268.5	9.09	21.89	2.64	14.4	2.23	4.68	2182	341	4.08	1.009	0.79	1.125	3.83
BC10B_2	168.7	294.6	32.17	143.2	35	11.29	48.1	6.64	38.6	228.6	7.96	19.54	2.28	12.81	1.83	2.08	2767	261.2	4.26	1.145	0.82	1.007	3.554
BC10B_3	214	313	30.8	143	28.2	9.4	33.2	5.3	26.2	170	6.03	16	2.05	9.6	1.49	2.1	8160	256	8.18	5.77	4.46	1.25	3.01

BC10B_4	214.5	347.6	36.38	161.2	39.7	11.16	50.7	8.04	46.6	262.6	9.22	23.53	2.67	15.84	2.19	4.45	2237	367.3	4.4	1.061	0.797	1.152	3.8
BC10B_5	234.5	330	34.2	144.5	33.1	10.27	43.9	6	36.1	209	6.92	16.95	1.94	11.9	1.7	2.56	2640	265.9	6.22	2.81	2.6	0.98	3.51
BC10B_6	235	348	36.5	161.8	34.3	11.07	45.3	6.63	37.6	226	7.59	17.8	2.11	13.17	1.91	3.09	2670	251.9	7.9	3.27	2.5	1.31	4.59
BC10B_7	252.4	405	39.8	180.3	41.2	11.26	51	6.73	41.1	246.2	8.07	19.57	2.48	13.49	1.99	2.74	3767	260.2	5.58	1.55	1.16	1.33	4.76
BC10B_8	34.2	57	5.5	24.6	5.5	2.35	9.1	1.26	8.8	68	1.86	6.1	0.64	5.07	1.19	0.86	2.72E+04	252.4	1.64	0.99	1.03	0.26	0.64
BC10B_9	129.2	191.4	19.1	83.5	19.1	5.32	23.2	3.29	19.2	122.3	3.84	10.12	1.14	7.51	1.18	1.2	20120	249.9	3.8	1.579	1.44	0.701	2.35
BC10B_10	219.3	355.2	35.74	164.6	37.5	10.53	46.6	6.56	39.8	225.7	7.73	18.76	2.16	12.65	2.07	1.81	2562	248.8	4.76	1.317	1.07	0.895	4.09
BC10B_11	194	335.3	37.49	174.9	40.9	12.59	54.8	7.79	42.9	256.6	8.94	21.89	2.61	14.55	2.13	3.34	2717	275.7	6.18	1.359	0.84	1.74	5.82
BC22A_1	983	1030	72.82	245.7	37.1	8.17	43.3	6.39	38.9	261	8.52	22.59	2.76	19.36	2.81	6.96	1030	354.1	7.79	1.73	5.85	37.52	6.91
BC22A_2	851	968	72.6	251.6	37.2	7.62	40.7	6.11	36	239.7	7.76	20.31	2.64	16.85	2.53	7.11	1028	355.3	7.63	1.89	4.57	25.43	6.495
BC22A_3	608	712	55.4	208	34.1	7.51	42.7	6.19	39.4	250.7	8.14	21.68	2.83	17.26	2.55	5.89	1630	330	8.3	4.5	6.1	18.55	4.73
BC22A_4	181	262	25.42	121.7	34.4	9.98	62.8	10.53	71.8	444.7	15.7	38.97	4.95	30.26	4.09	7.31	983	219.5	11.9	7.4	8.1	23.72	5.75
BC22A_5	728	792	57.4	209	36.2	9.17	51.1	8.06	50.9	337.8	11.17	29.25	3.55	24.35	3.48	6.79	1013	306.7	7.16	1.55	5.25	35.9	6.6
BC22A_6	774	829	60.4	220.5	37.1	9.08	48.2	7.91	49.8	322.4	10.85	28.85	3.71	22	3.24	6.5	1070	316	9.63	3.1	7.18	38.73	7.02
BC22A_7	677.5	790	60.9	233.1	38.6	8.95	50	7.42	47.9	307.7	10.12	27.05	3.47	21.82	3.08	9.03	1075	332.2	8.15	2.87	5.17	24.24	6
BC22A_8	737	831	62.1	232.4	38.1	8.54	51.2	7.35	46.5	303.5	10.03	27.24	3.34	21.36	3.17	7.25	1035	311.4	10.1	4.1	7.4	37.22	6.86
BC22A_9	493	566	45.1	178.4	37.5	9.93	58.1	9.11	62.3	398.3	13.8	35.2	4.23	26.8	3.92	6.86	1008	265.7	7.27	1.33	4.92	33.73	7.03
BC22A_10	771	893	68.5	250.5	39.4	8.31	47.7	6.57	41.6	272.6	9.27	23.85	2.98	19.3	2.8	7.78	1038	334	7.93	2.32	4.56	25.6	6.51
BC22A_11	370	436	37	153.9	34.5	9.36	56.3	9.73	64.6	409	14.33	37.4	4.69	29.4	3.91	6.86	993	251.6	8.08	2.67	5.94	35.48	6.61
BC22A_12	679	768	59.1	217.2	36.9	8.8	50.2	7.47	47.7	307.7	10.12	27.7	3.55	21.8	3.2	6.38	1021	298	8.6	2.66	6.9	37.27	6.98

BC22A_13	213	261.5	24.15	106.2	32.9	10.57	61.4	11.35	78.1	471.7	16.24	42.8	5.53	31.98	4.64	7.79	1017	225.5	9.16	2.54	5.72	33.03	7.91
BC22A_14	80.6	120	12.79	67.5	26.4	9.05	56.7	9.93	68.8	405.3	14.84	38.5	4.78	28.1	3.92	6.87	931	194.7	12.7	8.5	11	27.6	5.79
BC22A_15	73	107	10.67	55	21.4	6.93	47.4	8.98	63.7	386.7	13.88	36.35	4.42	25.5	3.74	5.67	928	190.2	10.4	7.2	11	18.66	4.34
BC22B_1	20.41	44.3	6.23	38	19.6	6.42	41.7	7.77	51.8	307	11.26	28.63	3.43	20.3	2.86	4.26	925	159.8	5.08	1.34	2.79	15.49	3.99
BC22B_2	9.1	19.96	2.82	19.4	9.7	3.45	23.6	4.22	30	189.6	6.68	17.7	2.06	12.62	1.63	2.65	875	148	2.57	1.64	1.54	2.11	1.308
BC22B_3	10.95	24.66	3.63	23.3	11.86	4.14	27.8	5.26	35	216.1	8.03	20.65	2.44	14.96	1.99	3.41	883	153.1	2.47	0.75	1.12	5.72	1.84
BC22B_4	9.86	21.06	2.84	19.42	9.95	3.06	22.7	4.13	28	178.1	6.51	16.29	1.87	11.03	1.42	2.8	892	158.6	2.9	2.6	1.83	0.794	0.766
BC22B_5	33.3	62.8	7.8	48	20.4	6.9	42.6	7.71	51.4	305.5	11.12	27.5	3.37	20.4	2.7	4.4	939	183.3	5.3	1.67	3.47	16.16	3.37
BC22B_6	26.6	51.5	6.27	40	16.8	5.59	40.5	6.95	47.8	291.8	10.63	28.03	3.23	19.9	2.56	4.19	904	172	3.48	1.09	2.47	14.21	2.78
BC22B_7	36.32	76.5	10.14	62	26.1	9.22	59.1	10.75	73.4	421.3	15.56	39.9	4.99	29.34	4.18	5.54	934	167.7	5.78	2.4	3.69	23.32	4.554
BC22B_8	23.08	49.7	6.75	43.6	19.8	6.92	46.5	8.56	58.5	343.8	12.45	32.82	4.12	23.37	3.24	4.77	902	160.4	5.49	1.57	2.79	18.64	4.12
BC22B_9	26.01	54.39	6.97	43.1	20.29	7.64	46.7	8.12	59.3	351.1	12.92	32.8	4.21	24.12	3.39	5.2	923	161.6	7.5	2.59	3.96	18.74	5.58
BC22B_10	13.25	25.71	3.48	22.6	9.38	3.52	24.2	4.14	31.9	182.8	6.52	17.22	2.19	12.18	1.639	3.37	915	172.4	2.59	1.75	1.85	5.72	1.28
BC22B_11	17.8	35.3	4.87	29.3	13.4	5.16	31.2	5.96	40.2	252.3	9.18	24.15	2.97	16.76	2.4	6.74	1005	163.7	5.3	3.3	3.8	11.6	2.52
BC22B_12	18.98	36.5	4.48	28	12.06	4.46	30.2	5.6	35.9	215.8	8.02	20.68	2.48	14.74	2.1	2.48	925	187.8	3.67	2.79	2.91	7.67	1.847
BC22B_13	9.55	20.29	2.85	18.7	9.15	3.46	23	4.31	30.6	182.9	6.56	17.58	2.2	12.6	1.72	3.9	842	163.8	2.38	1.41	1.87	6.1	1.313
BC22B_14	11.11	22.67	3.11	18.92	8.83	3.24	20.9	3.71	26.4	160.8	5.6	14.96	1.72	9.9	1.34	1.24	928	172.6	1.565	0.65	1.14	3.9	0.881
BC22C_1	17.6	33.1	2.92	15.2	9.9	2.07	12.5	4.72	24.4	169	5.4	15	1.54	7.8	1.34	4430	1.65E+05	189	162	117	113	0.009	1.51
BC22C_2	16.42	30.79	3.76	24.1	9.45	3.54	22.2	3.93	25.62	154.4	5.62	14.12	1.75	9.35	1.41	32.5	3080	183.4	5	3.8	3.2	0.0284	0.642
BC22C_3	13.1	25.97	3.39	20.4	8.46	3.08	22.2	3.64	25.25	141	5.24	13.49	1.486	9.48	1.29	0.66	990.3	168.3	8.6	8.4	7.7	0.0484	0.759

BC22C_4	13.93	27.7	3.29	21.2	9.34	2.87	21.6	3.63	24.34	141.5	5.19	12.98	1.54	9.08	1.299	3.82	1129	167	11.2	11	12.9	0.053	0.587
BC22C_5	9.22	18.34	2.3	16.18	6.51	2.4	17.8	3.06	21.26	131.1	4.45	12.36	1.47	8.5	1.22	0.64	945	158.6	5.3	5.4	3.2	0.07	0.591
BC22C_6	10.61	20.38	2.4	16.7	7.78	2.4	19	3.54	26.1	170.8	6.11	15.52	1.89	10.9	1.45	8.4	1144	151.1	29	22.3	27	0.06	0.566
BC22C_7	12.9	23.72	3	17.9	8.53	2.66	16.6	3.15	21.62	128.3	4.62	11.95	1.378	8.4	1.199	2.71	1001	157.7	14.6	15.1	13.7	0.077	0.567
BC22C_8	9.83	20.4	2.67	17.3	8.42	3.1	22.8	4.24	29.9	192.7	6.82	17.79	2.18	13.41	1.77	2.79	909	152.5	9.5	8.8	7.2	2.99	1.296

APPENDIX I – CALCITE TRACE ELEMENT DATA

	V	Mn	As	Sr	Y	Zr	La	Ce	Pr	Nd	Sm	Eu	Gd	Tb	Dy	Ho	Er	Tm	Yb	Lu
G_NIST612_0	39.15	38.07	37.52	78.75	38.07	38.12	35.85	38.72	37.19	36.02	38.16	35.04	36.86	36	36.01	38	38.1	38.03	39.19	36.96
G_NIST612_1	38.93	37.91	36.68	78.13	37.96	37.89	35.78	38.75	37.21	35.93	38.02	34.99	36.76	35.97	35.99	38.02	37.92	37.99	39.23	36.83
G_NIST612_2	38.9	37.97	37.06	78.31	37.88	37.91	35.69	38.63	37.11	35.73	37.95	34.85	36.58	35.87	35.9	37.81	37.88	37.89	39.1	36.75
G_NIST612_3	39.01	38.04	36.98	78.49	38.06	38.07	35.87	38.66	37.3	35.79	38.26	35.12	36.59	36.08	36.07	38.1	38.1	38.04	39.34	36.96
G_NIST612_4	38.96	38.19	37.02	78.42	38.01	37.98	35.83	38.83	37.24	36.01	38	34.94	36.69	36.02	35.98	37.98	37.9	38.05	39.15	36.9
G_NIST612_5	39.1	37.71	36.8	78.37	37.98	38.03	35.78	38.66	37.15	35.92	38.25	35.05	36.76	35.99	36.03	38.02	38.09	38	39.23	36.98
G_NIST612_6	38.99	37.96	36.98	78.29	37.86	37.98	35.76	38.67	37.09	35.93	38.12	34.96	36.62	35.93	35.96	37.94	37.95	38.05	39.31	36.85
G_NIST612_7	39.05	38.04	37.23	78.5	38.11	38.01	35.82	38.68	37.3	35.84	38.07	35.04	36.79	36.06	36.02	38.04	38.03	37.95	39.09	36.88
G_NIST612_8	39.1	37.99	37	78.5	38.04	38.15	35.91	38.84	37.27	35.99	38.16	35.07	36.83	36.07	36.19	38.09	38.08	38.14	39.35	37.02
G_NIST612_9	38.9	38.01	36.93	78.33	37.96	37.91	35.67	38.59	37.15	35.85	38.02	34.94	36.61	35.95	35.87	37.91	37.86	37.86	39.09	36.81
BC10_0	10.12	1740	3.13	185.6	20.35	545.5	22.16	37.43	4.589	17.4	3.13	0.684	2.669	0.381	2.54	0.567	1.711	0.258	1.826	0.303
BC10_1	9.78	1410	2.97	185.5	20.88	562.2	22.44	37.08	4.591	17.95	3.28	0.671	2.664	0.386	2.572	0.576	1.762	0.268	1.883	0.31
BC10_2	9.86	1590	2.96	185.89	20.8	555.5	22.41	37.14	4.544	17.64	3.31	0.664	2.709	0.384	2.527	0.552	1.71	0.268	1.91	0.297
BC10_3	10.03	1710	3.08	186	20.84	555	22.4	37.4	4.56	17.58	3.31	0.653	2.82	0.403	2.62	0.553	1.74	0.269	1.89	0.305

BC10_4	9.98	1790	3.16	185.3	20.64	548.3	22.33	37.09	4.536	17.19	3.08	0.65	2.66	0.401	2.605	0.555	1.719	0.261	1.843	0.287
BC10_5	10	1710	2.85	185.85	20.9	554.7	22.28	37.14	4.58	17.37	3.27	0.669	2.72	0.382	2.542	0.561	1.793	0.276	1.942	0.302
BC10_6	9.96	1790	3	187.3	20.7	550.7	22.34	37.08	4.584	17.36	3.16	0.612	2.548	0.397	2.568	0.556	1.743	0.26	1.873	0.283
BC10_7	10.1	1640	2.97	188.8	20.52	546.2	22.19	37.34	4.607	17.38	3.23	0.669	2.641	0.393	2.561	0.567	1.798	0.274	1.979	0.299
BC10_8	9.93	1860	2.9	187.8	20.92	551.3	22.23	36.85	4.57	17.44	3.29	0.643	2.586	0.383	2.581	0.573	1.744	0.262	1.906	0.299
BC10_9	9.99	960	2.86	186.05	20.83	558.4	22.25	36.97	4.496	17.54	3.22	0.669	2.674	0.386	2.633	0.58	1.835	0.264	1.914	0.298
BC10_10	9.9	1790	2.81	188.8	21.03	557	22.22	36.7	4.535	17.32	3.19	0.643	2.63	0.403	2.647	0.577	1.759	0.273	1.915	0.296
BC10_11	9.89	1010	2.72	185.1	20.4	549.6	22.22	37.24	4.535	17.58	3.21	0.65	2.597	0.386	2.601	0.548	1.682	0.2526	1.91	0.281
BC10_12	9.99	1160	2.59	187.6	20.68	546	22.17	37.04	4.47	17.39	3.23	0.637	2.581	0.386	2.64	0.548	1.728	0.26	1.898	0.2856
BC10_13	9.94	1870	2.7	190	20.68	538.1	22.64	37.63	4.476	17.45	3.19	0.612	2.591	0.389	2.481	0.544	1.678	0.262	1.905	0.319
BC10_14	10.04	2050	2.89	189	20.51	538.5	22.57	37.9	4.58	17.27	3.16	0.613	2.59	0.404	2.563	0.547	1.741	0.273	1.882	0.302
BC10_15	10.26	2250	2.86	190.1	20.63	546.6	22.42	38.25	4.553	17.59	3.19	0.671	2.62	0.391	2.558	0.556	1.701	0.268	1.871	0.317
BC10_16	10.02	1960	2.85	187.2	20.67	538.5	21.87	37.26	4.496	17.25	3.155	0.643	2.593	0.383	2.53	0.548	1.738	0.266	1.888	0.306
BC10_17	10.07	1980	2.88	187.4	20.43	541	22.08	38.15	4.576	17.58	3.14	0.671	2.663	0.387	2.661	0.56	1.685	0.26	1.905	0.292
BC10_18	9.92	1820	2.74	187.1	20.81	549.1	22.42	37.72	4.636	17.75	3.14	0.66	2.734	0.388	2.562	0.557	1.737	0.269	2.011	0.317
BC10_19	10.02	1040	20.8	184.6	20.63	545.1	22.59	38.87	4.662	17.86	3.26	0.671	2.756	0.374	2.655	0.552	1.701	0.261	1.806	0.293
VEIN_0	4.511	417	1.35	215.35	10.93	389.9	19.54	38.63	4.153	15.88	2.83	0.513	2.065	0.295	1.878	0.388	1.188	0.1775	1.194	0.189
VEIN_1	4.489	556	1.45	216.3	11.02	385.8	19.1	38.29	4.178	15.85	2.77	0.512	2.03	0.3	1.916	0.387	1.178	0.1815	1.292	0.2068
VEIN_2	4.504	162	1.21	214.87	10.44	390.5	19.07	38.18	4.161	15.64	2.697	0.486	1.88	0.291	1.829	0.35	1.077	0.18	1.203	0.196
VEIN_3	4.546	380	1.33	215.03	10.89	386.9	19.41	38.74	4.213	16.11	3	0.515	2.053	0.287	1.935	0.381	1.18	0.169	1.262	0.189
VEIN_4	4.472	2270	1.26	213.1	10.09	372.8	19.91	38.84	4.183	15.17	2.7	0.479	1.933	0.291	1.835	0.328	1.025	0.1585	1.139	0.1734
VEIN_5	4.501	2270	1.13	213.2	10.23	375.4	18.89	38.33	4.125	15.35	2.51	0.47	1.937	0.284	1.701	0.344	1.026	0.161	1.133	0.1787
VEIN_6	4.484	1420	1.23	214.6	10.14	375.1	19.58	38.67	4.095	15.31	2.78	0.472	1.86	0.287	1.71	0.354	1.081	0.171	1.092	0.185
VEIN_7	4.44	2020	1.17	213.6	10.42	371.2	19.39	39.58	4.176	15.66	2.79	0.512	1.95	0.273	1.838	0.35	1.14	0.1642	1.125	0.174
VEIN_8	4.612	1040	1.32	216	9.97	373.6	19.84	39.21	4.137	15.6	2.653	0.472	1.918	0.2598	1.751	0.335	1.023	0.17	1.108	0.179
VEIN_9	4.531	1320	1.34	218.7	9.99	373.4	18.58	38.21	4.09	15.44	2.68	0.464	1.964	0.283	1.69	0.347	1.066	0.1717	1.125	0.182
VEIN_10	4.515	376	1.47	213.9	10.419	386.4	19.05	38.48	4.168	15.81	2.598	0.525	1.955	0.282	1.802	0.368	1.112	0.1676	1.188	0.179

VEIN_11	4.574	369	1.32	214.7	10.2	380.9	18.83	38.46	4.132	15.29	2.78	0.474	2.025	0.285	1.767	0.345	1.077	0.158	1.185	0.189
VEIN_12	4.515	716	1.38	213.9	10.06	376.8	18.78	38.09	4.03	15.45	2.69	0.463	1.938	0.2788	1.727	0.347	1.036	0.172	1.153	0.1839
VEIN_13	4.518	494	1.23	215.3	10.25	388	18.9	37.83	4.087	15.7	2.71	0.459	1.964	0.283	1.772	0.365	1.096	0.1621	1.122	0.1915
VEIN_14	4.498	223	1.12	215.1	10.32	390.1	19.04	37.94	4.126	15.73	2.81	0.468	2.075	0.278	1.755	0.361	1.073	0.1685	1.161	0.1823
VEIN_15	4.444	1420	1.21	212.8	10.272	386.9	18.99	37.87	4.102	15.5	2.67	0.474	1.885	0.287	1.822	0.359	1.098	0.1687	1.156	0.19
VEIN_16	4.45	730	1.21	214.5	10.533	386.2	19.36	38.75	4.144	15.76	2.9	0.531	2.08	0.28	1.817	0.363	1.066	0.169	1.11	0.192
VEIN_17	4.485	1220	1.41	216.5	9.93	374.3	19.01	38.01	4.083	15.28	2.74	0.456	1.929	0.273	1.775	0.359	1.088	0.16	1.086	0.178
VEIN_18	4.387	1160	1.17	219.5	10.34	386.7	19.09	37.84	4.055	15.75	2.78	0.496	1.96	0.28	1.81	0.372	1.053	0.1603	1.147	0.1908
VEIN_19	4.44	2300	1.31	216.8	10.18	370.1	19.33	38.86	4.171	15.82	2.66	0.494	1.985	0.289	1.764	0.342	1.021	0.166	1.112	0.182
ORE_0	4.499	94	1.2	215.3	10.35	391.1	18.79	37.61	4.083	15.51	2.7	0.466	2.06	0.281	1.827	0.362	1.073	0.1662	1.24	0.182
ORE_1	4.486	303	1.26	216.1	10.23	382.5	18.72	37.75	4.123	15.31	2.62	0.481	1.898	0.285	1.771	0.359	1.069	0.164	1.152	0.1878
ORE_2	4.475	316	1.31	215.1	10.33	390	18.87	37.56	4.122	15.62	2.69	0.451	1.872	0.295	1.794	0.356	1.112	0.171	1.166	0.1856
ORE_3	4.529	181	1.25	216.8	10.306	386	18.76	37.74	4.137	15.63	2.64	0.454	1.919	0.277	1.765	0.369	1.133	0.1657	1.161	0.19
ORE_4	4.492	77	1.32	216.4	10.41	390.5	18.74	37.83	4.185	15.91	2.73	0.463	1.957	0.288	1.818	0.358	1.115	0.1668	1.154	0.1921
ORE_5	4.463	75	1.26	217.83	10.355	392.4	18.76	37.65	4.147	15.5	2.806	0.457	1.935	0.2824	1.781	0.375	1.098	0.1691	1.207	0.1906
ORE_6	4.645	64	1.32	217.2	10.43	392.4	18.89	37.97	4.116	15.84	2.799	0.481	1.959	0.275	1.823	0.369	1.146	0.171	1.196	0.188
ORE_7	4.5	66	1.38	218.2	10.39	391	18.91	38.05	4.193	15.76	2.704	0.465	1.941	0.29	1.818	0.365	1.076	0.1521	1.164	0.1784
ORE_8	4.561	47.3	1.23	216.5	10.41	391	18.71	37.66	4.114	15.29	2.7	0.464	1.988	0.2872	1.794	0.361	1.139	0.1745	1.174	0.1815
ORE_9	4.523	133	1.12	217.2	10.27	388.8	18.85	37.66	4.133	15.49	2.663	0.455	1.992	0.286	1.82	0.353	1.086	0.1691	1.203	0.1877
ORE_10	4.501	60.7	1.4	216.63	10.41	388.7	18.81	37.95	4.128	15.41	2.8	0.451	1.965	0.28	1.773	0.365	1.119	0.165	1.205	0.1785
ORE_11	4.502	168	1.36	218.1	10.45	390.7	18.99	38.09	4.164	15.48	2.64	0.472	1.945	0.27	1.811	0.351	1.065	0.1688	1.219	0.1904
ORE_12	4.539	109	1.37	217.7	10.262	390.3	18.75	37.79	4.186	15.53	2.78	0.486	1.926	0.279	1.757	0.368	1.044	0.1704	1.187	0.181
ORE_13	4.499	136	1.25	218.1	10.13	383.9	18.81	37.81	4.126	15.57	2.697	0.485	2.047	0.291	1.737	0.36	1.036	0.1665	1.082	0.1816
ORE_14	4.51	72	1.31	216.73	10.32	386.8	18.85	37.77	4.172	15.57	2.75	0.454	1.969	0.265	1.776	0.367	1.086	0.1667	1.159	0.1886
ORE_15	4.478	79.4	1.21	219.3	10.23	386.6	18.76	37.92	4.193	15.72	2.7	0.461	1.983	0.276	1.777	0.361	1.048	0.1716	1.218	0.191
ORE_16	4.431	203	1.23	217.7	10.159	381.7	18.76	37.84	4.126	15.22	2.789	0.492	1.934	0.2876	1.751	0.3525	1.03	0.1665	1.203	0.187
ORE_17	4.545	89	1.12	218.7	10.32	388.6	18.91	38.07	4.132	15.45	2.693	0.475	1.932	0.272	1.801	0.357	1.114	0.1649	1.137	0.185

ORE_18	4.568	261	1.3	217.2	10.344	390.7	18.8	37.75	4.113	15.58	2.604	0.479	1.973	0.268	1.816	0.375	1.104	0.1697	1.201	0.195
ORE_19	4.531	205	1.29	216.1	10.207	382.4	18.68	37.96	4.134	15.32	2.77	0.457	1.864	0.279	1.722	0.343	1.077	0.175	1.194	0.177
RML_0	10.44	580	3.26	179.6	23.49	629.4	25.18	42.54	5.111	19.69	3.69	0.749	3.01	0.463	2.97	0.653	2.005	0.301	2.079	0.333
RML_1	10.22	432	2.7	178.91	22.69	637.6	24.9	41.78	5.055	19.67	3.46	0.683	2.955	0.435	2.809	0.608	1.852	0.293	2.079	0.325
RML_2	10.3	612	2.66	178.21	22.44	634.6	24.75	41.22	4.937	19.3	3.55	0.66	2.912	0.423	2.827	0.603	1.937	0.283	2.088	0.331
RML_3	10.23	487	2.61	178.93	22.46	639.1	24.96	41.09	4.986	19.29	3.47	0.687	2.919	0.4428	2.84	0.597	1.878	0.293	2.176	0.324
RML_4	10.28	587	2.76	177.3	23.32	633.8	24.89	42.06	5.021	19.46	3.49	0.733	2.95	0.446	2.99	0.645	1.928	0.306	2.09	0.333
RML_5	10.22	373	2.83	177.61	22.54	640.6	24.67	41.3	4.997	19.35	3.5	0.676	2.906	0.434	2.797	0.598	1.887	0.296	2.135	0.315
RML_6	10.36	369	2.8	178.87	22.35	636.3	25.31	42.28	4.999	19.68	3.567	0.675	2.85	0.406	2.87	0.61	1.827	0.287	1.997	0.325
RML_7	10.33	380.8	2.69	177.18	22.51	634.9	24.86	41.36	4.942	19.25	3.617	0.692	3.019	0.434	2.777	0.599	1.873	0.289	2.058	0.323
RML_8	10.24	473	2.83	178.1	22.66	634.5	24.95	41.83	5.032	19.46	3.57	0.677	2.782	0.431	2.851	0.612	1.893	0.295	2.137	0.3269
RML_9	10.37	384.8	2.75	178.02	22.61	638.1	24.92	41.85	4.995	19.25	3.512	0.695	2.925	0.431	2.866	0.6	1.943	0.312	2.076	0.331
RML_10	10.34	421	3	178.68	22.46	628.5	24.78	41.61	5.011	19.24	3.49	0.716	2.985	0.432	2.832	0.595	1.87	0.276	1.996	0.328
RML_11	10.33	517	2.87	178	22.25	620	24.8	42.06	4.985	19.25	3.56	0.723	2.818	0.427	2.837	0.618	1.834	0.29	2.014	0.316
RML_12	10.36	664	2.77	176.7	22.06	623.9	24.7	40.92	4.93	19.5	3.59	0.687	2.819	0.418	2.888	0.593	1.842	0.294	2.075	0.319
RML_13	10.07	780	2.66	175.65	22.39	609	27.08	45.05	5.132	19.35	3.54	0.811	2.94	0.429	2.83	0.612	1.887	0.279	2.001	0.305
RML_14	10.21	561.7	2.63	176.05	22.67	628	25.28	42.8	5.031	19.52	3.62	0.747	2.998	0.447	2.937	0.632	1.868	0.294	1.994	0.328
RML_15	10.29	486	2.77	178.7	22.28	626.7	24.77	41.47	4.931	19.6	3.47	0.681	2.773	0.432	2.879	0.59	1.881	0.277	1.995	0.318
RML_16	10.14	512	2.7	177.1	22.19	626.6	24.58	41.49	5.003	19.38	3.44	0.681	2.98	0.426	2.824	0.604	1.852	0.292	2.023	0.316
RML_17	10.24	511.5	2.67	178.1	21.57	617.4	24.67	41.43	4.976	19.07	3.489	0.656	2.874	0.43	2.679	0.586	1.8	0.282	1.875	0.31
RML_18	10.51	628	2.73	177.5	21.58	618.2	24.36	41.43	4.945	19.16	3.42	0.639	2.77	0.427	2.778	0.602	1.811	0.273	1.979	0.32
RML_19	10.27	548.7	2.86	177.99	22.08	620.9	24.7	41.73	4.988	18.8	3.45	0.683	3.02	0.421	2.888	0.615	1.863	0.296	2.041	0.307